Research of Snow Detection in Akita Area Using MODIS Images

（MODIS 画像を用いた秋田県地域における積雪検知に関する研究）

Akita Prefectural University
Graduate School of Systems Science and Technology
Integrated Course of Systems Science and Technology
(Doctoral Course)

Paipai Pan

September, 2015

This page intentionally left blank.

Contents

Abstract

Snow, as one of the most important parameters of climate change, has been aroused more and more attention in many fields. However, most of snow cover detection results have low accuracy due to the effect of atmosphere, regional terrain and the underlying surface covered by snow. In the present work, several novel methods on snow cover detection were proposed to improve its accuracy. The work is divided into five chapters, which were described as follows.

In chapter 1, research background, which includes the current climate conditions of world and Japan, the significance of snow observations, observation methods of the snow and previous researches of snow cover detection using the satellite imagery data, is described. Meanwhile, developing snow cover detection methods with high accuracy as the research objectives is also presented. And the construction of this thesis is listed in this chapter.

In chapter 2, the study region and the used data are presented. In addition, the initial preprocessing steps before the snow cover detection conducted with proposed methods were also described in this chapter.

In chapter 3, in order to improve the discrimination accuracy of snow pixels in forest area, a new method with the combination of NDSI and NDVI is proposed. This method is proved to be applicable to Akita Prefecture. Compared to the MOD10_L2 data and NDSI alone results, it has been proved that the accuracy of proposed method for snow detection was improved about 11%. Therefore, it is feasible and effective to use the combination of NDSI and NDVI for the snow cover detection in Akita Prefecture of Japan with MODIS images. In addition, both GIS forest region data and the NDVI were used for forest area discrimination. The forest region was successfully classified with GIS and NDVI data for forest region classification in study area. Finally, the snow cover detection was conducted with proposed method for the study area. Comparing with the snow cover detection results without the forest area discrimination, the accuracy with GIS forest region data and with NDVI for the forest area discrimination were increased by 11.17% and 8.05%, respectively. And the

accuracy with GIS forest region data is about 3.12% higher than the NDVI discrimination method.

In chapter 4, first, the comparison of FLAASH and 6S code model for the atmospheric correction based on Terra/MODIS data and natural and geographic situation of Akita prefecture is studied. The results of snow cover detection without atmospheric correction and with FLAASH and 6S code model for atmospheric correction were also compared from December 2010 to April 2011. The snow cover detection accuracy was improved by 40% and 46% with FLAASH model and 6S code model for atmospheric correction. Moreover, the accuracy of snow cover detection with 6S code atmospheric correction is 6% higher than the FLAASH model.

Then, a new snow cover detection method based on visible red and blue channel from MODIS imagery under the cloud-free condition is proposed considering the influence of atmosphere, topographic features, snow covered underlying surface and the principle of the snow cover detection from MOD10_L2. The overall accuracy of the snow cover detection with proposed method is higher than both snow depth records of 31 observation stations and the results from MOD10_L2 products.

In addition, in order to operate the snow cover detection more effectively under the cloud condition, another new snow cover detection method is proposed to conduct the snow cover detection and eliminate the impact of cloud as much as possible. As it is difficult to remove a large area of cloud using information from optical sensors, predominantly sunny days (with cloud cover making up less than 5% of the acquired images) are selected for snow cover detection. In this method, snow and cloud are extracted from other ground surface features using red band 1 and blue band 3. Then, short-wave infrared (SWIR) band 6 and band 7 are used to detect and distinguish cloud. Finally, cloud is removed from snow to obtain a final snow cover map of Akita Prefecture. Compared with the MODIS snow products, in-situ snow depth data and previous snow cover detection method, the proposed method are proved to be more effective in study area, Akita Prefecture. Furthermore, the new proposed method is also further validated using data from Aomori Prefecture and the Mt. Chokaizan region.

In chapter 5, the conclusion and results of the whole study are described in this chapter.

Key words: Snow cover detection; MODIS; Akita Prefecture; Japan.

List of Figures

List of Tables

Chapter 1
Introduction

1.1 Research Background

1.1.1 The current climate conditions of World and Japan

Since the 1950s, the global scale climate changes are unprecedented over decades to millennia. The main reason is that gas emissions from the anthropogenic greenhouse have been increased since the pre-industrial era, and are now higher than ever. As a result, atmospheric concentrations of carbon dioxide, methane and nitrous oxide are unprecedented in at least the last 800,000 years. Atmospheric composition has become the dominant cause of the global climate warming since the mid-20th century [1].

Along with the advance of technology, the problem of the earth warming has become more and more serious, especially in recent 10 years. According to the latest global climate synthesis report, we can know that the earth temperature changes have warmed the atmosphere and ocean. Correspondingly, the earth is experiencing changes in precipitation, temperature, sea level rise and the intensity and frequency of cyclones [2]. Due to this reason, scientists have already observed alarming shifts in the natural world, including thawing permafrost, melting glaciers, and amounts of snow melting, which is threatening human and natural life [3].

Figure 1.1 shows the global average temperature changes from 1891 to 2013. It is obvious that the annual anomaly of temperature in 2013 is +0.20ºC above the average from 1981 to 2010. It is virtually certain that the global average surface temperature has risen at a rate of about 0.69ºC per century from a long time [4].

Based on the above data, we can make sure the global temperature has risen in recent years. Figure 1.2 shows the annual Japan average temperature changes from 1898 to 2013. Similarly, from this figure, we can also see that the average temperature of Japan in 2013 is 0.34ºC above the average from 1981 to 2010. It is virtually certain that the annual Japan average temperature has risen at a rate of about 1.14ºC per

century from a long time.

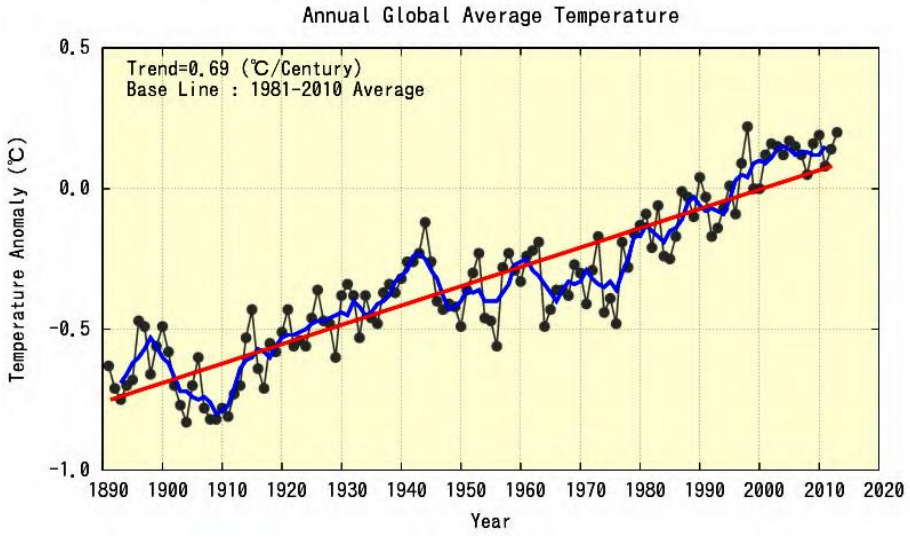

Figure 1.1: Annual global average temperature (Japan Meteorological Agency). [Note: Note: Black line with dots represents the temperature anomaly for each year. Blue line represents the five-year running mean, and red line represents the long-term linear trend.]

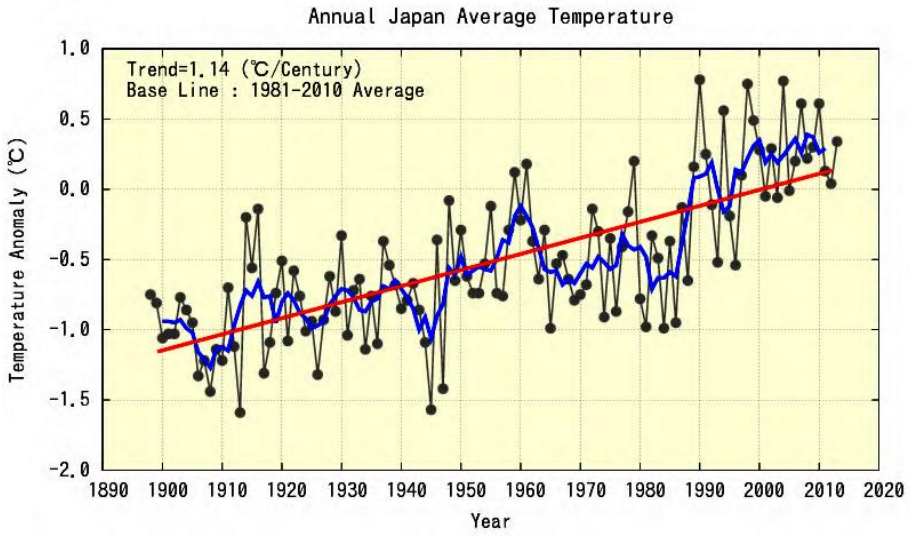

Figure 1.2: Annual Japan average temperature (Japan Meteorological Agency). [Note: Black line with dots represents the temperature anomaly for each year. Blue line represents the five-year running mean, and red line represents the long-term linear trend.]

From Figure 1.2, it is noticeable that in the late 1980s, temperature began to show a rapid warming trend and appeared the warmest record since the 1990s. This trend is similar to that of annual global average temperature (Figure 1.1) [4].

Figure 1.3 (a), Figure 1.3 (b), and Figure 1.3 (c) show the snow depth conditions in the Sea of Japan Side of Japan from 1962 to 2013, which is published by Japan Meteorological Agency. From these three figures, we can obtain the annual average snow depth ratio in 2013 is 140% relative to the average from 1981 to 2010 for the Sea of Japan side of northern Japan (Figure 1.3 (a)), 69% for the same side of eastern Japan (Figure 1.3 (b)), and 57% for the same side of western Japan (Figure 1.3 (c)). And the annual average snow depth had a peak in the early 1980s followed by a decline until around the early 1990s. The annual average of snow depth ratio on the Sea of Japan side in these three figures shows decline trend [4].

From the above statistical data, we can make sure to conclude that the annual average snow depth is decreasing. Therefore, snow cover observation has become an immediate problem.

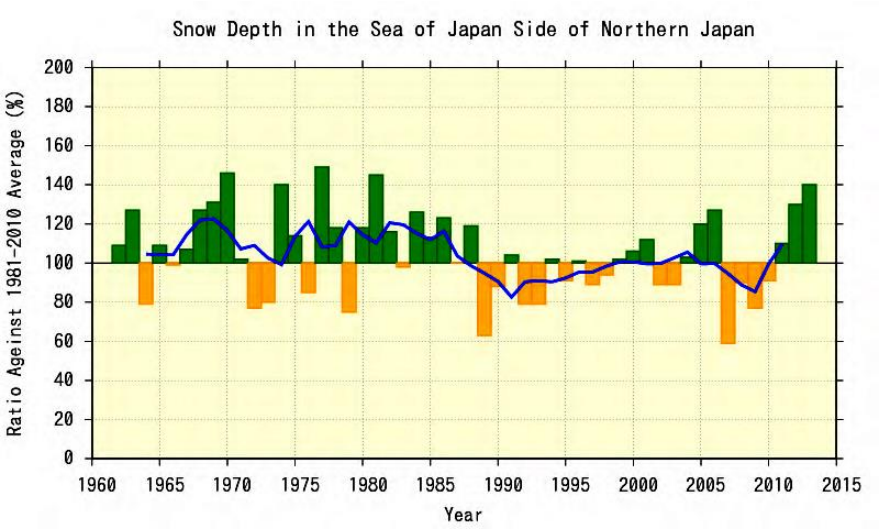

Figure 1.3 (a): Snow depth in the Sea of Japan Side of Northern Japan from 1962 to 2013 (Japan Meteorological Agency).

1.1.2 The significance of snow observations

As a most active natural factor and an important component of the cryosphere, snow not only impacts the heat balance of global season and climate change, but also has an important impact on the global water cycle, industrial and agricultural processes [5], [6], [7].

Observation for snow cannot only improve the management of regional water

resources effectively, but also contributes to the ecological environment construction, environment protection and agricultural production [8]. Therefore, it is very important to study the snow cover conditions and their effects on the global climate.

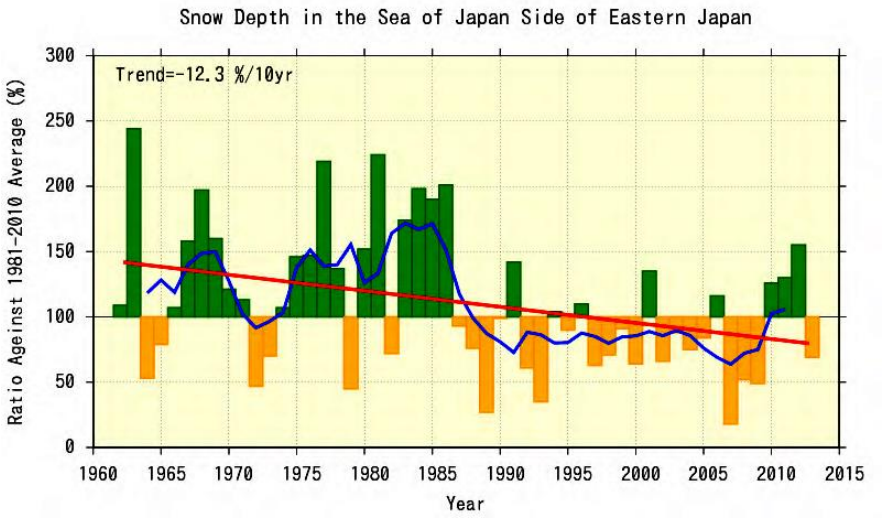

Figure 1.3 (b): Snow depth in the Sea of Japan Side of Eastern Japan from 1962 to 2013 (Japan Meteorological Agency).

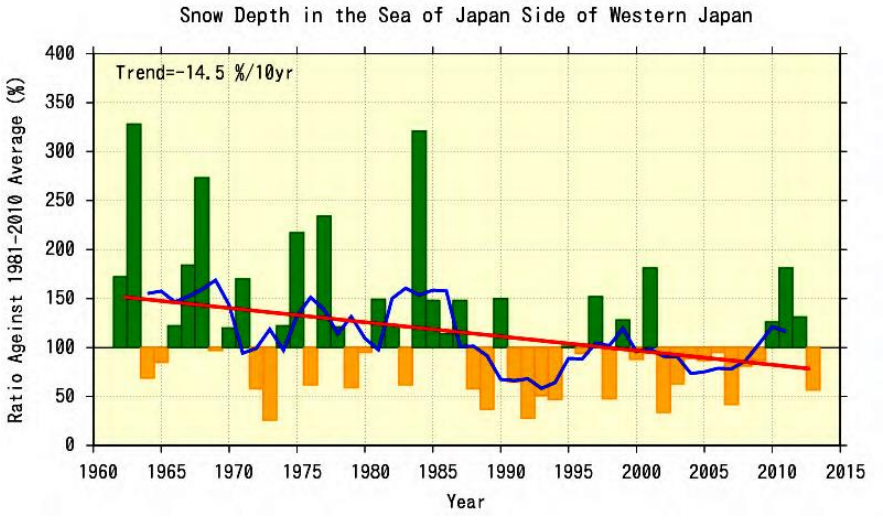

Figure 1.3 (c): Snow depth in the Sea of Japan Side of Western Japan from 1962 to 2013 (Japan Meteorological Agency).
Note: Annual averages are presented as ratios against the baseline (the 1981 – 2010 average). Bars represent the snow depth ratio for each year. Blue line represents the five-year running mean, and red line represents the long-term linear trend.

In 1970, the snow was defined as a main role in the formation of condensate due to the decline or the deposition of ice particles as a result of sublimation role by the

World Meteorological Organization (WMO), United Nations Educational Scientific, Cultural Organization (UNESCO) and International Association of Hydrological Sciences (IAHS) [9]. In fact, the snow is a mixture of ice crystals, liquid water, and air [10]. Therefore, the snow has all kinds of properties, such as the grain size and shape, water content, surface roughness, depth and presence of impurities. Thus, snow can affect all aspects of the global climate and human life.

1.1.3. Observation methods of the snow

Previously, studies of snow cover detection have been conducted using data from hydrometeorological stations as the traditional observation method, which have been found to be reliable over long periods. However, the distribution of such hydrometeorological stations is inhomogeneous and, particularly in remote rural areas, missing measurements, incorrect measurements, and inconsistent observation times occasionally affect datasets [11]. For this reason, it is difficult to use these data for conducting snow cover detection correctly over large areas.

With the development of science and technology, surveying the snow using aircraft has become more and more useful and popular. This method can make up for the shortcomings of traditional methods. In addition, it can observe snow cover conditions in the remote places at one time. The most important is that this method can identify the properties of snow beyond the recognition capability of eyes. However, the aircraft is often affected by the cloud and weather, and its cost is very high. Therefore, the application of this method is also limited and do not meet the more widely research for snow cover [12].

Nowadays, the development of satellite remote sensing technology has prompted much research and methodological development using information from the visible, infrared, and microwave spectra based on the optical, electric, and thermal properties of snow [13], [14]. The high reflectance of snow makes it easy to extract from other ground surface features, with the exception of cloud [15], [16]. New studies and methods enable the synchronous detection of snow cover over a wide range of wavelengths, including information on snow cover from beyond the visible range. Additionally, using these techniques, the same regions can be repeatedly investigated for prolonged periods. Therefore, these methods have improved the inadequacies of

traditional methods and have improved the depth, breadth, accuracy, and efficiency of snow cover detection.

1.1.4. Previous researches of snow cover detection with the use of satellite imagery data

Recently, several snow cover detection studies have been conducted using satellite data from the National Oceanic and Atmospheric Administration (NOAA) [17], [18], Landsat [19], and moderate resolution imaging spectroradiometer (MODIS) [16], [20].

Hall et al. [21] proposed the normalized difference snow index (NDSI), by which snow can be identified using a corresponding threshold. This method has been widely used and recognized by the National Aeronautics and Space Administration's (NASA's) MODIS group [22], [23]. At present, the NDSI is being used as the standard for acquiring snow cover data. However, recognizing the snow signal within satellite data from mountainous and forested areas is proving to be problematic because the snow may be covered by dense vegetation in these terrain types.

Klein et al. [24] reported this problem and proposed a method by combining the NDSI and the normalized difference vegetation index (NDVI) for evaluating the snow and vegetation mixed pixels in heavily vegetated regions. The accuracy of the results and the feasibility of this method have been derived. However, several studies and experiments have also found the errors in snow cover detection by combination of , NDSI and NDVI because the necessary preprocessing were not performed [25], [26].

Spectral mixing is an inherent problem in dense vegetation, which results in the few image pixel spectrum can represent the pure surface features [27], [28]. Adams and Smith [29], [30] proposed a Linear spectral mixture analysis (SMA) method to resolve this spectral mixing problem [31]. They mainly assumed the variability of the pixel-to-pixel in one image resulted from different proportions of spectrum values. One mixed pixel's spectrum could be calculated by a linear combination of the spectrum value weighted by all the values area within this pixel. These researches estimated that electromagnetic radiation scattering and absorption is resulted from one single component on the surface features [27], [32].

Another inherent problem is the subpixel in the remote sensing. Generally speaking, subpixel of the snow cover is disturbed by the unpredictable variability from subpixel from non-snow surface cover [33]. To overcome this problem, researching for subpixel of snow cover has been conducted in many studies [34], [35], [36], [37]. Among these methods, Rosenthal et al. [38] had proposed the spectral mixture algorithm was the effective technique to solve this snow cover subpixel problem and it has been proven to be an effectiveness method in alpine areas. However, this method can be only applied to the small scale areas and not considered the land cover type under the snow cover [39].

There are also many studies about snow cover detection methods, such as snow melt and accumulation [40], Melt Area Detection Index (MADI) [41] and snowfall detection [42] and so on. These methods have obtained definite achievements in a certain extent.

However, all of the above methods are not applicable to the Akita Prefecture, because there are a lot of mountains and forests. It is due to the fact that the snow cover detection in mountains and forests is strongly affected by atmospheric and topographic variations. First, the reflectance of real ground surface features received by satellite sensors can be hindered by particles and aerosols in atmosphere [43]. Second, snow cover information can be masked or disturbed by shadows produced by surface relief and terrain [44]. Therefore, atmospheric and topographic corrections are necessary before effective snow cover detection in forested and mountainous areas.

1.2 Research Objectives

In this study, the main factors of the snow cover detection, such as the atmosphere, the terrain, the underlying surface of snow and cloud, are concerned and considered. The Akita Prefecture of Japan as the study area is selected. The main objective of this research is to propose new and most effective method for snow cover detection, which is applicable in Akita Prefecture. The accuracy of snow cover detection is improved and the proposed method is expected to be used in every place of the whole world. In this work, the MODIS images from Terra satellite and Aqua satellite are the main study use images data.

1.3 Construction of Thesis

The construction of this thesis is shown in below.

Chapter 1 Introduction

The background and objectives of this study are mainly described.

Chapter 2 Study Region, Used Data and Initial Processing Steps

The study region which includes Akita prefecture and Tohoku region, satellite data which includes MODIS imagery data and landsat satellite operational land imager data, digital elevation model data, in-situ data which includes automated meteorological data acquisition system data and road snow information system data, and Initial processing steps which includes geographic correction, study area clipping, atmospheric correction (CREFL_SPA and 6S code) and topographic correction, are mainly described.

Chapter 3 Snow Cover Detection via Normalized Difference Indexes

In this chapter, the study area image of completed atmospheric correction and topographic correction is used to snow cover detection. In section 3.2, a new method with the combination of NDSI and NDVI, which is applicable to Akita Prefecture, is proposed. Compared to the MOD10_L2 data and NDSI alone results, the proposed new method showed high accuracy in snow cover detection. In section 3.3, GIS forest region data and the NDVI were adopted for the forest area discrimination based on Terra/MODIS data and natural and geographic situation of the Tohoku region. Image comparisons between GIS forest region data and the NDVI forest area discrimination were investigated. The results of snow cover detection without the forest area discrimination and with GIS forest region data and the NDVI for the forest area discrimination were also compared to prove the effective of forest discrimination.

Chapter 4 Snow Cover Detection with Visible Red and Blue Bands

This chapter is divided into three parts. In section 4.2, FLAASH and 6S Code as the two most effective atmospheric correction methods are investigated and compared. The atmospheric correction based on atmospheric radiation transfer model, which can restore the real surface features reflectance from the top of the atmosphere, are investigated and compared. In addition, the snow cover detection without atmospheric correction is also conducted to compare with the results with FLAASH and 6S code model for atmospheric correction. In section 4.3, a new snow cover detection method based on visible red and blue bands from MODIS imagery data is proposed for Akita prefecture under the sunny cloud-free conditions. The 5 typical images of clear days during the whole year are observed, and the threshold values by investigating these 5 typical images and their corresponding 2-dimensional scatter plots in bands 1 and 3 are confirmed. The effectiveness of the proposed method is investigated via the comparisons with the MOD10_L2 products and in-situ snow depth data from 31 observation stations across the whole study area. As is known to all, cloud disturbances pose a significant barrier to effective snow cover detection. It is difficult to remove a large area of cloud using information from optical sensors. So in section 4.4, predominantly sunny days (with cloud cover making up less than 5% of the acquired images) are selected for snow cover detection in order to eliminate the impact of cloud as much as possible. In this section, a new snow cover detection algorithm is proposed uses MODIS image data and is validated for the Akita Prefecture, Japan. Snow and cloud are extracted from other ground surface features using red band 1 and blue band 3. Then, short-wave infrared (SWIR) band 6 and SWIR band 7 are used to detect and distinguish cloud. Finally, cloud is separated from snow to obtain a final snow cover map of Akita Prefecture. The new proposed method is further validated using data from Aomori Prefecture and the Mt. Chokaizan region.

Chapter 5 Conclusion

The conclusions and results of this study are mainly described.

Chapter 2
Study Region, Used Data and Initial Processing Steps

2.1. Study Region

In this work, Akita Prefecture and Tohoku Region of Japan as the study region are selected, and the Aomori Prefecture and Mt. Chokaizan Region as the test region are chosen in Chapter 4.

2.1.1. Akita Prefecture

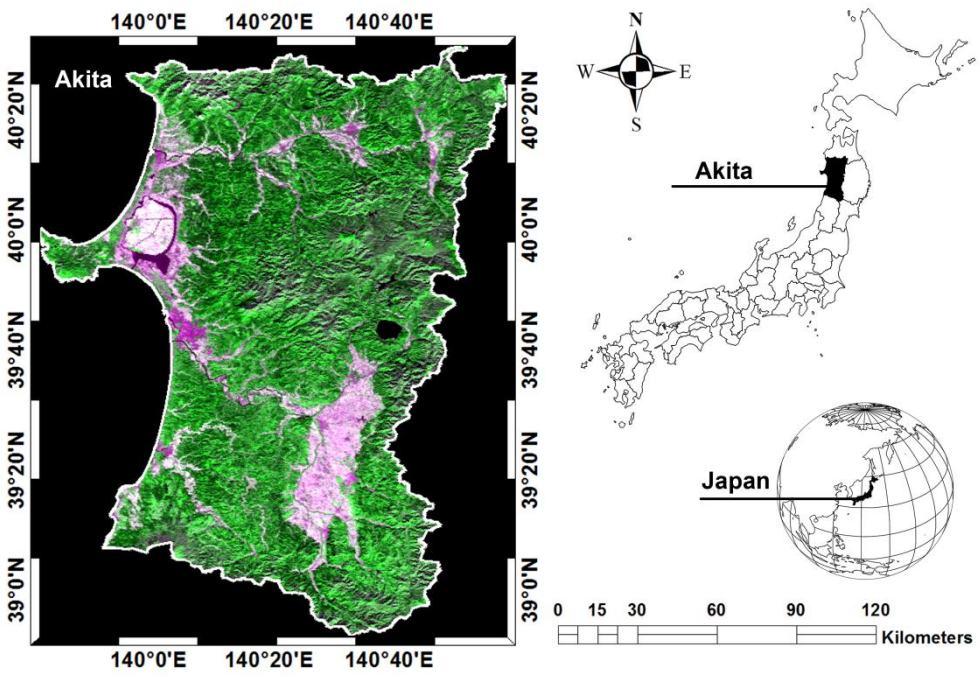

Figure 2.1: The MODIS image in Akita prefecture of Japan taken on the October 8, 2012, which is the 250 m true color image synthesized from RGB 121. The green part in the left image represents vegetation and other parts represent no vegetation. The right figure represents the location of Akita prefecture in Japan.

Akita Prefecture, (between 38°52′23″N and 40°30′40″N, and 139°41′32″E and

140°59′43″E) [45], with an area of 11,636.28 km² [46], is located in the northeast region of northern Honshu, the main island of Japan as shown in Figure 2.1. It faces the Sea of Japan in the west and is bordered by four other prefectures: Aomori in the north, Iwate in the east, Miyagi in the southeast and Yamagata in the south.

Akita prefecture is the typical climate of the Sea of Japan, winter is long and summer is short. Its four seasons are distinct. Winter is very cold with short frost-free period, and summer is hot with less sunshine and abundant rainfall [4], the annual rainfall is about 1800 mm [48]. The warm and cold Tsushima currents result in significant amounts of snowfall in Akita prefecture during the winter, with annual snowfall around 377 cm. The general average thickness of the snow is 48 cm. And the maximum and minimum temperatures during the snowy season are −4.82˚C and −11.26˚C, respectively. The terrain of Akita prefecture is high in east and low in west. There are the Ou Mountains in the east boundary, and the Dewa Mountains with basins in the central, and coastal plains in the western. Due to the Dewa Mountains run parallel cross the central region of the prefecture, the whole region has been divided into two big areas, their climates are different. There are often a lot of snow cover in inland and few snow cover in coastal area [49].

Due to sparsely populated and almost no industrial in the Akita prefecture, rice planting in agricultural production is very developed and ranked third in Japan. In addition, more than 70% [50] is covered by forests in the whole prefecture. The majority forests are coniferous and deciduous, and account for around 54.71% and 41.48% of the forested area in the whole prefecture, respectively [50]

Akita prefecture is selected as the study area in this work for the following three reasons: First, Akita is the typical climate of the Sea of Japan, with abundant snowfall in winter. Because of the influence of the sea wind, coastal areas have relatively few snow cover on the ground and there are plenty of snow cover on the ground in inland area, which can help to clearly judge the snow cover detection method is effective or not. Second, Akita prefecture is a village with large area and high density of forests. Tree species are relatively simple, mainly are coniferous and deciduous forests. Hence, whether the snow cover detection method can detect the snow pixels hidden by forest or not can be clearly evaluated. Third, due to there are many mountains and large terrain variations in Akita, we can clearly evaluate whether the snow cover detection method can detect the snow pixels in the large terrain variation regions or not.

2.1.2. Tohoku Region

The Tohoku region, (between 36°47′29″N and 41°33′22″N, and 139°09′53″E and 142°04′21″E) [51], with an area of 66,890 km², consists of the northeastern portion of Honshu which is the largest island of Japan as shown in Figure 2.2. It includes six prefectures which are Akita, Aomori, Fukushima, Iwate, Miyagi and Yamagata.

The climate of Tohoku region is divided into four groups which are the coast region of Sea of Japan, the region of Nasu volcanic belt piedmont and west side (basin), the region of east side and the other areas except for the Nasu volcanic belt piedmont (basin), and the coast region of Pacific Ocean.

The climate of the Sea of Japan side group consisted by the coast region of Sea of Japan, and the region of Nasu volcanic belt piedmont and west side (basin) is the climate of the Sea of Japan. The weather is very high temperature in summer because of the Foehn wind. On the contrary, there is less daylight hours and easily become a heavy snowfall region, especially the snowfall of basin on the west side of the Mt. Ou often heavy.

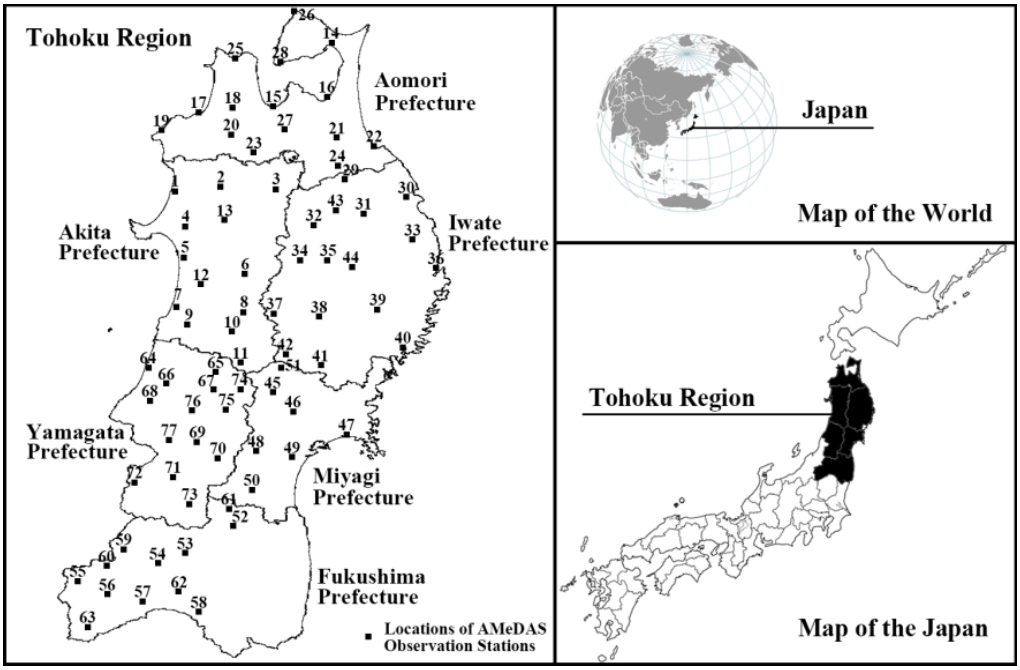

Figure 2.2: Study area of Tohoku Region

The climate of the region of east side and the other areas except for the Nasu

volcanic belt piedmont (basin) is both a Pacific Ocean side climate and inland climate. During the summer, the days of the high temperature caused by the Foehn wind and the days of low temperatures caused by cloudy weather in the Pacific Ocean coastal areas are more. While, sunny days in the Pacific Ocean side are more than the weather of the coast region of Sea of Japan.

The climate of the coast region of Pacific Ocean is both a Pacific Ocean side climate and marine climate. During the summer, the weather is often under the low temperature and sunny days are more. The snowfall is often less, and atmosphere is often dried [52].

Around 70% of Tohoku region is covered by rich forest. It was chosen as a study area in this work because of its weather is influenced by the climate of Sea of Japan and Pacific directly, and the snowfall is abundant on one side of the Sea of Japan. On the contrary, snowfall is seldom on the other side of the Pacific. In addition, most of the areas in the whole region are covered by forests and tree species (coniferous and deciduous) are relatively single.

2.2. Used Data

2.2.1. Satellite Data

In this study, the MODIS imagery of Earth Observing System (EOS) Terra satellite and Aqua satellite as the main process data are used in the whole study, and the Operational Land Imager (OLI) of Landsat 8 satellite as the test data are used in Chapter 4.

2.2.1.1. MODIS Imagery Data

Moderate Resolution Imaging Spectroradiometer (MODIS), a key instrument for snow cover detection, provides high radiometric sensitivity (12 bit) in 36 spectral bands with the wavelength ranging from 0.4 μm to 14.4 μm aboard the Terra (EOS AM-1) satellite which was launched on December 18, 1999 [53], and the Aqua (EOS PM-1) satellite which was launched on May 4, 2002 [54]. Two bands are observed at a nominal resolution of 250 m at nadir, with five bands at 500 m, and the other 29 bands at 1 km [55] as shown in Table 2.3 (a) and (b). Terra's orbit around the earth is timed so that it passes from north to south across the equator at local time 10:30 in the

morning, while Aqua passes south to north over the equator at local time 13:30 in the afternoon. A ±55-degree scanning pattern at the EOS orbit of 705 km achieves a 2,330 km swath and provides global coverage every one to two days.

Table 2.3 (a): The Specifications of MODIS from bands 1 to 19

Primary Use	Band	Bandwidth[1]	Spectral Radiance[2]	Required SNR[3]
Land/Cloud/	1	620 - 670	21.8	128
Aerosols Boundaries	2	841 - 876	24.7	201
	3	459 - 479	35.3	243
Land/	4	545 - 565	29	228
Cloud/	5	1230 - 1250	5.4	74
Aerosols Properties	6	1628 - 1652	7.3	275
	7	2105 - 2155	1	110
	8	405 - 420	44.9	880
	9	438 - 448	41.9	838
	10	483 - 493	32.1	802
Ocean Color/	11	526 - 536	27.9	754
Phytoplankton/	12	546 - 556	21	750
Biogeochemistry	13	662 - 672	9.5	910
	14	673 - 683	8.7	1087
	15	743 - 753	10.2	586
	16	862 - 877	6.2	516
	17	890 - 920	10	167
Atmospheric Water Vapor	18	931 - 941	3.6	57
	19	915 - 965	15	250

MODIS has 44 standard data products. They can enable us to improve our understanding of global dynamics and processes occurring in the earth, oceans, and atmosphere, playing a major role in the development of predictive models of global climate change, the status of the melting ice and snow and agricultural production. MODIS products are organized into different processing levels. Level 0 product is raw digital number images. Level 1 product includes uncalibrated and calibrated radiance values. Level 2, 3 and 4 products have more processing and are derived from lower level products [56].

As MODIS has the characteristics of high observed frequency and wide spectral range, the observation period is short and coverage is wide. It can not only monitor

the sudden changing natural disasters in real-time, but also improve the observation ability for the earth complex systems and the identification ability for the earth's surface. In addition, the satellite images covering the entire Akita prefecture can be obtained almost every day.

Table 2.3 (b): The Specifications of MODIS from bands 20 to 36

Primary Use	Band	Bandwidth[1]	Spectral Radiance[2]	Required NE[Δ]T(K)[4]
	20	3.660 - 3.840	0.45(300K)	0.05
Surface/	21	3.929 - 3.989	2.38(335K)	2
Cloud Temperature	22	3.929 - 3.989	0.67(300K)	0.07
	23	4.020 - 4.080	0.79(300K)	0.07
Atmospheric	24	4.433 - 4.498	0.17(250K)	0.25
Temperature	25	4.482 - 4.549	0.59(275K)	0.25
Cirrus Clouds	26	1.360 - 1.390	6	150(SNR)
Water Vapor	27	6.535 - 6.895	1.16(240K)	0.25
	28	7.175 - 7.475	2.18(250K)	0.25
Cloud Properties	29	8.400 - 8.700	9.58(300K)	0.05
Ozone	30	9.580 - 9.880	3.69(250K)	0.25
Surface/	31	10.780 - 11.280	9.55(300K)	0.05
Cloud Temperature	32	11.770 - 12.270	8.94(300K)	0.05
	33	13.185 - 13.485	4.52(260K)	0.25
Cloud Top Altitude	34	13.485 - 13.785	3.76(250K)	0.25
	35	13.785 - 14.085	3.11(240K)	0.25
	36	14.085 - 14.385	2.08(220K)	0.35

[1] Bands 1 to 19 are in nm; Bands 20 to 36 are in µm

[2] Spectral Radiance values are (W/m^2 -µm-sr)

[3] SNR = Signal-to-noise ratio

[4] NE(Δ)T = Noise-equivalent temperature difference

Note: Performance goal is 30-40% better than required

Therefore, we chose it from the consideration of data collection interval for snow detection in Akita Prefecture of Japan. In this work, MODIS Level-1 B data was obtained from the Level 1 and Atmosphere Archive and Distribution System (LAADS) website [57].

2.2.1.2. Landsat Satellite Operational Land Imager Data

Landsat represents the world's longest continuously acquired collection of

space-based moderate-resolution land remote sensing data. Four decades of imagery provides a unique resource for those who work in agriculture, geology, forestry, regional planning, education, mapping, and global change research. So far, there are 8 satellites of Landsat series launched to the space. Among these satellites imagery data, the TM, ETM+ and OLI imagery are often widely used in the remote sensing research industry [58].

In this work, Landsat Satellite Operational Land Imager Data are used in Chapter 4. The operational land imager (OLI) is a multispectral instrument with nine bands onboard the Landsat 8 satellite, which was launched on February 11, 2013. It includes 30 m resolution in eight bands covering the visible, near infrared, and SWIR spectra, and 15 m resolution in one panchromatic band [58]. The Landsat 8 satellite images the entire Earth every 16 days. In this work, OLI bands 3, 4, 5, and 6 image data are used for validating the results of the proposed snow cover detection method. The OLI data used in this work were provided by the Earth Resources Observation and Science Center (EROS), freely available to download from the USGS Global Visualization Viewer (GloVis) within 24 h of reception [59].

2.2.2. DEM Data

Digital Elevation Model (DEM) is a digital geographic dataset of elevations in xyz coordinates. It produces a data file that contains the elevation of the terrain over a specified area, usually at a fixed grid interval over the surface of the Earth. It is used for extracting terrain parameters, creating relief maps, rectifying satellite imagery, analyzing terrain in geomorphological and physical geographical applications, and terrain corrections [60].

In this work, American National Aeronautics and Space Administration (NASA) Shuttle Radar Topographic Mission (SRTM) DEM data with 90 m resolution are used to conduct the topographic correction across the study area. SRTM 90 m DEM is available for over 80% of the entire globe, including Japan, and its vertical error is reported to be less than 16 m. So far, the SRTM 90 m DEM data have 4 versions [61], and in this study, the latest version 4 is selected as the highest quality SRTM dataset. Currently, DEM data are distributed by the United States Geological Survey (USGS) free of charge and can be obtained from the National Map Seamless Data Distribution System website [61].

2.2.3. In-situ Data

In this study, two kinds of In-situ data are used. One is the Automated Meteorological Data Acquisition System (AMeDAS) data which is used in the whole study, and the other one is the Road Snow Information System (RSIS) data which is used in Chapter 4 for comparing results from the proposed method.

2.2.3.1. AMeDAS Data

Automated Meteorological Data Acquisition System (AMeDAS) snow depth is an automated measuring data. It is supersonic snow depth gauge measuring. Hourly observation data of snow depth (cm) and its maximum value among 24 hours are recorded in time. Maximum will not be recorded if one or more missing exists. The difference between observed value and previous value (one hour before) of snow depth for daily data will be accumulated if it is greater than 0 cm. The AMeDAS system operated from November 1, 1974, and currently comprises 1,300 stations (over 1,100 are unmanned operation) throughout Japan, with an average separation of 17 km. For about 280 stations (manned or unmanned) located in the areas with heavy snowfall, their snow depth has also been observed [62].

Table 2.4: The latitude, longitude and altitude of 13 observation stations.

Stations	Latitude (N)		Longitude (E)		Altitude (m)
	Degree	Minute	Degree	Minute	
Kazuno	40	12.9	140	47.2	123
Yunodai	38	57.6	140	31.7	335
Aniai	39	59.6	140	24.2	120
Noshiro	40	11.9	140	1.9	6
Akita	39	43	140	5.9	6
Honjo	39	21.6	140	3.3	11
Takanosu	40	13.6	140	22.3	29
Kakunodate	39	36.2	140	33.4	56
Yokote	39	19.2	140	33.3	59
Yuzawa	39	11.2	140	27.8	74
Gojome	39	56.3	140	6.9	6
Yashima	39	14.1	140	8.2	46
Taishouji	39	31.6	140	14	20

Akita Local Meteorological Observatory started the operation of AMeDAS from

1974. And so far, there are 36 observation stations which are being carried out in the whole prefecture [63].

In this study, AMeDAS snow depth data was used to make the objective fact judgment and compared with the results of proposed method. 13 observation stations have been selected in this study, which are Kazuno, Yunodai, Aniai, Noshiro, Akita, Honjo, Takanosu, Kakunodate, Yokote, Yuzawa, Gojome, Yashima and Taishouji.

Table 2.4 shows the latitude and longitude coordinates and altitude of 13 observation stations for the snow depth observation in Akita Prefecture, and Figure 2.5 shows the space geographic distributions of 13 observation stations in Akita Prefecture. AMeDAS snow depth data were obtained from Japan Meteorological Agency website [64].

2.2.3.2. RSIS Data

Road Snow Information System (RSIS) is also an automated measured observation network developed by the Akita Construction Department Road Division used for gathering snow depth and snowfall data on the road surface and outside of the road across the entire Akita prefecture. In this system, snowfall sensor, frozen road detection sensor and workstation are combined online, and then snowfall and freezing information are collected in real-time. It is intended to give information for timely snow removal, anti-freezing agent spraying, and optimization and faster on the road surface management in winter. RSIS was operated in 1996, and currently comprises 31 observation stations throughout the whole Akita prefecture [65]. It can record hourly observation data (cm) of snow depth over 24 hour periods.

In this work, in order to evaluate the effectivity of the proposed method for the snow cover detection results, RSIS snow depth data from the 25 observation stations which can provide the long time and continuous observation record data obtained from the Akita Construction Department Road Division are selected in Chapter 4.

2.3. Initial Processing Steps

The preprocessing of satellite remote sensing images is necessary for the further snow detection. It can be mainly divided into four steps: geographic correction, study area clipping, atmospheric correction and topographic correction (the sequence is different according to atmospheric correction method).

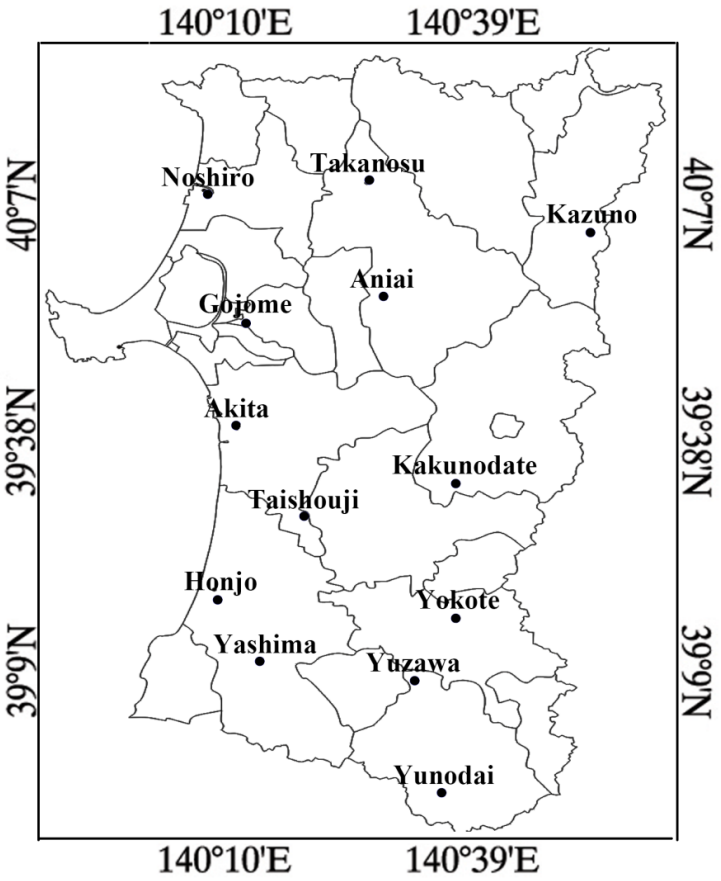

Figure 2.5: The space geographic distributions of 13 observation stations.

2.3.1. Geographic Correction

In order to remove internal and external distortions and precisely identify the location of each pixel on the earth, the MODIS Swath Reprojection Tool (MRT Swath) is applied for geographic correction of image [66]. The MRT Swath was developed by the Land Processes Distributed Active Archive Center (LP DAAC) for MODIS Level 1B products and Level 2 land product data. It is available from the website of LP DAAC in USGS [67]. The MODIS Level 1B Geolocation file is used since all the projections require the corresponding additional inputs. Hence, the MODIS Geolocation Dataset (MOD03) is also used here. During this process, the format type of the output file is GeoTIFF, the resampling type is nearest neighbor, the projection type is geographic, and the output pixel size is 0.0045 degree at 500 m spatial resolution [66].

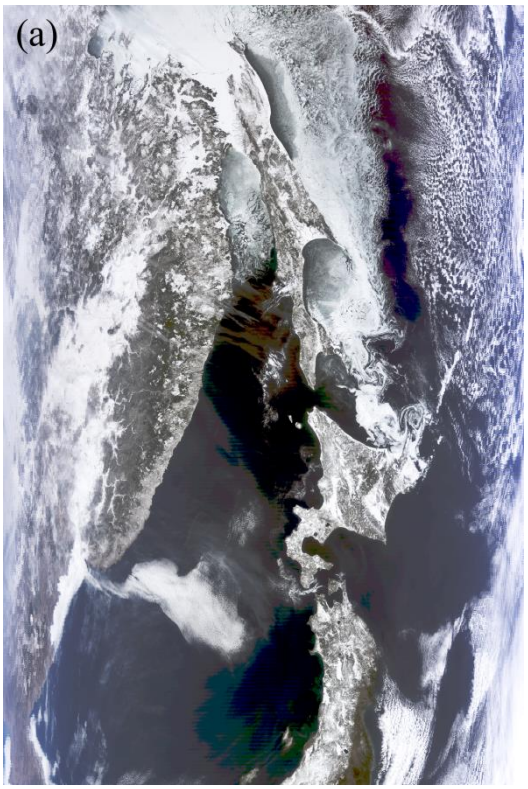

Figure 2.6 (a): Images of before geographic correction on the February 22, 2011.

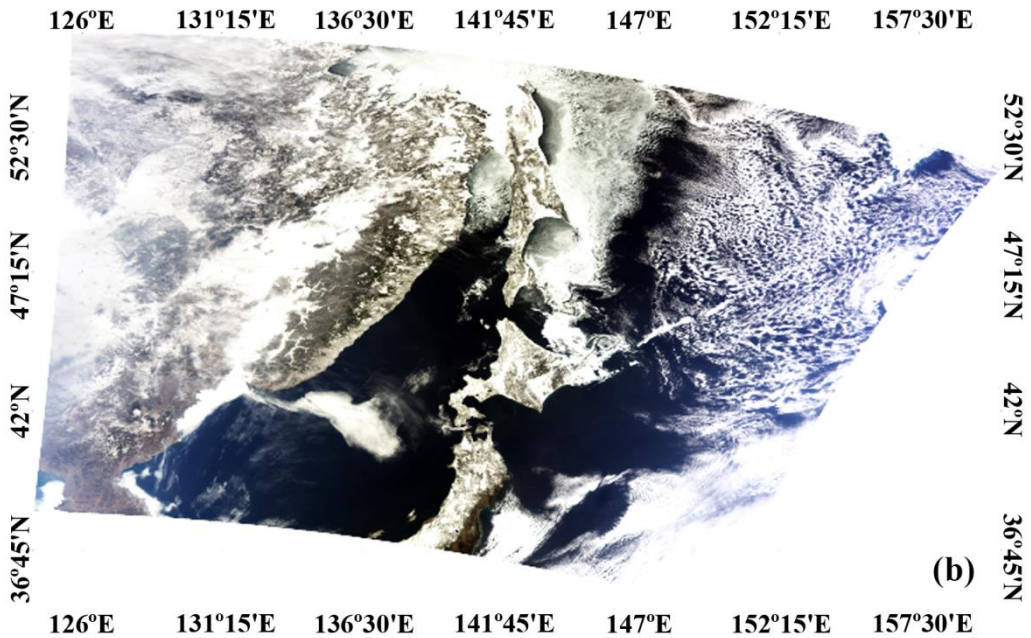

Figure 2.6 (b): Images of after geographic correction on the February 22, 2011.

Figure 2.6 (a) and (b) show the comparison images of before (a) and after (b) geographic correction. From these figures, we can know that each pixels of image have geographic coordinates such as latitude and longitude information by geographic correction. This is the foundation for the study area clipping.

2.3.2. Study Area Clipping

The administrative regional boundaries of Akita Prefecture are used to clip the acquired image in order to remove those areas that do not belong to the Akita Prefecture and decrease the number of calculations necessary. Copyright for this information belongs to the Esri Japan Corporation, and can be obtained from the ShapeFile Library website [68].

2.3.3. Atmospheric Correction

The MODIS Level 1B product has been calibrated, yet its reflectance only represents the apparent surface reflectance at the top of atmosphere and not the real ground surface reflectance. A considerable amount of water vapor, carbon dioxide, ash, and smoke dust can lead to atmosphere scattering and absorbance, which are the primary factors responsible for generating error in snow cover detection. To eliminate these errors, the MODIS image should be atmospherically corrected to return real ground surface reflectance of the target area [69], [70], [71], [72]. In this work, the CREFL_SPA software and 6S Code method were used for the atmospheric correction.

2.3.3.1 CREFL_SPA

The CREFL_SPA is an Open Source software package which is provided by NASA. The algorithm is based on the 6S Radiative Transfer Model and could perform a simple atmospheric correction with MODIS in visible, near-infrared, and short-wave infrared bands (bands 1 through 16). It processes MODIS Aqua and Terra Level 1B DB data to create the MODIS Level 2 Corrected Reflectance product. It corrects for molecular (Rayleigh) scattering and gaseous absorption (water vapor and ozone) using climatological values for gas contents. It requires no real-time input of ancillary data. The CREFL_SPA can be obtained from the Direct Readout Laboratory (DRL) website [73].

Figure 2.7 (a) and (b) show the comparison images of before and after atmospheric

correction. (a) is the image of before atmospheric correction and (b) is the image of after atmospheric correction. From the figure, we can see that (b) is obviously clearer than (a). That is because atmospheric correction has eliminated the effect of atmosphere.

2.3.3. 6S code

In this work, the second simulation of a satellite signal in the solar spectrum (6S) code model is used for atmospheric correction in Chapter 4. The 6S code model is a basic radiative transfer (RT) code used for the calculation of Look Up Tables (LUTs) in the MODIS atmospheric correction algorithm [74], [75]. This method cannot be affected by the study target, target type, or background, and it can be used in the spectral bands of several satellite sensors because of the intrinsic combination of topography, weather, spectrum, and other parameters [76]. It can be calculated online, and is obtained from the website of the MODIS land surface reflectance science computing facility, 6S Vector Code [77].

Table 2.8 (in Chapter 4.3) presents the parameters of the 6S code atmospheric correction with MODIS images from the Terra satellite, acquired on April 6, 2011. From Table 2.8, it can be seen that the 6S code atmospheric correction includes geometrical conditions, an atmospheric model, target and sensor altitudes, spectral conditions, and ground reflectance and signal. For these, the date for the geometrical conditions is obtained from the satellite image file name. Solar and sensor zenithal and azimuthal angles are the average values for the study area as calculated from MOD03. According to the manual of the 6S code atmospheric correction, a study area image acquired on April 6 belongs to mid latitude winter. For the aerosol models, “Rural,” “Urban” and “Tropospheric” are usually used to represent small, large, and very small amounts of atmospheric aerosols, respectively.

“Maritime” is usually used to represent the effects at the border of continents and oceans. In this work, “Maritime” is chosen because Akita Prefecture is located on the border of the continent and the ocean. Visibility is obtained from the Sendai Aviation Weather Station Akita Airport Branch of JMA, and was 20 km at the time of MODIS image acquisition. The target altitude is the average altitude of the 36 AMeDAS observation stations in Akita Prefecture.

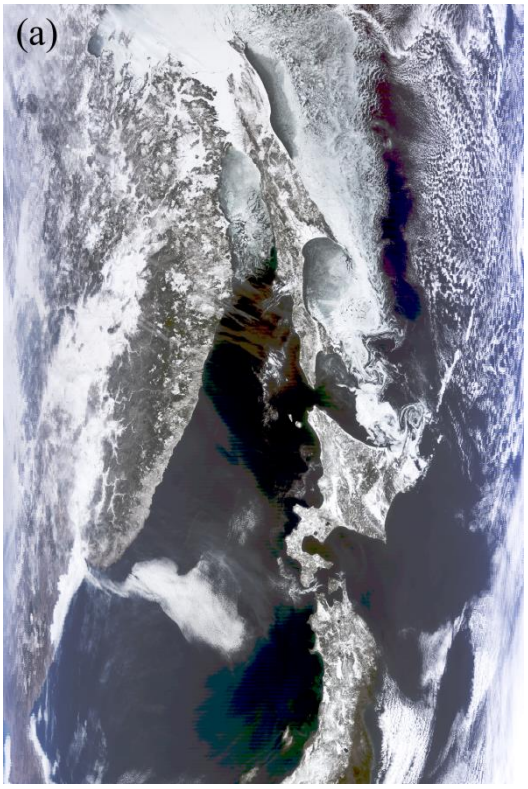

Figure 2.7 (a): Comparison images of before atmospheric correction.

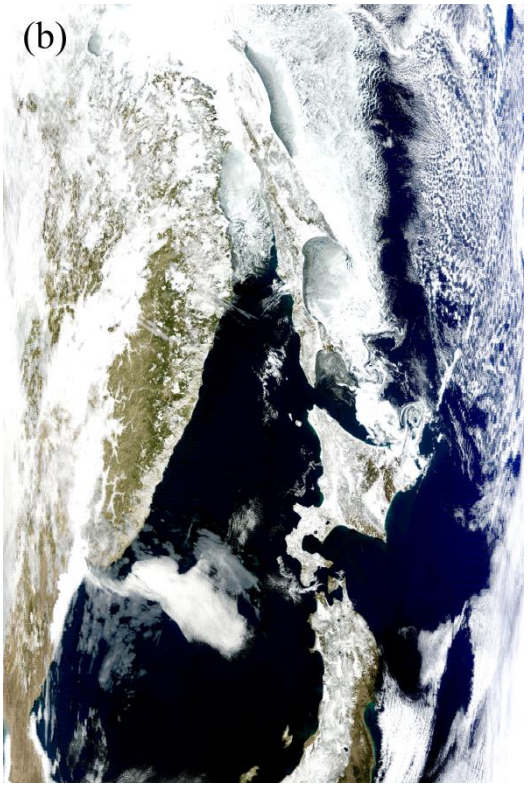

Figure 2.7 (b): Comparison images of after atmospheric correction.

Table 2.8 (in Chapter 4.3)Parameters of the 6S code atmospheric correction.

Parameter Name		Input Parameter
Geometrical Conditions (User's)	Month	4
	Day	6
	Solar Zenithal Angle	40.91
	Solar Azimuthal Angle	143.73
	Sensor Zenithal Angle	43.00
	Sensor Azimuthal Angle	-96.49
Atmospherical Model	Atmospheric Profile	Mid latitude Winter
	Aerosol Model	Maritime Model
	Visibility (km)	20
Target & Sensor Altitude	Target Altitude (km)	-0.097
	Sensor Altitude	(-1000) Satellite Level
Spectral Conditions	Bands (μm)	MODIS Band 1 (0.6100 to 0.6850)
		MODIS Band 3 (0.4500 to 0.4825)
		MODIS Band 6 (1.6000 to 1.6650)
		MODIS Band 7 (2.0575 to 2.1825)
Ground Reflectance	Ground Reflectance Type	Homogeneous Surface
	Directional Effects	Directional Effects
	Specify Surface Reflectance	MODIS operational BRDF
Signal	Atmospheric Correction Mode	Atmospheric Correction with BRDF

For the spectral condition, MODIS bands 1, 3, 6, and 7 are selected as they represent the bands that need to be corrected with this method. As over 70% of the area of Akita Prefecture is covered by forests, there may be considerable impact from the bidirectional reflectance distribution function (BRDF) during the process of snow cover detection using MODIS images. Therefore, in order to eliminate the impact of BRDF to the greatest possible extent, the ground reflectance type of the study area is assumed to be a homogeneous surface, with the existence of directional effects.

Next, the MODIS operational BRDF is selected and input weights are chosen for the Lambertian kernel, Ross Thick kernel, and Li Sparse kernel as 0.5, 0.5, and 0.5, respectively. Atmospheric correction with BRDF is selected for the atmospheric correction model. Finally, atmospheric correction coefficients x_a, x_b, and x_c are

obtained for the calculation of the real surface reflectance, using Equations (1) and (2):

$$y = x_a \times (measured\ radiance) - x_b \quad (1)$$

$$acr = y / (1 + x_c \times y) \quad (2)$$

where *measured radiance* is the apparent surface reflectance and *acr* is the real ground surface reflectance.

Table 2.9 (in Chapter 4.2): The parameters of the 6S code atmospheric correction.

Parameter Items		Parameter Values
Geometrical Conditions (User's)	Month	4
	Day	2
	Solar Zenithal Angle	42.513333
	Solar Azimuthal Angle	141.155259
	Sensor Zenithal Angle	50.785289
	Sensor Azimuthal Angle	95.193096
Atmospherical Model	Atmospheric Profile	Midlatitude Winter
	Aerosol Model	Maritime Model
	Visibility (km)	20
Target & Sensor Altitude	Target Altitude (km)	-0.097
	Sensor Altitude	(-1000) Satellite Level
Spectral Conditions	Spectral Conditions	MODIS Band 1
		MODIS Band 3
Ground Reflectance	Ground Reflectance Type	Homogeneous Surface
	Directional Effects	Directional Effects
	Specify Surface Reflectance	MODIS operational BRDF
Signal	Atmospheric Correction Mode	Atmospheric Correction with BRDF

Table 2.9 (in Chapter 4.2) lists the detailed parameters of the 6S code atmospheric correction with MODIS images from the Terra satellite acquired on April 2, 2014, 10:00 AM (Japan Standard Time (JST)).

2.3.4. Topographic Correction

The study area Akita prefecture is a mountainous region with rugged terrain. Changes in reflected brightness can be caused by irregular topography from the 70% forest and mountain coverage of Akita Prefecture. Therefore, this phenomenon can lead to inconsistent reflectances from similar or identical ground surface features, resulting in reduced accuracy in remote sensing image classification. Thus, topographic correction is conducted on the image data in order to improve the image classification and accuracy of snow cover detection.

Many methods and algorithms have been proposed for topographic correction, including ratio algorithms [78], the cosine correction method [79], and the image processing workbench method [80]. These algorithms are able to eliminate the topographic effect only partly in the study area because the radiation changes caused by the terrain are not simple or constant and can show frequent fluctuations. Every pixel in the MODIS image may include a number of different terrain shadows, slopes, aspects, and other small interactions [81]. Thus, it is difficult to fully correct for the topography with such a physical-based approach [82], [83], [84], [85]. In this study, a shadowing function algorithm developed by Hapke [83] is adopted to reduce topographic effects across the Akita region. This is based on the following four assumptions: (1) all relevant objects are large compared to the wavelength of light so that geometric optics apply; (2) the mean slope of the rough surface is assumed to be reasonably small; (3) multiple scatterings of light from one macroscopic surface facet to another are neglected; and (4) the surface is made of facets titled at a variety of angles that have no preferred direction in the azimuth, but whose zenith angle can be described by a Gaussian distribution [83].

Given a Gaussian surface with an average slope $\bar{\theta}$, the Hapke shadowing function [83] can be expressed in two separate cases: (1) $\theta_0 < \theta$ and (2) $\theta_0 \geq \theta$, where θ_0 and θ are the solar zenith angle and the viewing zenith angle, respectively.

When $\theta_0 < \theta$,

$$S(\mu_0, \mu) = \frac{\mu_e(\xi)}{\mu_e(0)} \frac{\mu_0}{\mu_{0e}(0)} \frac{\chi(\bar{\theta})}{1 - f(\xi) + f(\xi)\chi(\bar{\theta})\left[\mu_0 / \mu_{0e}(0)\right]}, \quad (3)$$

$$\mu_{0e}(\xi) = \chi(\bar{\theta})\left[\mu_0 + \sqrt{1-\mu_0^2}\tan(\bar{\theta}) \times \frac{\cos(\xi)E_2(\theta) + \sin^2(\xi/2)E_2(\theta_0)}{2 - E_1(\theta) - \xi/\pi E_1(\theta_0)}\right], \text{and} \quad (4)$$

$$\mu_e(\xi) = \chi(\bar{\theta})\left[\mu + \sqrt{1-\mu^2}\tan(\bar{\theta}) \times \frac{E_2(\theta) - \sin^2(\xi/2)E_2(\theta_0)}{2 - E_1(\theta) - \xi/\pi E_1(\theta_0)}\right], \quad (5)$$

When $\theta_0 \geq \theta$,

$$S(\mu_0, \mu) = \frac{\mu_e(\xi)}{\mu_e(0)} \frac{\omega_0}{\mu_{0e}(0)} \frac{\chi(\bar{\theta})}{1 - f(\xi) + f(\xi)\chi(\bar{\theta})\left[\mu_0 / \mu_e(0)\right]}, \quad (6)$$

$$\mu_e(\xi) = \chi(\bar{\theta})\left[\mu + \sqrt{1-\mu^2}\tan(\bar{\theta}) \times \frac{\cos(\xi)E_2(\theta_0) + \sin^2(\xi/2)E_2(\theta)}{2 - E_1(\theta_0) - \xi/\pi E_1(\theta)}\right], \text{ and} \quad (7)$$

$$\mu_{0e}(\xi) = \chi(\bar{\theta})\left[\mu_0 + \sqrt{1-\mu_0^2}\tan(\bar{\theta}) \times \frac{E_2(\theta_0) - \sin^2(\xi/2)E_2(\theta)}{2 - E_1(\theta_0) - \xi/\pi E_1(\theta)}\right], \quad (8)$$

Where,

$$\chi(\bar{\theta}) = \frac{1}{\sqrt{1 + \pi\tan^2(\bar{\theta})}}, \quad (9)$$

$$E_1(\chi) = \exp\left(-\frac{2}{\pi}\cot(\bar{\theta})\cot(\chi)\right), \quad (10)$$

$$E_2(\chi) = \exp\left(-\frac{1}{\pi}\cot^2(\bar{\theta})\cot^2(\chi)\right), \quad (11)$$

$$f(\xi) = \exp(-2\tan(\xi/2)), \quad (12)$$

and ξ is the phase angle.

The mean slope angle $\bar{\theta}$ is defined by

$$\tan(\bar{\theta}) = \frac{2}{\pi}\int_0^{\pi/2} \alpha(\xi)\tan(\xi)d\xi\,, \tag{13}$$

where $\alpha(\xi)$ is the normalized slope distribution function.

Dubayah [82] has a related effective or apparent reflectance to true reflectance using topographic factors as follows:

$$r_R(\Omega_0,\Omega) = r(\Omega_{0e},\Omega_e)S(\Omega_0,\Omega)\,, \tag{14}$$

where $r_R(\Omega_0,\Omega)$ is the effective or apparent reflectance and $r(\Omega_{0e},\Omega_e)$ is the true reflectance. Ω_0 and Ω are the solid angles denoting the illumination direction and viewing direction, respectively. Ω_{0e} and Ω_e are the equivalent angles of Ω_0 and Ω considering roughness effects. $S(\Omega_0,\Omega)$ is the shadowing function.

Before the topographic correction, the SRTM 90 m DEM data are conducted to be resampled by the geographic projection and cut with the administrative regional boundary ShapeFile data of Akita prefecture at 500 m resolution. Then, image registration in pixel level is conducted for matching the study area image. Finished the all above steps, the obtained SRTM 90 m DEM data are applied for topographic correction.

Chapter 3
Snow Cover Detection via Normalized Difference Indexes

3.1 Introduction

The Normalized Difference Snow Index (NDSI) as a snow detection method has aroused more and more attention, and its feasibility has been proved by several reporters. However, the accuracy of NDSI alone has failed to meet the expected requirement. The snow cover detection is not only affected by the atmosphere, but also influenced by the regional terrain and the underlying surface covered by snow. Due to this reason, in section 3.2, the snow detection in Akita Prefecture located in the Tohoku region of Japan was conducted through the combination of NDSI and NDVI (Normalized Difference Vegetation Index). Because of the large area of mountains and forests in the rugged Akita Prefecture region, the surface reflectance was retrieved from the top of vegetation after atmospheric and topographic corrections. Furthermore, in order to reduce the effect of the misclassification of snow and vegetation cover, a Normalized Difference Vegetation Index (NDVI) model was used to discriminate the snow and forest pixels. Compared to the MOD10_L2 data and NDSI alone results, the combination of NDSI and NDVI showed high accuracy in snow cover detection.

In addition, during the process of the forest and non-forest region classification, GIS forest region data is always used to discriminate forest region usually [86]. Therefore, in section 3.3, GIS forest region data and the NDVI are adopted for the forest area discrimination based on Terra/MODIS data and natural and geographic situation of the Tohoku region. The whole work is conducted in the environment of the Interface Definition Language (IDL). During the forest area discrimination, the GIS forest region data and the NDVI are input and calculated. Then, we investigate image comparisons between GIS forest region data and the NDVI forest area discrimination. The results of snow cover detection without the forest area discrimination and with GIS forest region data and the NDVI for the forest area discrimination are also compared from December 2013 to April 2014.

3.2 Snow Cover Detection via NDSI and NDVI

3.2.1 Methodology

In this study, data MOD02HKM (MODIS/Terra Calibrated Radiances 5-Min L1B Swath 500m Collection 4 and 5 product data), MOD03-Geolocation (MODIS geolocation product), MOD10_L2 (The MODIS/Terra Snow Cover 5-Min L2 Swath 500m data set), AMeDAS snow depth, DEM and geographic coordinates data of 13 observation stations were applied for the snow detection in Akita Prefecture. In addition, ShapeFile (Region boundary and regional mesh of Akita Prefecture) data were used to cut the image into the study area shape. Its copyright belongs to the Esri Japan Corporation, and the data can be obtained from ShapeFile library website [68]. Image photography time is from December 2010 to April 2011. And the process flowchart is shown in Figure 3.1.

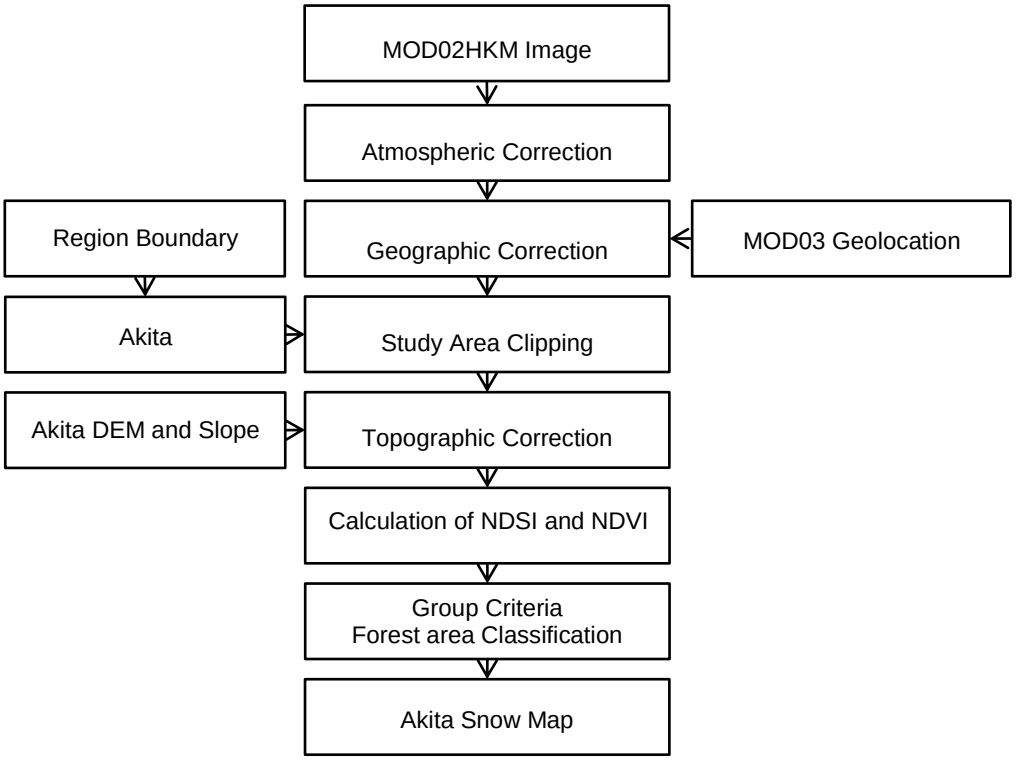

Figure 3.1: the flowchart of snow cover detection

In this work, the preprocessing steps including geographic correction, study area

clipping, atmospheric correction and topographic correction are completed as shown in Figure 3.1. And the detailed information is shown in the chapter 2.

3.2.2. NDSI

The NDSI (Normalized Difference Snow Index) is useful for the detection of snow and separating snow pixels from most clouds. Principle is mainly based on the fact that snow is considerably more reflective in the visible than in the short wave Infrared (SWIR) part of the spectrum, and the reflectance of most clouds remains high in the short wave Infrared (SWIR), while the reflectance of snow is low [87], [88]. As the NDSI does not depend on the reflectance in a single band, and is insensitive to a wide range of illumination conditions [56]. Hence, it can partially normalize atmospheric effects.

The $NDSI$ was calculated with the following formula:

$$NDSI = (band_4 - band_6)/(band_4 + band_6) \quad (15)$$

In which $band_4$ and $band_6$ represent the reflectance value of band 4 and band 6 of MODIS.

3.2.3. NDVI

The NDVI (Normalized Difference Vegetation Index) is an index using Near Infrared (NIR) and red (R) channel ratio to reflect the plant growth status and spatial distribution of vegetation density. As it has advantages of high vegetation detection sensitivity and wide range of the vegetation coverage detection, hence can eliminate the shadow of the Terrain and community structure and weaken the noise which was produced by solar altitude and atmosphere and radiated interference [89]. Thus, $NDVI$ can reflect the background impact of plant canopy.

The $NDVI$ was calculated with following formula:

$$NDVI = (band_2 - band_1)/(band_1 + band_2) \quad (16)$$

In which $band_1$ and $band_2$ represent the reflectance value of band 1 and band 2 of MODIS.

3.2.4. Snow Cover Detection with NDSI

In generally, when 50% or more of the areas are covered with snow, the threshold value of $NDSI$ is 0.4. This value is obtained from TM images and has been proved in the area of Sierra Nevada, California [21]. However, the selection of the threshold value for $NDSI$ is different as the area and time difference, and the range is between from 0.2 to 0.5. In this study, the threshold value of $NDSI$ was selected as 0.45 (The average value of $NDSI$ images in the whole study area during the period of December 2010 to April 2010) by the repeated tests and the comparison of multi-temporal images.

When the value of $NDSI$ is larger than 0.45, the extracted substances are the mixture of snow and water. In order to extract the snow from the water, we decided to use the reflectance value of $band_2$ which is larger than 0.11 to extract the snow from the water. Meanwhile, using the reflectance value of $band_4$ which is larger than 0.10 to eliminate pixels which are not snow but the values of $NDSI$ are also larger than 0.453.

However, if the snow cover was detected just with the $NDSI$ value as 0.45, the reflectance of underlying surface will be ignored. As a result, the accuracy of snow detection was decreased because of the no detection for the snow pixels when the $NDSI$ values are below 0.45. The spectrum reflectance of snow itself and the influence of underlying surface on the changes of snow reflectance should be considered in order to improve the accuracy of snow detection.

3.2.5. Relation of the snow reflectance and snow depth

Most of researchers have found that the snow reflectance can be affected by snow depth. Figure 3.2 shows the changing curve of the fine snow reflectance with different snow depth. The wavelength is 555 nm. From the figure, we can see that the reflectance of snow increases with increasing of the snow depth when it is below 30 cm. The reflectance is toward stability after the snow depth over 30 cm. It indicates

that the reflectance of pure snow is a little higher than no pure snow.

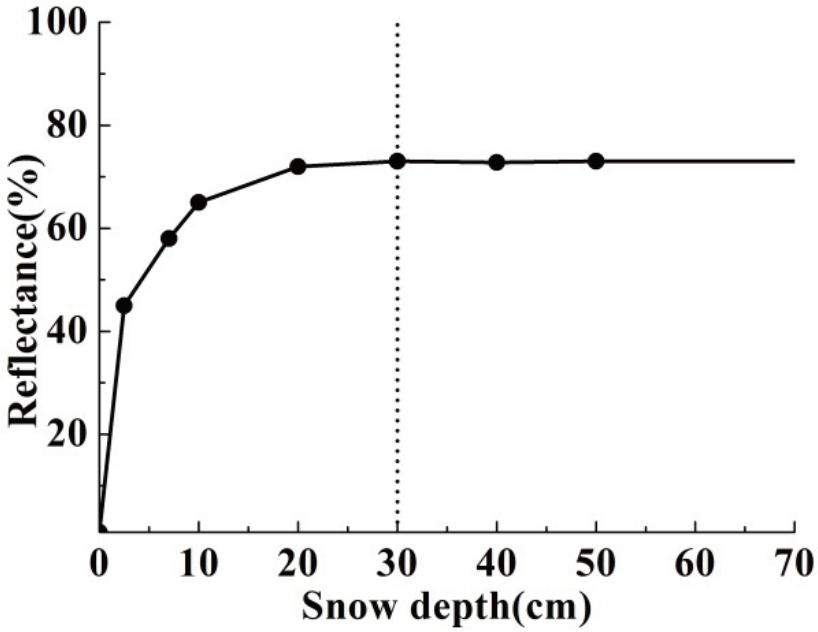

Figure 3.2: The relation curve of the snow reflectance and snow depth.

In other words, when the depth of snow covered on other surfaces is equal or over than 30 cm, we suppose that the reflectance obtained by satellite sensor is the reflectance of pure snow, the pixel on image is pure representing snow only. Otherwise, the pixel is mixed representing snow and other features.

3.2.6. Discussion for the combination of NDVI and NDSI

In Akita prefecture, the strong wind in winter blows snow from the coast to inland mountain area, thus the accumulation of snow on the ground is relatively small (generally less than 30 cm). Most of the regions are in heavy snow areas, snow depth is over 100 cm. From the 13 observation stations, we can find that Noshiro, Akita and Honjo are located at coastal regions, while the others are located in the mountain areas and basin areas. As mountain areas are covered by forests which are coniferous trees (54.71%) and deciduous broad-leaved trees (41.48%), thus snow will not stack on top of the trees and leaves, but fall to the root parts of the trees and will be concealed by the forest. Image pixels reflect the spectrum of the mixture of snow and forests at this moment. Therefore, the underlying surface covered by snow in Akita prefecture can

be attributed to the forests.

In order to discriminate and extract the pixels of forests, the NDVI was used to identify and classify the pixels of study areas on February 22, 2011. Figure 3.3 shows NDVI image and forests classification image of the study area. (a) is the grayscale image of NDVI in study area; (b) is the binary image of forests classification in study area, white represents forest and black represents non-forest. From (a), we can see that the value of NDVI is from -1 to 1. The minus values indicate cloud, water, snow and so on due to their high reflectivity in the visible light range. 0 indicates rock and soil, because the values are analogously equal in NIR and R range.

When NDVI is larger than 0, it indicates vegetation, and the values of NDVI increase with the vegetation coverage. The snow depth of Akita is over 30 cm in winter, most of the vegetation are covered by snow except the ever green vegetation such as forests (mainly are coniferous and deciduous broad-leaved trees). So the discriminated pixels of vegetation belong to forests. In this study, when NDVI is larger than 0.2, we think that the ground coverage are forests in study area after repeated tests as shown in (b).

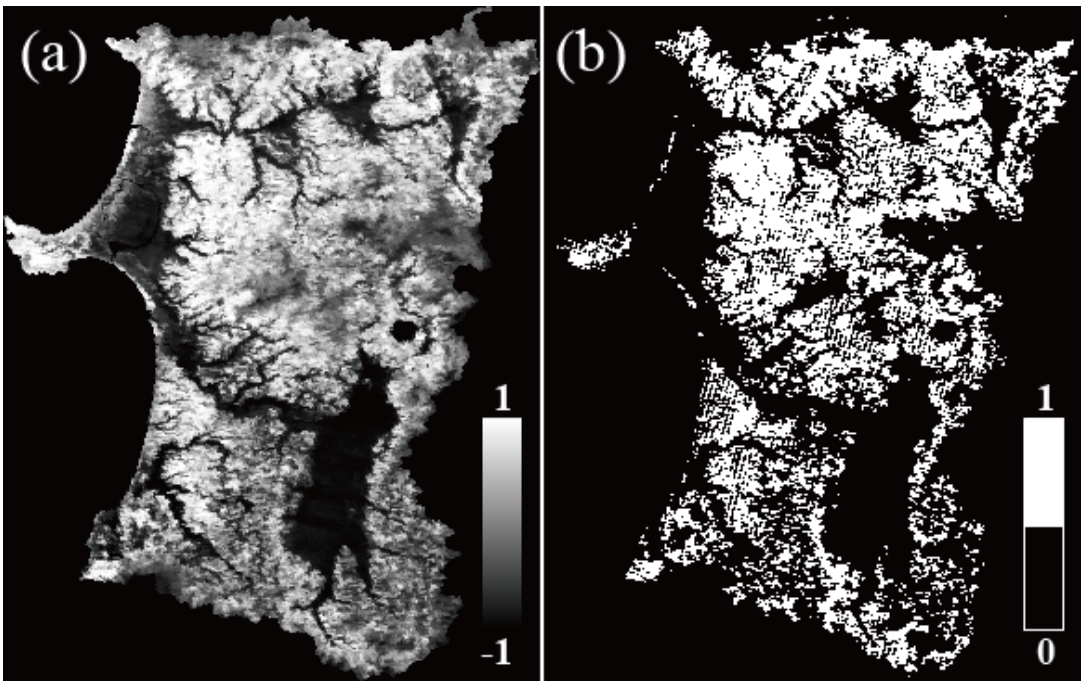

Figure 3.3: Images of before and after forests classification.

Table 3.4: The snow detection results from AMeDAS (I), MOD10_L2 (II), NDSI (III) and the combination of NDVI and NDSI (IV).

Stations	12/1/2010				12/17/2010				1/27/2011				2/15/2011				2/22/2011				2/28/2011				3/9/2011				3/19/2011				3/28/2011				4/6/2011			
	I	II	III	IV	I	II	III	IV	I	II	III	IV	I	II	III	IV	I	II	III	IV	I	II	III	IV	I	II	III	IV	I	II	III	IV	I	II	III	IV	I	II	III	IV
Kazuno	6	1	1	1	8	1	1	1	74	1	1	1	73	1	1	1	61	1	1	1	45	1	1	1	52	1	1	1	38	1	1	1	23	1	1	1	0	0	0	0
Yunodai	0	1	0	0	15	1	1	1	155	1	1	1	138	1	1	1	120	1	1	1	107	1	1	1	123	1	1	1	124	1	1	1	117	1	1	1	84	1	1	1
Aniai	1	1	1	1	13	1	1	1	123	1	1	1	105	1	1	1	94	0	1	1	79	1	1	1	96	1	1	1	91	1	1	1	89	1	1	1	1	1	1	1
Noshiro	0	1	0	0	8	0	1	1	26	1	1	1	18	1	1	1	0	1	1	0	0	1	0	0	0	1	1	1	0	0	1	1	0	0	1	1	0	0	0	0
Akita	0	0	1	1	8	1	1	1	32	1	1	1	28	1	1	1	11	1	1	1	0	0	0	0	3	1	1	1	6	0	0	0	13	1	1	1	0	0	0	0
Honjo	0	1	0	0	7	1	1	1	57	1	1	1	52	1	1	1	32	1	1	1	14	1	1	1	0	1	1	1	0	1	0	0	6	1	1	1	0	1	0	0
Takanosu	1	1	1	1	7	0	1	1	66	0	1	1	64	1	1	1	51	1	1	1	38	1	1	1	47	1	1	1	28	1	1	1	3	0	1	1	0	1	0	0
Kakunodate	0	0	1	0	5	1	0	1	89	0	1	1	92	1	1	1	74	0	1	1	62	1	1	1	69	1	1	1	66	1	1	1	54	1	1	1	5	1	1	1
Yokote	2	1	1	1	21	1	1	1	136	1	1	1	133	1	1	1	115	1	0	1	91	1	1	1	103	1	1	1	91	1	1	1	72	1	1	1	18	1	1	1
Yuzawa	0	0	0	0	24	1	1	1	144	1	1	1	130	1	1	1	112	1	1	1	98	1	1	1	111	1	1	1	105	1	1	1	101	1	1	1	64	1	1	1
Gojome	0	0	1	1	5	1	1	1	49	1	1	1	36	1	1	1	23	1	1	1	5	1	0	1	0	1	1	0	0	1	1	0	10	0	1	1	0	1	1	0
Yashima	0	0	1	0	27	1	1	1	154	1	0	1	138	1	1	1	117	1	0	1	95	1	1	1	115	1	1	1	98	1	1	1	88	1	1	1	40	1	1	1
Taishouji	0	0	1	0	14	1	1	1	79	1	1	1	94	1	1	1	72	1	1	1	63	1	1	1	73	1	1	1	60	1	1	1	43	1	0	1	0	0	1	0

Note:

I: Records of Snow Depth (cm) from AMeDAS II: Results from MOD10_L2 III: Results from NDSI IV: Results from NDVI and NDSI

"0": Snow Free "1": Snow Covered

For the snow detection in forests, the NDSI threshold value was decreased to 0.38, which was the minus of NDSI average value and standard deviation. Therefore, through the combination of NDVI and NDSI, we can distinguish the mixed pixels in forest areas of Akita Prefecture, so as to improve the accuracy of snow detection.

Table 3.4 shows the comparison results of the AMeDAS data, MOD10_L2 product, NDSI alone data and the proposed method for detecting snow in study area from December 2010 to April 2011. We divided the 13 observation stations into 3 types according to their positions for accuracy comparison, including mountain areas (Kazuno, Yunodai, Aniai, Yashima and Taishoji), plain areas (Noshiro, Akita, Honjo and Gojome) and basin areas (Takanosu, Kakunodate, Yokote and Yuzawa).

In the Table, I shows the records of the AMeDAS snow depth. II shows the results from MOD10_L2 products, III shows the results from NDSI, and IV shows the results from the combination of NDVI and NDSI. Meanwhile, "1"represents snow covered and "0"represents snow free. From the table, we can know that their average accuracy for detecting snow are respectively 98% (II), 88% (III) and 100% (IV) in mountain areas, 65% (II), 70% (III) and 85% (IV) in plain areas, 85% (II), 92.5% (III) and 100% (IV) in basin areas. In addition, the average accuracy by time is respectively 83.06% (II), 83.83% (III) and 94.61% (IV).

We used the final results of snow detection as examples to analyze the mistake judgement of snow cover detection on February 22, 2011 as shown in Figure 3.5. (a) is the results from MOD10_L2 product, (b) is NDSI alone results and (c) is the results from proposed method. From Table 3.4, we can find that the final results of using above 3 methods for snow detection are different at Aniai, Noshiro, Kakunodate, Yokote and Yashima observation stations.

The snow depth record is 0 cm in Noshiro from AMeDAS snow depth records on February 22, 2011. However, there are snow covered according to the results of (a) and (b), while there is no snow covered in (c). It might due to the Noshiro observation station is located near the coast. The snow is blown away by the strong sea wind. Hence, there is no snow in Noshiro observation station.

At Yashima and Aniai observation stations, the AMeDAS snow depth records are 117 cm and 94 cm respectively. However, there is snow covered according to (a) and (c), while there is no snow covered according to (b) in Yashima observation station. And there is no snow covered according to (a), while there is snow covered according

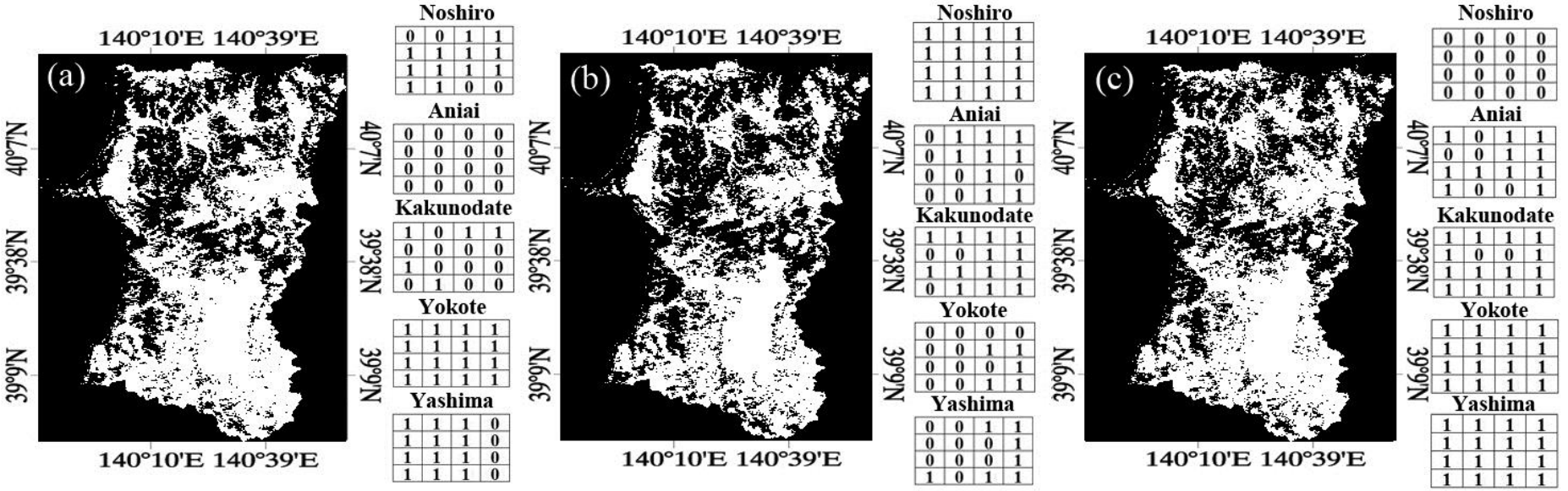

Figure 3.5: The final results of snow detection with II, III and IV.

to (b) and (c) in Aniai observation station. Analyzing the reasons, we think that due to these two observation stations are located in the mountain areas, the snow pixels are covered with forests, therefore error detections are caused. In Yokote and Kakunodate observation stations, the AMeDAS snow depth records are respectively 115 cm and 74 cm. However, there are snow covered according to (a) and (c), while there is no snow covered according to (b) in Yokote observation station. And there is no snow covered according to (a), while there is snow covered according to (b) and (c) in Kakunodate observation station. Both method II and III appear error detections. Because the Yokote observation station is located in the southeast edge of the Yokote Basin and is adjacent to Mahiru Mountain, and the Kakunodate observation station is located in the northwest corner of the Yokote Basin and is adjacent to Dewa Mountain. These two stations are both located in the slope surface of the terrain. It is due to the method II is not corrected by topographic correction, and although method III is corrected by topographic correction, it is possible that pixels of above two stations are covered by forests on the MODIS images at 500 m resolution. Therefore, they are handled as pure pixels and the threshold value of NDSI is not lowered. Due to this reason, the error detections are caused. Thus, the proposed method in this study is feasible to detect snow covered in Akita Prefecture of Japan and its accuracy is higher than other two methods.

3.3. Comparison of GIS and NDVI Forest Region Discrimination on Snow Cover Detection in Tohoku Region

3.3.1. Methodology

In this work, MOD09GA (the MODIS Surface Reflectance Daily L2G Global 1 km and 500 m), MOD03-geolocation and MOD35 Cloud Mask data were used. They were obtained from the website of the Level 1 and Atmosphere Archive and Distribution System (LAADS).

The MOD09GA provides 500 m surface reflectance images in the sinusoidal projection. However, in order to match the GIS forest region data and Tohoku region administrative zone file, the MOD09GA data was geographic corrected with the MODIS Swath Reprojection Tool (MRT Swath) software obtained from LP DAAC

website [90]. MOD03-Geolocation data was used here as the auxiliary file. Then, geographic corrected data was clipped by Tohoku region administrative zone file. The calculation of Normalized Difference Snow Index (NDSI) and NDVI was conducted before the forest region discrimination. Cloud pixels were removed in study area with MOD35 cloud mask product. Finally, snow cover was detected in forest region and non-forest region to generate the results map in Tohoku region of Japan as shown in Figure 3.6.

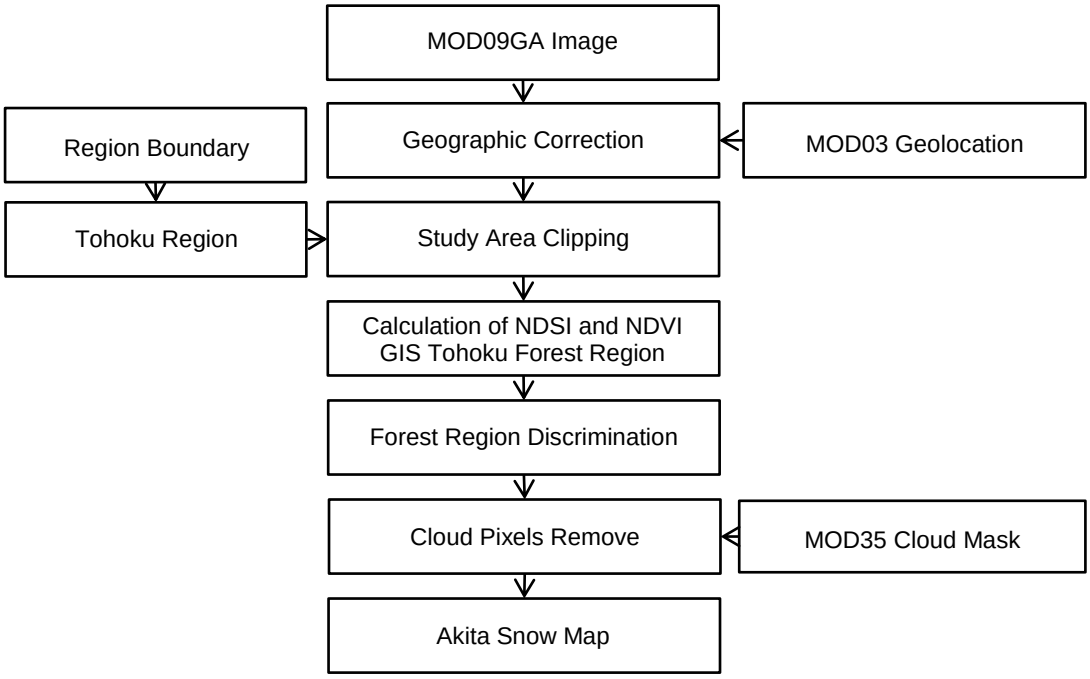

Figure 3.6: the flowchart of snow cover detection in this study.

3.3.2. The NDSI and NDVI

Snow cover of the Tohoku region was detected by the combination of $NDSI$ and $NDVI$, which were calculated with Equations (15) and (16), respectively.

Final snow cover detection results were achieved through following two groups of grouped criteria. In one group, value of $NDSI$ was greater than 0.40, $band_2$ was greater than 0.11 and $band_4$ was greater than 0.10. In the other group, value of $NDVI$ was greater than 0.35, value of $NDSI$ was greater than 0.10, $band_2$ was greater than 0.11 and $band_1$ was greater than 0.1 in forest area.

3.3.3. Forest Region Discrimination

According to the above snow cover detection criteria, we can know that the forest region discrimination was conducted by the NDVI. In order to easily compare forest area discrimination results, the GIS forest region file was used to discriminate the forest region of study area. Then, we conducted the snow cover detection through the same criteria as above without using the NDVI. Meantime, the image without the forest region discrimination was also used to conduct the snow cover detection under the criteria of the value of $NDSI$ was greater than 0.10, $band_2$ was greater than 0.11 and $band_4$ was greater than 0.10.

3.3.4. The Comparison of Forest Region Discrimination

Figure 3.7 shows the comparison images of without the forest region discrimination (a) composited by MODIS bands 1, 4 and 6, with GIS forest region data (b) and the NDVI (c) forest region discrimination on April 14, 2014. Snow has high reflectance in visible spectrum (bands 1 and 4) and low reflectance in short wave infrared (SWIR, band 6), and the reflectance of cloud is high whether in visible and SWIR or not, so the snow in (a) is displayed as yellow and that of cloud is showed nearly to white. Compared to (a), from (b), it can be seen that the whole forest area was extracted by GIS forest region data whether there are snow or not. However, only the edge forest regions were extracted by NDVI from (c), because NDVI uses near infrared (band 2) and red channel (band 1) ratio to reflect the plant growth status and spatial distribution of vegetation density, while the forest was covered by thick snow in mountains and forest center.

3.3.5. The Results Comparison of Snow Cover Detection

Figure 3.8 shows the snow cover detection results comparison of without the forest region discrimination (a), with GIS forest region data (b) and the NDVI (c) forest region discrimination on April 14, 2014. The snow cover of both (b) and (c) are much more than (a), because just the snow in mountains and forest center was detected by (a), but not in the edge areas. This is because the forest region was not extracted before snow cover detection, the snow covered by vegetation cannot be discriminated. Moreover, the snow was detected more in (b) than in (c). It is because forest region

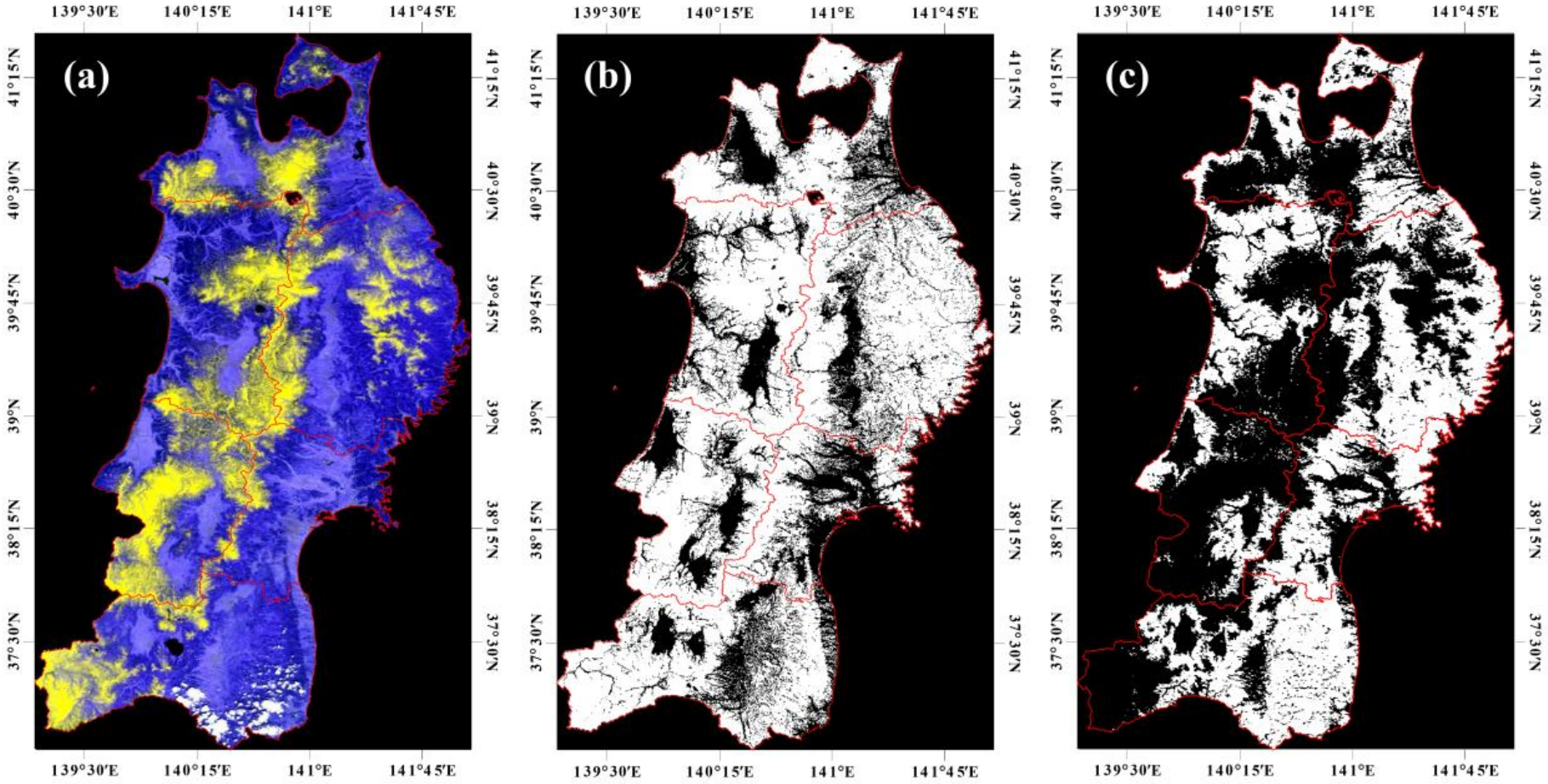

Figure 3.7 The comparison of without the forest region discrimination (a), with GIS forest region data (b) and the NDVI (c) forest region discrimination on April 14, 2014.

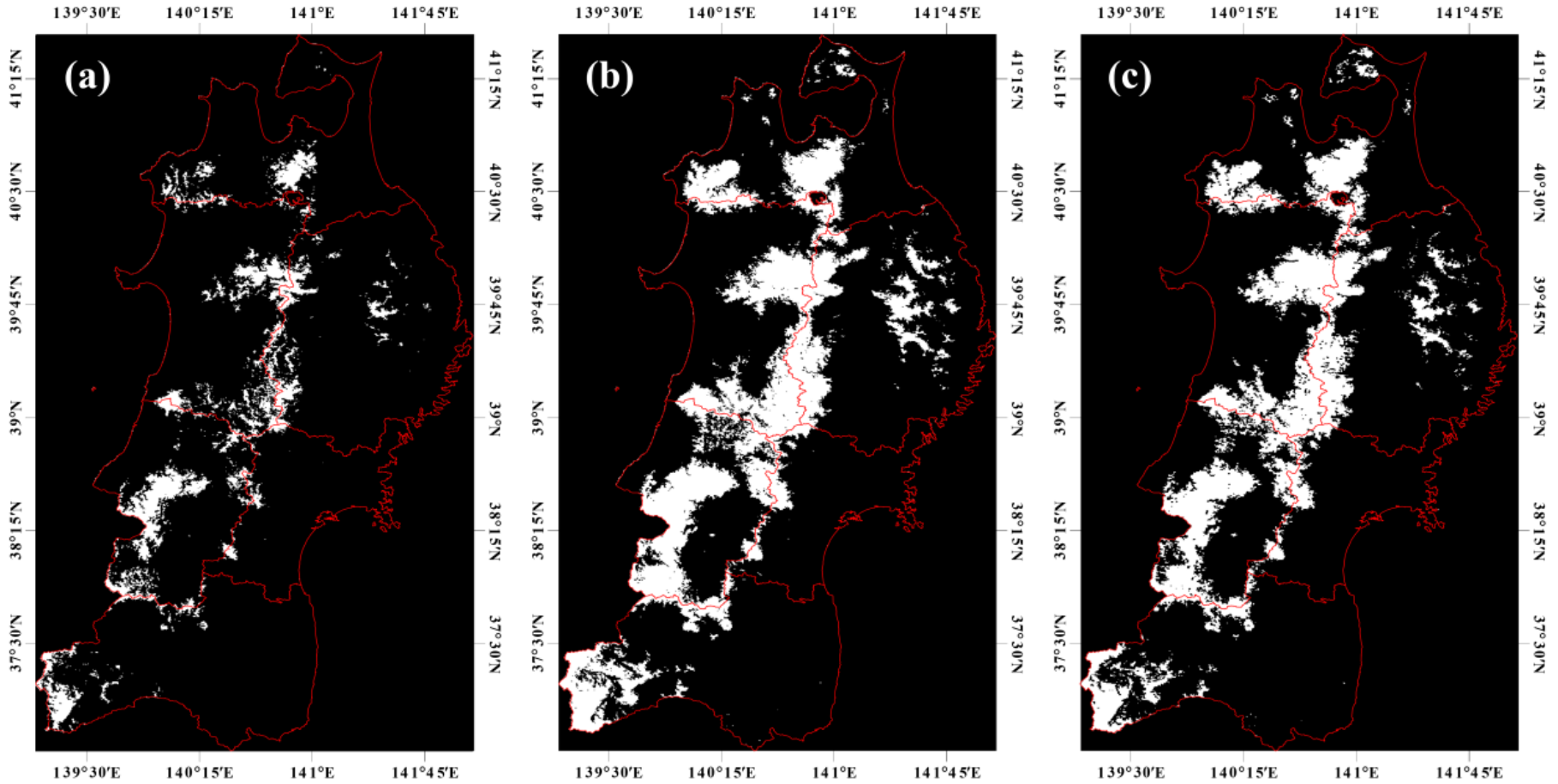

Figure 3.8: The snow cover detection results comparison of without the forest region discrimination (a), with GIS forest region data (b) and the NDVI (c) forest region discrimination on April 14, 2014.

can be detected by GIS forest region data consistent with the real distribution of forest in study area, but the threshold of NDVI is determined by the defined polygon of a scatter plot of the NDSI and NDVI indices, the error is relatively larger.

3.3.6. Assessment with AMeDAS Data

In this work, AMeDAS snow depth data was used for the objective judgment and verifying results of snow cover detection. 77 observation stations have been selected as shown in Figure 3.9.

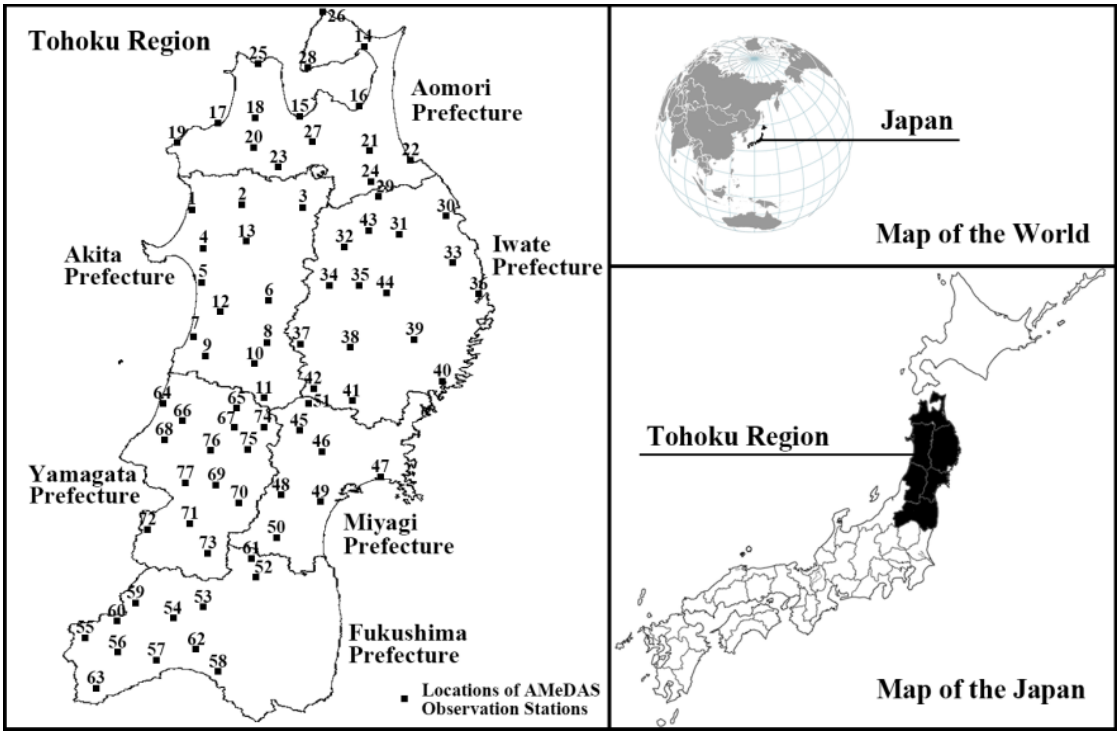

Figure 3.9: Study area of Tohoku Region, Japan and Locations of AMeDAS observation stations.

3.3.7. The Statistics Results Comparison of Snow Cover Detection

The average accuracy of snow cover detection was calculated from 77 observation stations in snowy season from December 2013 to April 2014 as shown in Table 3.10.

The accuracy of without the forest region discrimination (a), with GIS forest region data (b) and the NDVI (c) forest region discrimination are 78.18%, 89.35% and 86.23%, respectively, as shown in Figure 3.11. Moreover, it also can be found that the snow cover detection accuracy of with GIS forest region data is higher than with the

Table 3.10: The results comparison of snow cover detection with different methods from 77 observation stations (1-16).

Station ID	Prefecture	Station Name	Latitude(N)		Longitude(E)		2013/12/26				2014/1/24				2014/2/26				2014/3/4				2014/4/14			
			Degree	Minute	Degree	Minute	AMeDAS	a	b	c	AMeDAS	a	b	c	AMeDAS	a	b	c	AMeDAS	a	b	c	AMeDAS	a	b	c
1	Akita Prefecture	Noshiro	40	11.9	140	1.9	0	0	0	0	28	0	1	1	17	1	1	1	0	0	0	0	0	0	0	0
2		Takanosu	40	13.6	140	22.3	8	0	1	1	42	1	1	1	44	1	1	1	30	0	1	1	0	0	0	0
3		Kazuno	40	12.9	140	47.2	8	0	1	1	40	1	1	1	34	1	1	1	26	1	1	1	0	0	0	0
4		Gojome	39	56.3	140	6.9	5	0	0	0	40	1	1	1	44	1	1	1	27	0	1	1	0	0	0	0
5		Akita	39	43	140	5.9	0	0	0	0	37	1	1	1	24	1	1	1	1	0	1	1	0	0	0	0
6		Kakunodate	39	36.2	140	33.4	25	1	1	1	91	1	1	1	83	1	1	1	70	1	1	1	0	0	0	0
7		Honjo	39	21.6	140	3.3	1	0	1	0	43	1	1	1	10	0	1	0	0	0	1	1	0	0	0	0
8		Yokote	39	19.2	140	33.3	48	1	1	1	161	1	1	1	142	1	1	1	125	1	1	1	0	0	1	1
9		Yashima	39	14.1	140	8.2	43	1	1	1	117	1	1	1	94	1	1	1	78	1	1	1	0	0	0	0
10		Yuzawa	39	11.2	140	27.8	52	1	1	1	135	1	1	1	112	1	1	1	102	1	1	1	0	0	0	1
11		Yunotai	38	57.6	140	31.7	80	1	1	1	177	1	1	1	173	1	1	1	154	1	1	1	49	1	1	1
12		Daishoji	39	31.6	140	14	32	1	1	1	108	1	1	1	91	1	1	1	69	1	1	1	0	0	0	0
13		Aniai	39	59.6	140	24.2	30	1	1	1	120	1	1	1	130	1	1	1	111	1	1	1	0	1	1	1
14	Aomori Prefecture	Mutsu	41	17	141	12.6	1	0	1	0	45	1	1	1	49	1	1	1	46	1	1	1	0	0	0	0
15		Aomori	40	49.3	140	46.1	14	1	1	1	60	1	1	1	65	1	1	1	55	1	1	1	0	0	0	0
16		Noheji	40	53.1	141	9.6	0	0	0	1	47	1	1	1	50	1	1	1	44	1	1	1	0	0	0	0

a: Results of Snow Cover Detection without Classifying the Forest Area

b: Results of Snow Cover Detection from Classifying the Forest Area with GIS data

c: Results of Snow Cover Detection from Classifying the Forest Area with NDVI

1: Snow Covered

0: Snow Free

Table 3.10: The results comparison of snow cover detection with different methods from 77 observation stations (17-32).

Station ID	Prefecture	Station Name	Latitude(N)		Longitude(E)		2013/12/26				2014/1/24				2014/2/26				2014/3/4				2014/4/14			
			Degree	Minute	Degree	Minute	AMeDAS	a	b	c	AMeDAS	a	b	c	AMeDAS	a	b	c	AMeDAS	a	b	c	AMeDAS	a	b	c
17		Ajigasawa	40	46.6	140	12.3	4	0	1	1	38	1	1	1	22	0	1	1	9	0	0	0	0	0	0	0
18		Goshogawara	40	48.5	140	27.5	10	1	1	1	58	1	1	1	48	1	1	1	31	1	1	1	0	0	0	0
19		Fukaura	40	38.7	139	55.9	6	0	1	1	24	0	0	0	21	0	1	1	8	0	1	1	0	0	0	0
20		Hirosaki	40	36.7	140	27.3	17	1	1	1	60	1	1	1	67	1	1	1	51	1	1	1	0	0	0	0
21		Towada	40	35.7	141	14.8	0	0	0	0	25	1	1	1	55	1	1	1	34	1	1	1	0	0	0	0
22	Aomori	Hachinohe	40	31.6	141	31.3	1	0	0	0	8	0	0	0	35	0	1	1	22	1	1	0	0	0	0	0
23	Prefecture	Ikarigaseki	40	28.9	140	37.2	20	1	1	1	68	1	1	1	63	1	1	1	50	1	1	1	0	0	0	0
24		Sannohe	40	23	141	15.4	0	0	0	0	19	1	1	1	51	0	1	1	31	1	1	1	0	0	0	0
25		Imabetsu	41	10.8	140	28.9	13	0	1	1	61	1	1	1	68	1	1	1	59	1	1	1	0	0	0	0
26		Oma	41	31.6	140	54.7	0	0	0	0	19	1	1	1	21	1	1	1	16	0	1	1	0	0	0	0
27		Sukayu	40	38.9	140	50.9	143	1	1	1	334	1	1	1	370	1	1	1	359	1	1	1	340	0	1	1
28		Wakinosawa	41	8.7	140	49.3	7	0	0	0	48	1	1	1	39	0	1	1	38	1	1	1	0	0	0	0
29		Ninohe	40	17.9	141	17.9	0	0	0	0	14	0	0	0	40	1	1	1	25	1	1	1	0	0	0	0
30	Iwate	Kuji	40	10.1	141	44.9	0	0	0	0	0	0	0	0	43	1	1	1	27	1	1	1	0	0	0	0
31	Prefecture	Kuzumaki	40	2.3	141	26.2	6	0	1	0	20	1	1	1	63	1	1	1	40	1	1	1	0	0	0	0
32		Iwatematsuo	39	57.1	141	3.9	4	0	1	1	24	1	1	1	18	1	1	1	0	0	0	0	0	0	0	0

a: Results of Snow Cover Detection without Classifying the Forest Area

b: Results of Snow Cover Detection from Classifying the Forest Area with GIS data

c: Results of Snow Cover Detection from Classifying the Forest Area with NDVI

1: Snow Covered

0: Snow Free

Table 3.10: The results comparison of snow cover detection with different methods from 77 observation stations (33-48).

Station ID	Prefecture	Station Name	Latitude(N)		Longitude(E)		2013/12/26				2014/1/24				2014/2/26				2014/3/4				2014/4/14			
			Degree	Minute	Degree	Minute	AMeDAS	a	b	c	AMeDAS	a	b	c	AMeDAS	a	b	c	AMeDAS	a	b	c	AMeDAS	a	b	c
33	Iwate Prefecture	Iwaizumi	39	50.8	141	47.7	0	0	0	0	0	0	0	0	48	1	1	1	29	1	1	1	0	0	0	0
34		Shizukuishi	39	41.8	140	58.5	10	1	1	1	32	1	1	1	25	1	1	1	8	0	1	1	0	0	0	0
35		Morioka	39	41.9	141	9.9	2	0	1	0	14	0	1	1	5	0	0	0	2	0	1	1	4	0	0	0
36		Miyako	39	38.8	141	57.9	0	0	0	0	1	0	1	0	27	1	1	1	15	0	1	1	2	0	0	0
37		Yuda	39	18.6	140	46.6	58	1	1	1	201	1	1	1	200	1	1	1	185	1	1	1	116	0	1	1
38		Kitakami	39	17.3	141	6.6	0	0	0	0	32	1	1	1	14	1	1	1	0	0	0	0	0	0	0	0
39		Tono	39	20.3	141	32.6	0	0	0	0	15	0	1	1	19	0	1	0	2	0	1	0	0	0	0	0
40		Ofunato	39	3.8	141	42.8	2	0	0	1	3	0	1	0	1	0	0	0	1	0	1	1	1	0	0	0
41		Ichinoseki	38	56	141	7.5	0	0	0	0	7	0	1	0	2	0	0	0	0	1	1	1	0	0	0	0
42		Matsurube	39	0.7	140	51.9	65	1	1	1	159	1	1	1	146	1	1	1	124	1	1	1	8	0	1	1
43		Okunakayama	40	3.6	141	13.5	22	1	1	1	61	1	1	1	81	1	1	1	66	1	1	1	0	0	0	0
44		Kuzakai	39	39	141	21.2	24	1	1	1	45	1	1	1	54	1	1	1	44	1	1	1	0	0	0	0
45		Kawatabi	38	44.6	140	45.6	12	0	0	0	55	1	1	1	50	1	1	1	35	1	1	1	0	0	0	0
46	Miyagi Prefecture	Furukawa	38	35.9	140	54.7	0	0	0	0	6	0	0	0	10	1	1	1	0	1	0	0	0	0	0	0
47		Ishinomaki	38	25.6	141	17.9	2	0	1	0	1	0	0	0	2	0	0	0	0	0	0	0	0	0	0	0
48		Nikkawa	38	18.2	140	38.2	5	0	1	0	8	0	1	1	31	1	1	1	12	0	1	1	0	0	0	0

a: Results of Snow Cover Detection without Classifying the Forest Area

b: Results of Snow Cover Detection from Classifying the Forest Area with GIS data

c: Results of Snow Cover Detection from Classifying the Forest Area with NDVI

1: Snow Covered

0: Snow Free

Table 3.10: The results comparison of snow cover detection with different methods from 77 observation stations (49-63).

Station ID	Prefecture	Station Name	Latitude(N)		Longitude(E)		2013/12/26				2014/1/24				2014/2/26				2014/3/4				2014/4/14			
			Degree	Minute	Degree	Minute	AMeDAS	a	b	c	AMeDAS	a	b	c	AMeDAS	a	b	c	AMeDAS	a	b	c	AMeDAS	a	b	c
49	Miyagi Prefecture	Sendai	38	15.7	140	53.8	0	0	0	0	2	0	1	1	3	0	0	0	1	1	1	1	0	0	0	0
50		Shiroishi	38	0.9	140	36.7	0	0	0	0	0	0	0	0	12	1	1	1	0	0	0	0	0	0	0	0
51		Komanoyu	38	54.8	140	49.7	49	1	1	1	108	1	1	1	115	1	1	1	96	1	1	1	6	1	1	1
52	Fukushima Prefecture	Fukushima	37	45.5	140	28.2	2	1	0	0	3	0	0	0	15	0	0	0	4	0	1	0	0	0	0	0
53		Inawashiro	37	33.1	140	6.5	23	1	1	1	54	1	1	1	54	1	1	1	36	1	1	1	0	0	0	0
54		Wakamatsu	37	29.3	139	54.6	13	1	1	1	32	1	1	1	37	1	1	1	18	1	1	1	0	0	0	0
55		Tadami	37	20.6	139	18.8	56	1	1	1	150	1	1	1	181	1	1	1	165	1	1	1	78	0	1	1
56		Nango	37	15.9	139	32.2	59	1	1	1	128	1	1	1	155	1	1	1	133	1	1	1	0	0	0	0
57		Tajima	37	12.4	139	47.7	19	1	1	1	46	1	1	1	79	1	1	1	61	1	1	1	0	0	0	0
58		Shirakawa	37	7.9	140	12.9	2	0	0	0	1	0	0	1	30	1	1	1	10	1	1	0	1	0	0	0
59		Nishiaizu	37	35.3	139	39.4	19	1	1	1	61	1	1	1	72	1	1	1	57	1	1	1	0	0	0	0
60		Kaneyama	37	28.4	139	31.7	28	1	1	1	106	1	1	1	125	1	1	1	112	1	1	1	0	0	0	0
61		Moniwa	37	53.5	140	26.2	10	1	1	1	19	1	1	1	31	1	1	1	19	0	1	1	0	0	0	0
62		Yumoto	37	16.6	140	3.8	29	1	1	1	63	1	1	1	95	1	1	1	76	1	1	1	0	0	0	0
63		Hinoemata	37	1.4	139	23.2	99	1	1	1	133	1	1	1	199	1	1	1	170	1	1	1	75	0	1	1

a: Results of Snow Cover Detection without Classifying the Forest Area

b: Results of Snow Cover Detection from Classifying the Forest Area with GIS data

c: Results of Snow Cover Detection from Classifying the Forest Area with NDVI

1: Snow Covered

0: Snow Free

Table 3.10: The results comparison of snow cover detection with different methods from 77 observation stations (64-77).

Station ID	Prefecture	Station Name	Latitude(N)		Longitude(E)		2013/12/26				2014/1/24				2014/2/26				2014/3/4				2014/4/14			
			Degree	Minute	Degree	Minute	AMeDAS	a	b	c	AMeDAS	a	b	c	AMeDAS	a	b	c	AMeDAS	a	b	c	AMeDAS	a	b	c
64		Sakata	38	54.5	139	50.6	2	0	0	0	9	0	0	1	2	0	0	0	2	0	1	0	0	0	0	0
65		Kaneyama	38	52.7	140	19.9	55	1	1	1	145	1	1	1	144	1	1	1	133	1	1	1	0	0	1	1
66		Karikawa	38	48	139	58.4	0	0	0	0	28	1	1	1	40	1	1	1	21	1	1	1	0	0	0	0
67		Shinjo	38	45.4	140	18.7	51	1	1	1	134	1	1	1	132	1	1	1	121	1	1	1	0	0	1	1
68		Kushibiki	38	40.3	139	50.9	0	0	0	0	16	0	1	1	21	1	1	1	4	0	0	0	0	0	0	0
69		Aterazawa	38	22.2	140	11.5	23	1	1	1	49	1	1	1	52	1	1	1	33	1	1	1	0	1	1	1
70	Yamagata	Yamagata	38	15.3	140	20.7	8	1	1	1	15	0	1	1	25	1	1	1	15	0	1	1	0	0	0	0
71	Prefecture	Nagai	38	6.3	140	0.9	29	1	1	1	76	1	1	1	67	1	1	1	50	1	1	1	0	0	0	0
72		Oguni	38	4.7	139	44.1	47	1	1	1	139	1	1	1	136	1	1	1	117	1	1	1	0	0	0	0
73		Yonezawa	37	54.7	140	8.6	28	1	1	1	67	1	1	1	82	1	1	1	65	1	1	1	0	0	0	0
74		Mukaimachi	38	45.5	140	31	55	1	1	1	134	1	1	1	130	1	1	1	117	1	1	1	0	1	1	1
75		Obanazawa	38	36.5	140	24.7	53	1	1	1	121	1	1	1	146	1	1	1	139	1	1	1	0	0	1	1
76		Hijiori	38	36.4	140	9.8	104	1	1	1	252	1	1	1	305	1	1	1	273	1	1	1	151	0	1	1
77		Oisawa	38	23.4	139	59.6	127	1	1	1	209	1	1	1	240	1	1	1	213	1	1	1	117	1	1	1

a: Results of Snow Cover Detection without Classifying the Forest Area

b: Results of Snow Cover Detection from Classifying the Forest Area with GIS data

c: Results of Snow Cover Detection from Classifying the Forest Area with NDVI

1: Snow Covered

0: Snow Free

NDVI, and improved by 3.12%.

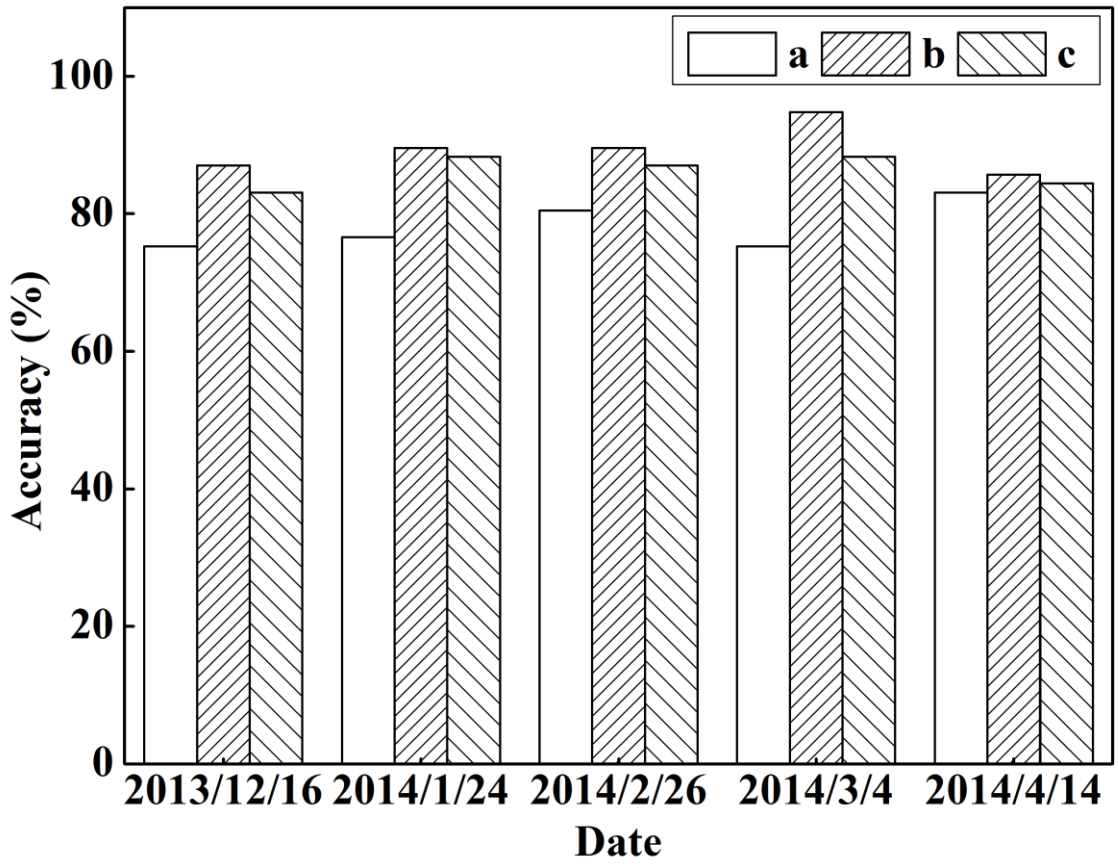

Figure 3.11: The statistics results of snow cover detection from above three situations.

3.4 Summary

The MOD10_L2 product is not preprocessed by atmospheric correction and topographic correction, which caused many error detections for snow. In this chapter, a new method for snow detection via the combination of NDSI and NDVI based on the terrain features and the underlying surface covered by snow of Akita Prefecture in Japan was proposed. The Terra MODIS Level-1 B product data were used during the period of December 2010 to April 2011. Then, 13 observation stations which have the AMeDAS snow depth records were selected. In order to improve the accuracy of snow detection, the preprocessing was conducted before the snow detection. It includes atmospheric correction with CREFL_SPA, geographic correction with MRT, study area cutting and topographic correction with a shadowing function method. Considering the effect of the underlying surface covered by snow, we took advantage of the

NDVI to distinguish the mixed pixels of the snow and forests. And the threshold value of NDSI was correspondingly lowered to improve the detecting accuracy for snow in forests. It has been proved that the accuracy of proposed method for snow detection was improved about 11% compared to the results of the MOD10_L2 product and NDSI alone. Therefore, it is feasible and effective to use the combination of NDSI and NDVI for the snow cover detection in Akita Prefecture of Japan with MODIS images.

In addition, in order to investigate the effectiveness of the GIS and NDVI data to forest region classification in study area, GIS forest region data and the NDVI were also used for forest area discrimination with Terra/MODIS data of Tohoku region in Japan during snowy season from December 2013 to April 2014 in. Then the snow cover detection was conducted in study area. The results show that the accuracy of without the forest area discrimination, with GIS forest region data and with the NDVI for the forest area discrimination are 78.18%, 89.35% and 86.23%, respectively. Comparing with the snow cover detection results without the forest area discrimination, the accuracy with GIS forest region data and with NDVI for the forest area discrimination were increased by 11.17% and 8.05% respectively. And the accuracy with GIS forest region data is higher about 3.12% than the NDVI.

Chapter 4
Snow Cover Detection
with visibile Red and Blue Bands

4.1 Introduction

Generally, the accuracy of the snow cover detection can be affected by atmosphere [91]. Therefore, atmospheric correction as the necessary preprocessing should be conducted to get real surface reflectance.

Recently, lots of methods have been done to improve the validity on the atmospheric correction. For example, the histogram matching method [69], [92], [93], dark object method [94], invariant object method [95], contrast reduction method [96], and LOWTRAN [97] model and so on. However, most of these methods and models based on some special and ideal conditions and their application is limited. Currently, FLAASH and 6S code model are the most widely used in the field of remote sensing earth science. FLAASH is a first-principles atmospheric correction tool. It incorporates the MODTRAN 4 radiation transfer code and can define relative solar position, atmospheric, aerosol and scattering models parameters [93]. The 6S code is a basic RT code used for calculation of lookup tables in the MODIS atmospheric correction algorithm [98]. This method cannot be limited by study target, target type and back ground. It combined the topography, weather, spectrum and other parameters, can be used in spectral bands of several satellite sensors [99].

Therefore, in section 4.2, FLAASH and 6S code model are adopted for the atmospheric correction based on Terra/MODIS data and natural and geographic situation of Akita prefecture. FLAASH model is calculated in the environment of the Interface Definition Language (IDL). The applied 6SV1 is a vector version of the 6S radiative transfer code. It can simulate the reflection of solar radiation, spectral and geometrical conditions [100]. The parameter items and values of FLAASH and 6S code model are input during the atmospheric correction, then image comparisons between FLAASH and 6S code model atmospheric correction are investigated. The results of snow cover detection without atmospheric

correction and with FLAASH and 6S code model for atmospheric correction are also compared from December 2010 to April 2011 [101].

After comparing the results from the FLAASH and 6S code atmospheric correction, 6S code method is used to atmospheric correction in the following studies of snow cover detection as the necessary preprocessing step.

In section 4.3, a new snow cover detection method based on visible red and blue bands from MODIS imagery data is proposed for Akita prefecture under the sunny cloud-free conditions. This method is applied in order to more effectively detect the snow cover. Furthermore, the 5 typical images of clear days during the whole year are observed, and the threshold values by investigating these 5 typical images and their corresponding 2-dimensional scatter plots in bands 1 and 3 are confirmed. The effectiveness of the proposed method is investigated via the comparing with the MOD10_L2 products and in-situ snow depth data from 31 observation stations across the whole study area. The overall accuracy, over-estimation error and under-estimation error of snow cover detection are calculated and applied to evaluate the effectiveness of the proposed method [102].

As we know, cloud disturbances pose a significant barrier to effective snow cover detection. The NASA MODIS land team has produced a cloud mask algorithm, named the MODIS cloud mask, for separating cloud from clear sky data, and has obtained a series of cloud products [103], [104]. The cloud mask algorithm is intended to be applied during data preprocessing, and includes inputs of surface type, altitude, and snow distribution. However, the cloud product can be affected by the condition of the sensor because of the information from many bands is used [105]. In a previous study, Tekeli et al. [106], observed the distribution of snow cover in the eastern mountainous regions of Turkey. During their study process, they found that land type, topography variations, short-term climate change, and the particular snow mapping algorithms used in the cloud mask products can all affect the accuracy of snow cover detection. The snow-covered areas may be underestimated by the MODIS snow product because of seasonal changes, particularly in early spring when the snow begins to melt. The accuracy of snow cover detection can also be affected by the orientation of mountain slopes and solar angles. An overestimation of cloud in the MODIS cloud mask product may result in an underestimation of snow, as potential snow pixels will be masked by the cloud detection. Hall and Riggs [107] identified this problem as the most significant source of detection error in the MODIS snow products. As it is difficult to remove a large area of cloud using information from optical sensors, predominantly sunny days (with

cloud cover making up less than 5% of the acquired images) are selected for snow cover detection in order to eliminate the impact of cloud as much as possible. In section 4.4, a new snow cover detection algorithm is proposed uses MODIS image data and is validated for the Akita Prefecture, Japan. Snow and cloud are extracted from other ground surface features using red band 1 and blue band 3. Then, short-wave infrared (SWIR) band 6 and SWIR band 7 are used to detect and distinguish cloud. Finally, cloud is separated from snow to obtain a final snow cover map of Akita Prefecture. The new proposed method is further validated using data from Aomori Prefecture and the Mt. Chokaizan region [108].

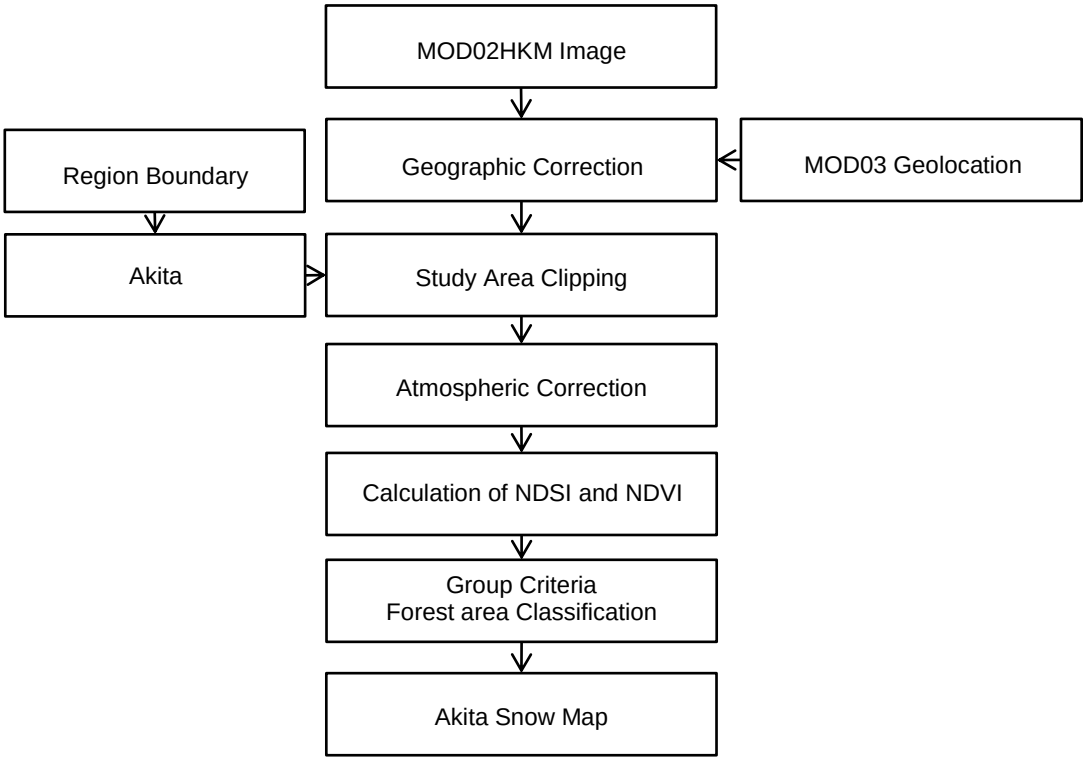

Figure 4.1: the flowchart of snow cover detection

4.2. Comparison of FLAASH and 6S Code Atmospheric Correction on Snow Cover Detection

4.2.1. Snow Cover Detection Method

In this work, firstly, data MOD02HKM (MODIS/Terra Calibrated Radiances 5-Min L1B Swath 500m Collection 4 and 5 product data) was geographic corrected with the MODIS Swath Reprojection Tool (MRT Swath) software, which can be obtained from LP DAAC

website. MOD03-Geolocation (MODIS geolocation product) data as the auxiliary file was used here. Then, geographic corrected data was clipped by Akita prefecture administrative zone file, which can be obtained online. Next is the atmospheric correction. Following is the calculation of Normalized Difference Snow Index (NDSI) and Normalized Difference Vegetation Index (NDVI). In the end, generate the results map of snow cover in Akita prefecture of Japan. Figure 4.1 shows the flowchart of snow cover detection in this study.

FLAASH		6S Code	
Parameter Items	Parameter Values	Parameter Items	Parameter Values
Flight Date	April 6th, 2011	Date	6th, April
Flight Time GMT(HH:MM:SS)	1:25:05	Solar Zenithal Angle	40.91
Latitude	39.6915	Solar Azimuthal Angle	143.73
Longitude	140.344	Sensor Zenithal Angle	43.00
Sensor Type	MODIS	Sensor Azimuthal Angle	-96.49
Atmospheric Model	Midlatitude Winter	Atmospheric Profile	Midlatitude Winter
Aerosol Model	Rural	Aerosol Model	Continental Model
Initial Visibility (km)	20	Visibility (km)	20
Ground Elevation (km)	0.097	Target Altitude (km)	-0.097
Sensor Altitude (km)	705	Sensor Altitude	(-1000) Satellite Level
Pixel Size (m)	500	Spectral Conditions	MODIS Band 1- Band 7
Ground Refectance Type	none	Ground Reflectance Type	Homogeneous Surface
Directional Effects	none	Directional Effects	No Directional Effect
Specify Surface Reflectance	none	Specify Surface Reflectance	Mean Spectral Value of Green Vegetation
Atmospheric Correction Mode	none	Atmospheric Correction Mode	Atmospheric Correction with BRDF
Reflectance	none	Reflectance	1

Table 4.2: The parameters comparison in the processes of FLAASH and 6S Code Methods.

4.2.2. Atmospheric Correction Method

In the process of FLAASH atmospheric correction, the latitude and longitude are the center coordinates of the whole Akita prefecture. Akita is the agriculture prefecture and industry

rarely, so rural was chosen in aerosol model. In addition, due to the resolution of MODIS image is relatively no high, so water retrieval and adjacency correction were not conducted. In the process of 6S code atmospheric correction, solar zenithal angle, solar azimuthal angle, sensor zenithal angle and sensor azimuthal angle are all the average values which were calculated from MOD03-geolocation. Target Altitude is the average value of 36 observation stations which were distributed by Akita Local Meteorological Observatory of Japan Meteorological Agency (JMA). The mean spectral value of green vegetation was used in specify surface reflectance. Atmospheric correction was conducted with BRDF (Bidirectional Reflectance Distribution Function), and the reflectance value was set as 1. Visibility data was obtained from the Sendai aviation weather center Akita airport branch of JMA. In this work, visibility data 20 km at 10:00 am was adopted because of the Terra/MODIS image was taken at 10:25 am of Japan standard time as shown in Table 4.2.

4.2.3. The NDSI and NDVI

The combination method of NDSI and NDVI was used to detect the snow cover of Akita. The $NDSI$ and $NDVI$ were calculated with following Equations (15) and (16), respectively.

Final snow cover detection results were achieved through two groups of grouped criteria. In one group, value of $NDSI$ was greater than 0.45, $band_2$ was greater than 0.11 and $band_4$ was greater than 0.10. In the other group, value of $NDVI$ was greater than 0.3, value of $NDSI$ was greater than 0.38, $band_2$ was greater than 0.11 and $band_1$ was greater than 0.1 in forest area.

4.2.4. The Comparison of Atmospheric Correction

Figure 4.3 shows the RGB (143) comparison images of without atmospheric correction (a), with FLAASH atmospheric correction (b) and with 6S code atmospheric correction (c). A_X, B_X, C_X and D_X are the magnified image of forest area, agricultural area, lake area and snow area respectively. It shows that the image is dark and the objects are fuzzy in (a), but (b) and (c) are clearer than (a). Moreover, the same feature in (b) and (c) can correspond to more different reflectance because of the real reflectance range became wider after correction and contained more abundant features information. Meanwhile, they have more sense of visual layering. That is because atmospheric correction has eliminated the effect of atmosphere. It

also shows that (c) is much clearer than (b), and the visual layering sense is much better. It suggests that the 6S code model is a more effective method than FLAASH model for atmospheric correction.

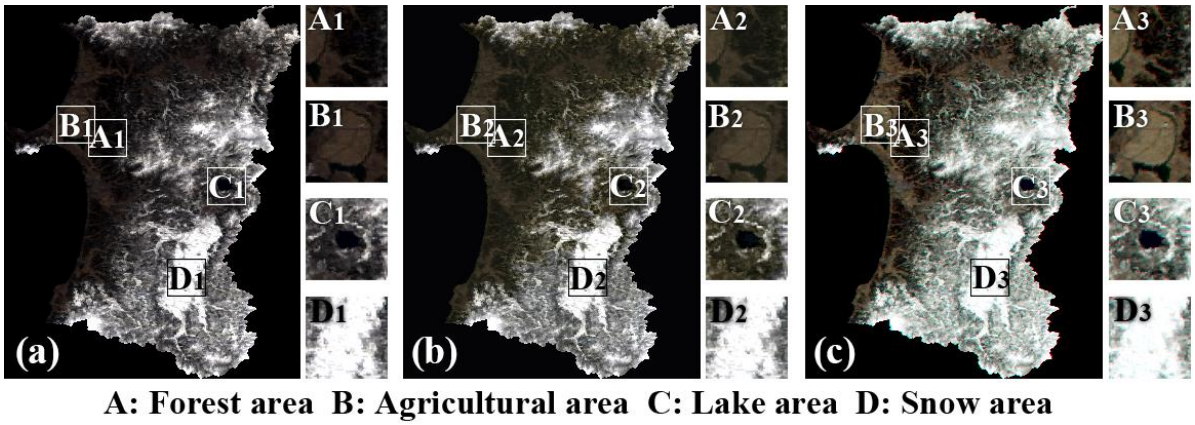

Figure 4.3: The RGB (143) combined comparison images of without and with atmospheric correction. ((a) Without Atmospheric Correction; (b) With FLAASH Atmospheric Correction; (c) With 6S Code Atmospheric Correction.)

4.2.5. The Results Comparison of Snow Cover Detection

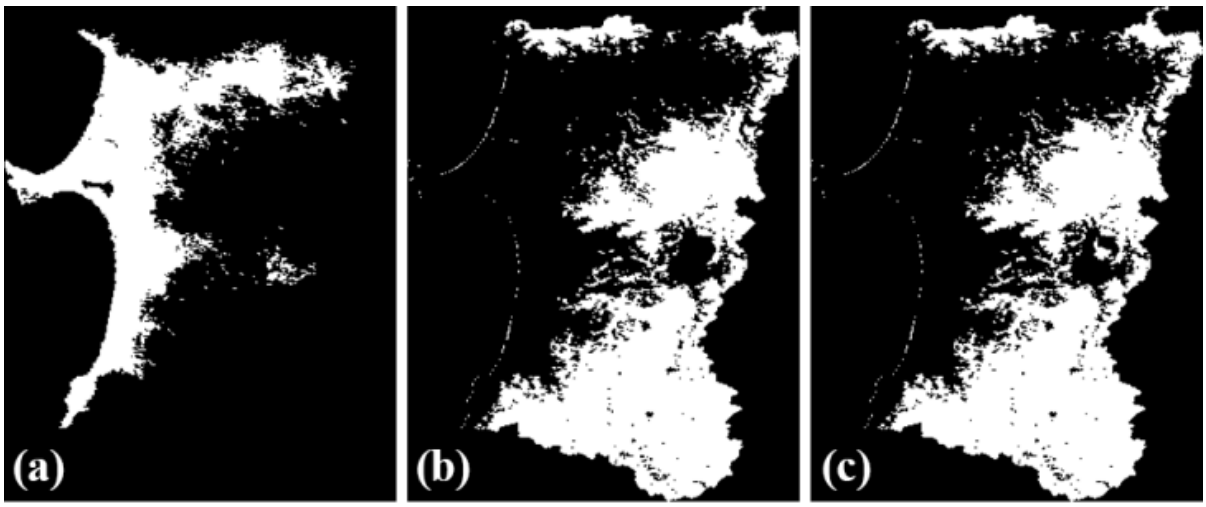

Figure 4.4: The snow cover detection results comparison images of without and with atmospheric correction. ((a) Without Atmospheric Correction; (b) With FLAASH Atmospheric Correction; (c) With 6S Code Atmospheric Correction.)

Figure 4.4 shows the results comparison images of snow cover detection without

atmospheric correction (a), with FLAASH atmospheric correction (b) and with 6S code atmospheric correction (c). The snow was not detected in the forest and mountain areas without atmospheric correction from (a) because that solar radiation and ground reflected radiation were scattered and absorbed by atmosphere, which increased the average luminance value of the atmosphere. These scattering and absorption superposed on the radiation signal of ground surface features and recorded together with satellite remote sensing imagery. As a result, the contrast and sharpness of images were decreased, and the radiation signals were distortion. However, after the atmospheric correction, the real reflectance of ground surface was mainly restored, and the more surface feature information was appeared as shown in Figure 4.4 (b) and (c). As a result, the snow cover in forest and mountain areas were successfully detected, which improved the accuracy of snow cover detection.

4.2.6. The Statistics Results Comparison of Snow Cover Detection

In this work, AMeDAS snow depth records of 10 observation stations which distributed in the whole Akita prefecture were chosen to verify the results of snow cover detection with the combination of NDSI and NDVI as shown in Figure 4.5.

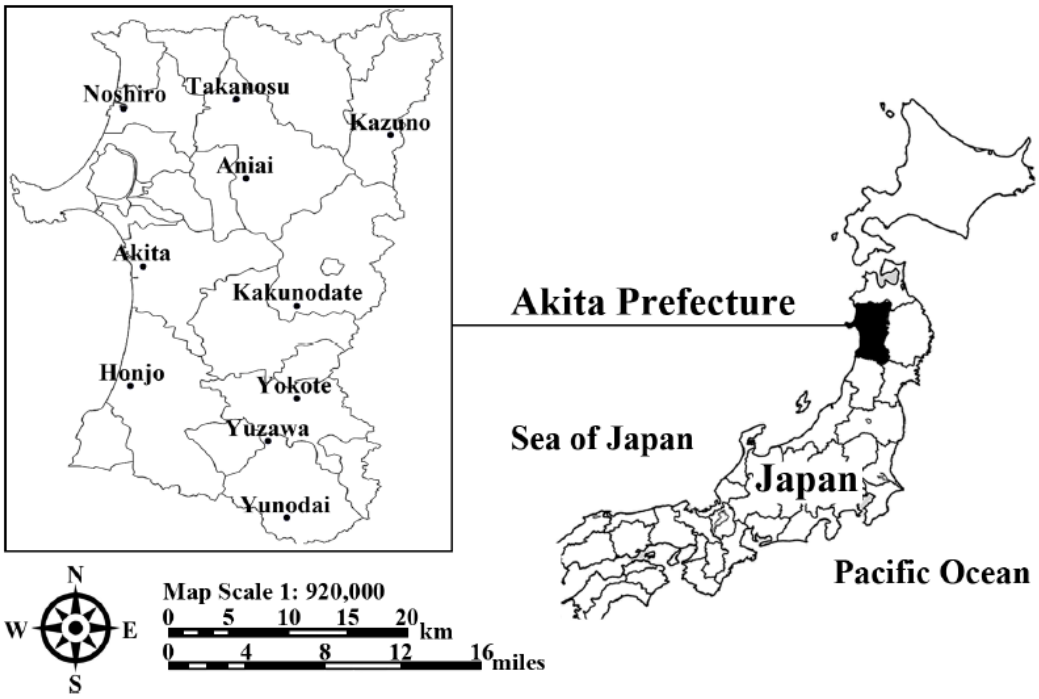

Figure 4.5: Study area of Akita Prefecture, Japan.

Table 4.6: The statistics results of snow cover detection

Stations	Latitude (N)	Longitude (E)	12/1/2010				1/27/2011				2/15/2011				3/9/2011				4/6/2011			
			AMeDAS	a	b	c	AMeDAS	a	b	c	AMeDAS	a	b	c	AMeDAS	a	b	c	AMeDAS	a	b	c
Kazuno	40°12.9′	140°47.2′	6	0	1	1	74	1	1	1	73	1	1	1	52	1	1	1	0	1	0	0
Yunodai	38°57.6′	140°31.7′	0	1	0	0	155	0	1	1	138	1	1	1	123	1	1	1	84	1	1	1
Aniai	39°59.6′	140°24.2′	1	1	1	1	123	0	1	1	105	0	1	1	96	1	1	1	1	1	0	0
Noshiro	40°11.9′	140°1.9′	0	1	0	0	26	0	0	0	18	0	1	1	0	0	0	0	0	1	0	0
Akita	39°43′	140°5.9′	0	1	1	0	32	0	1	1	28	0	0	1	3	0	1	1	0	1	0	0
Honjo	39°21.6′	140°3.3′	0	1	0	0	57	0	0	1	52	1	1	1	0	0	0	1	0	1	0	0
Takanosu	40°13.6′	140°22.3′	1	0	1	1	66	1	1	1	64	1	1	1	47	0	1	1	0	1	0	0
Kakunodate	39°36.2′	140°33.4′	0	0	1	1	89	1	1	1	92	1	1	1	69	1	1	1	5	0	0	1
Yokote	39°19.2′	140°33.3′	2	0	1	1	136	1	1	1	133	1	1	1	103	1	1	1	18	0	1	1
Yuzawa	39°11.2′	140°27.8′	0	0	0	0	144	0	1	1	130	1	1	1	111	0	1	1	64	0	1	1

Notice: a: Results of Snow Cover Detection without Atmospheric Correction

b: Results of Snow Cover Detection with FLAASH Atmospheric Correction

c: Results of Snow Cover Detection with 6S Atmospheric Correction

0: Snow Free

1: Snow Covered

Table 4.6 shows the statistics results of snow cover detection compared with 10 AMeDAS stations. In this table, AMeDAS represents the records of the AMeDAS snow depth. It is obviously to see that the accuracy of snow cover detection without atmospheric correction is 46%, with FLAASH atmospheric correction is 86% and with 6S code atmospheric correction is 92%. Moreover, it also can be found that the effect of 6S code is higher than FLAASH model, and improved by 6%.

4.3. Snow Cover Detection Based on Visible Red and Blue Channel from MODIS Imagery Data

4.3.1 Methodology

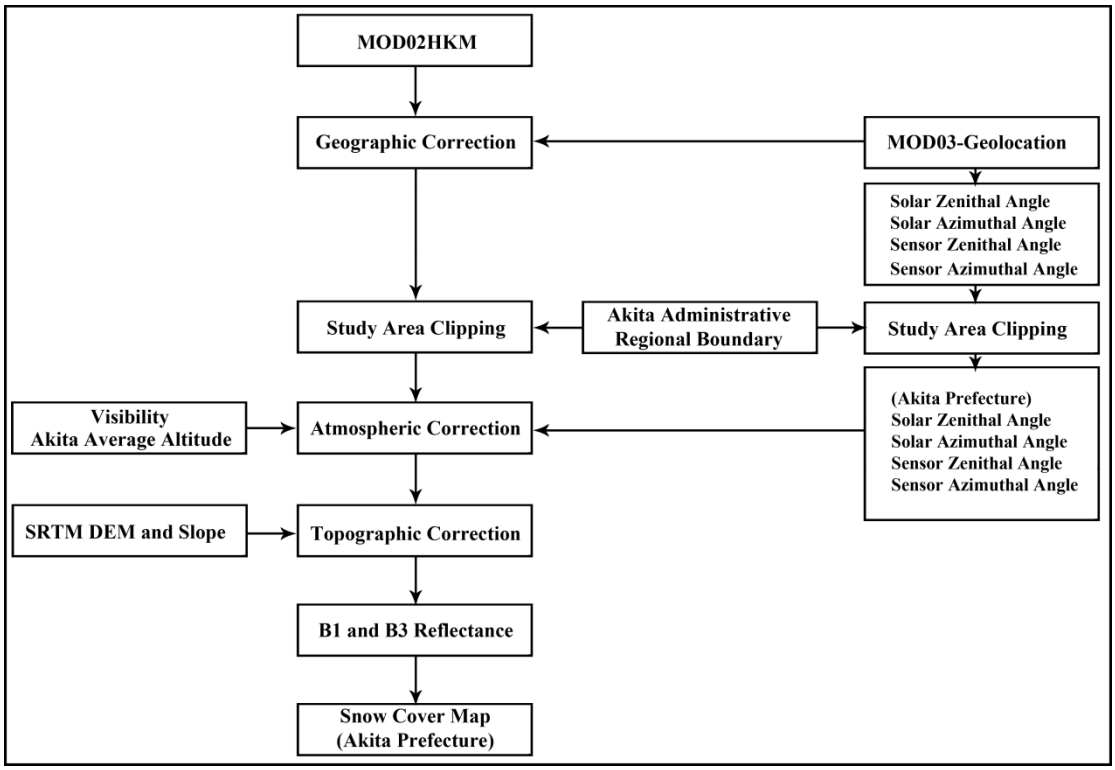

Figure 4.7: The flowchart of the snow cover detection method proposed in this study.

In this study, the MODIS/Terra Calibrated Radiances 5-Min L1B Swath 500 m (MOD02HKM) product data, the MODIS geolocation product (MOD03-Geolocation) data, the MODIS/Terra Snow Cover 5-Min L2 Swath 500 m (MOD10_L2) product data, the administrative regional boundary ShapeFile data of Akita prefecture, visibility and average altitude data of Akita prefecture, the RSIS snow depth data, the AMeDAS snow depth data, the SRTM 90 m DEM data,

geographic coordinates data of 31 observation stations are applied for the snow cover detection in Akita prefecture.

Figure 4.7 shows the flowchart of the snow cover detection method proposed in this study. The pre-processing including geographic correction, study area clipping, atmospheric correction and topographic correction are conducted before the snow cover detection. Then the reflectance images of band 1 (red, 0.620 - 0.670 μm) and band 3 (blue, 0.459 - 0.479 μm) are obtained and used to detect the snow cover pixels by setting their threshold values. Finally, the snow cover detection results of the study area are obtained. Here, it is necessary to clear that the whole operation process of this study is conducted at Interface Description Language (IDL) language environment platform.

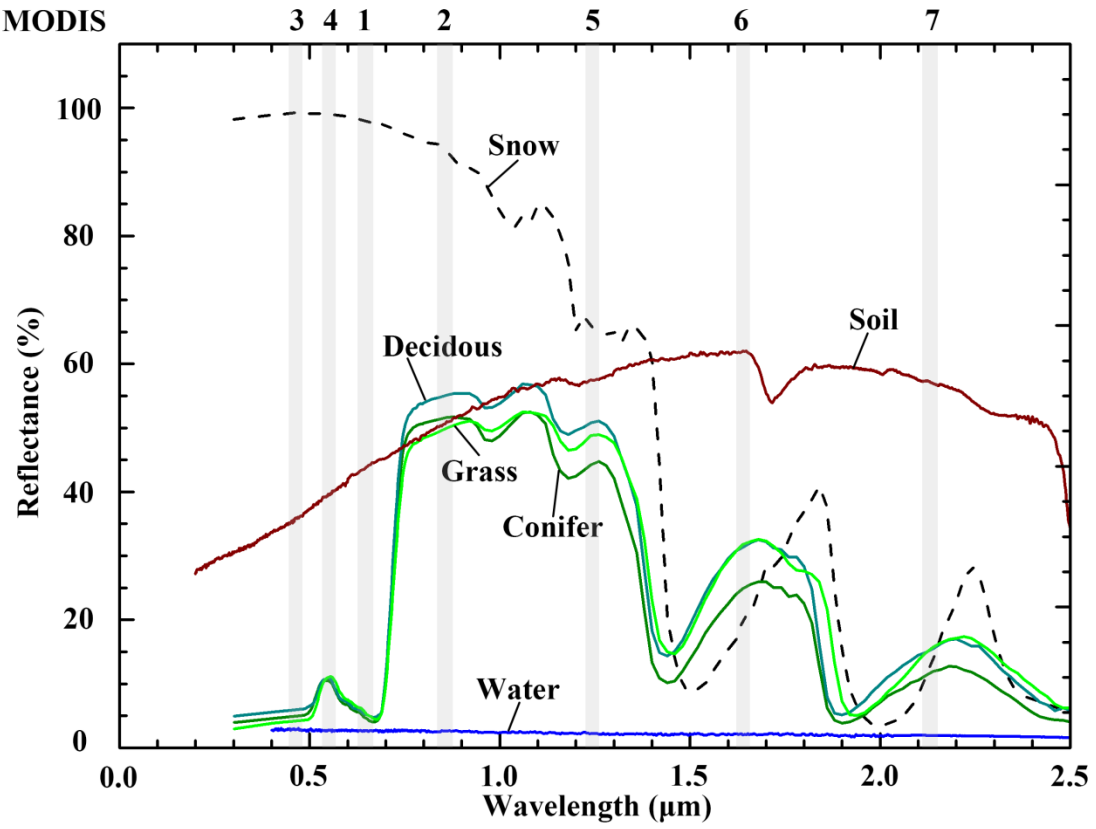

Figure 4.8: Spectral reflectance curves of snow, soil, vegetation (deciduous, conifer and grass) and water.

4.3.2. Spectral Analysis

The MODIS imagery of the real ground surface reflectance in the study region can be obtained after completion of the above pre-processing operations.

In order to analyze the spectrum distribution of the ground surface substances in bands 1 and 3 within the study area, the spectrums of the ground surface substances in accordance with clear day conditions of Akita prefecture are searched and produced from the relevant spectral libraries. Figure 4.8 shows the ideal standard reflectance spectrums of the various representative ground surface substances in Akita prefecture, such as snow, soil, deciduous, conifer, grass and water.

From Figure 4.8, it can be seen that the reflectance spectrums of different substances can be clearly distinguished in the visible red band 1, blue band 3 and green band 4 (0.545 - 0.565 μm). In these three bands, the reflectance of snow is the highest, followed in order by soil and other vegetation (deciduous, conifer and grass). Vegetation has much lower reflectance because of the strong chlorophyll absorption among these three wavelengths. The reflectance of water is only 5%, which is the smallest in all of the substances. Due to green vegetation shows a small reflectance peak in band 4, there may be some difficulties during the identification of mixed snow and green vegetation pixels. Therefore, the visible bands 1 and 3 are selected to detect and distinguish snow pixels from other ground surface substances in this work.

4.3.3. The Snow Distribution of Study Area in Different Periods

In order to investigate the snow cover distribution at different periods in the study area, we selected 5 types of typical snow cover distribution situations images from May 2012 to April 2014 on clear days as the training images and are shown in Figure 4.9.

Figure 4.9 shows the true color images composited by MODIS images of the Terra satellite at 500 m spatial resolution in different periods. The winter of Akita prefecture is from the late December to early February, so the whole study area is almost covered by snow as shown in Figure 4.9 (a). The white area represents snow cover, its brightness increased with the snow cover becoming thicker. The deep green area represents the bared vegetation, because the snow cover on the branches are

blown down by the strong sea wind, which lead to some of the forest is exposed. On the other hand, there is no snow cover over the Tazawa Lake and shows black colors because it keeps ice-free all the year round. From Figure 4.9 (b), it can be seen that some of snow cover began to melt in March, but there are still snow cover in most of the study area. In fact, all of snow cover distributed in the mountain and basin areas of inland but not in the coastal area. It is because that the snow cover in coastal area was blown to the inland by strong sea wind. Therefore, the bared soil in the coastal area shows the dark brown. In addition, there is also no snow cover on the Hachirougata Choseichi in the southeast of Oga Peninsula.

In May, the weather of the whole study area warms into spring, most of snow cover has been melted, and there is only snow cover on the top of mountains in inland as shown in Figure 4.9 (c). The dark brown area is the bared land with the buds of green vegetation like grass, and the dark green area is the forest. Meantime, the Tazawa Lake on the satellite images begins to show the blue color due to the strong light of sun.

With the study area entering into the late June, almost all of snow cover has been melted due to the continuous high temperature of summer. There is only still a little snow cover on the peak of Mt. Chokaizan which locates in the southwest corner of the Akita prefecture as shown in Figure 4.9 (d). It is because that the altitude of Mt. Chokaizan is 2,236 m and the temperature on the top of the mountain is much lower. Other places across the whole study area have a large area of the vegetation and the bared land has become the agricultural land. They show the bright green color from the satellite images.

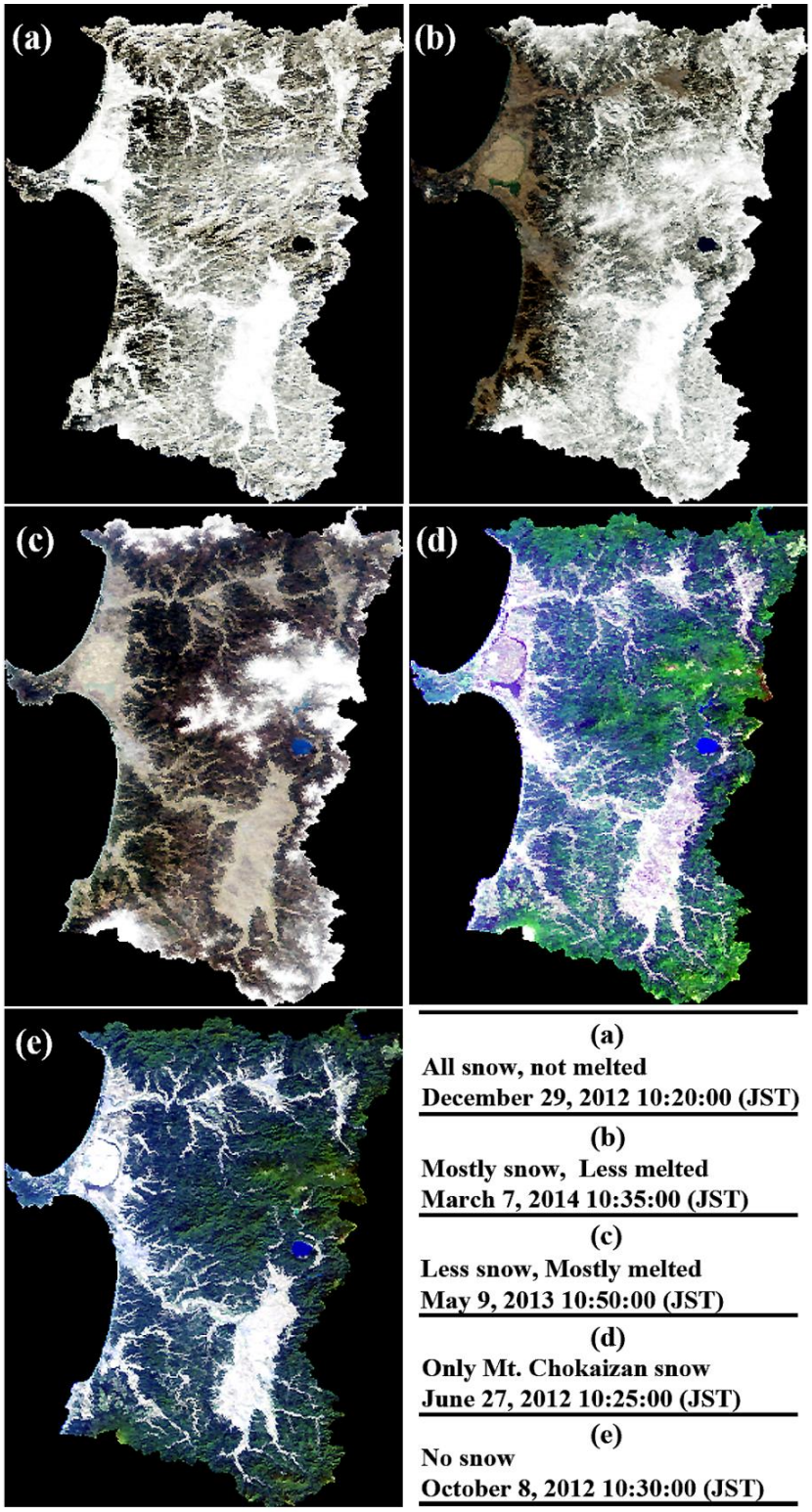

Figure 4.9: The true color images composited by MODIS images of Terra satellite at 500 m spatial resolution in different periods (a) 10:20:00 AM on December 29, 2012, snow was not melted; (b) 10:35:00 AM on March 7, 2014, snow was melted a little; (c) 10:50:00 AM on May 9, 2013, mostly snow was melted; (d) 10:25:00 AM on June 27, 2012, snow covered only on Mt. Chokaizan; (e) 10:30:00 AM on October 8, 2012, no snow.

In October, the study area enters into the alternate season of summer and autumn. Due to the continuous high temperature of summer in July, August and September, there is not any snow cover even on the Mt. Chokaizan as shown in Figure 4.9 (e). At this time, the forest is still lush and shows dark green. And due to the harvest of the crops, the agricultural land turns into bared land again. But the brightness on the satellite images is higher than before because only weeds are left.

4.3.4. 2 Dimensional Scatter Plot Analysis

Based on the above analysis, we conclude that when the reflectance value of one pixel is greater than the soil, this pixel will be judged as the snow pixel. From Figures 4.10 (a)-(e), the largest reflectance values of soil pixels in visible bands 1 and 3 are 0.458 and 0.60, respectively. Therefore, in this work, the threshold values are determined as greater than 0.458 in band 1 and greater than 0.60 in band 3.

A 2-dimensional scatter plot density distribution can further illustrate the pixel distributions of various substances in the study area. Figure 4.10 shows the 2-dimensional scatter plot density distributions of the above 5 types of training images in visible red band 1 and blue band 3. Figures 4.10 (a)-(e) are the 2-dimensional scatter plot density distributions across the whole study area which represent that there are all snow cover and not melted situation, at 10:20:00 AM on the December 29, 2012, there are mostly snow cover and less melted situation, at 10:35:00 AM on the March 7, 2014, there are less snow cover and mostly melted situation, at 10:50:00 AM on the May 9, 2013, there are only snow cover on the top of the Mt. Chokaizan, at 10:25:00 AM on the June 27, 2012, and there are no snow cover situation, at 10:30:00 AM on the October 8, 2012, respectively. The density distribution location of each substance in the 2-dimensional scatter plot is marked in these 5 types of different figures.

From Figure 4.10, it is obvious that snow pixels decreased from (a) to (d) until it disappeared in (e). The reflectance values of images from (a) to (e) also decreased along with the snow pixels decreasing in the MODIS visible red band 1 and blue band 3. Combining with the composited true color images in Figure 4.9, from Figure 4.10 (a), it can be seen that there are only 3 types substances which are snow, vegetation (conifer and deciduous forest) and water. Due to all of the study area are

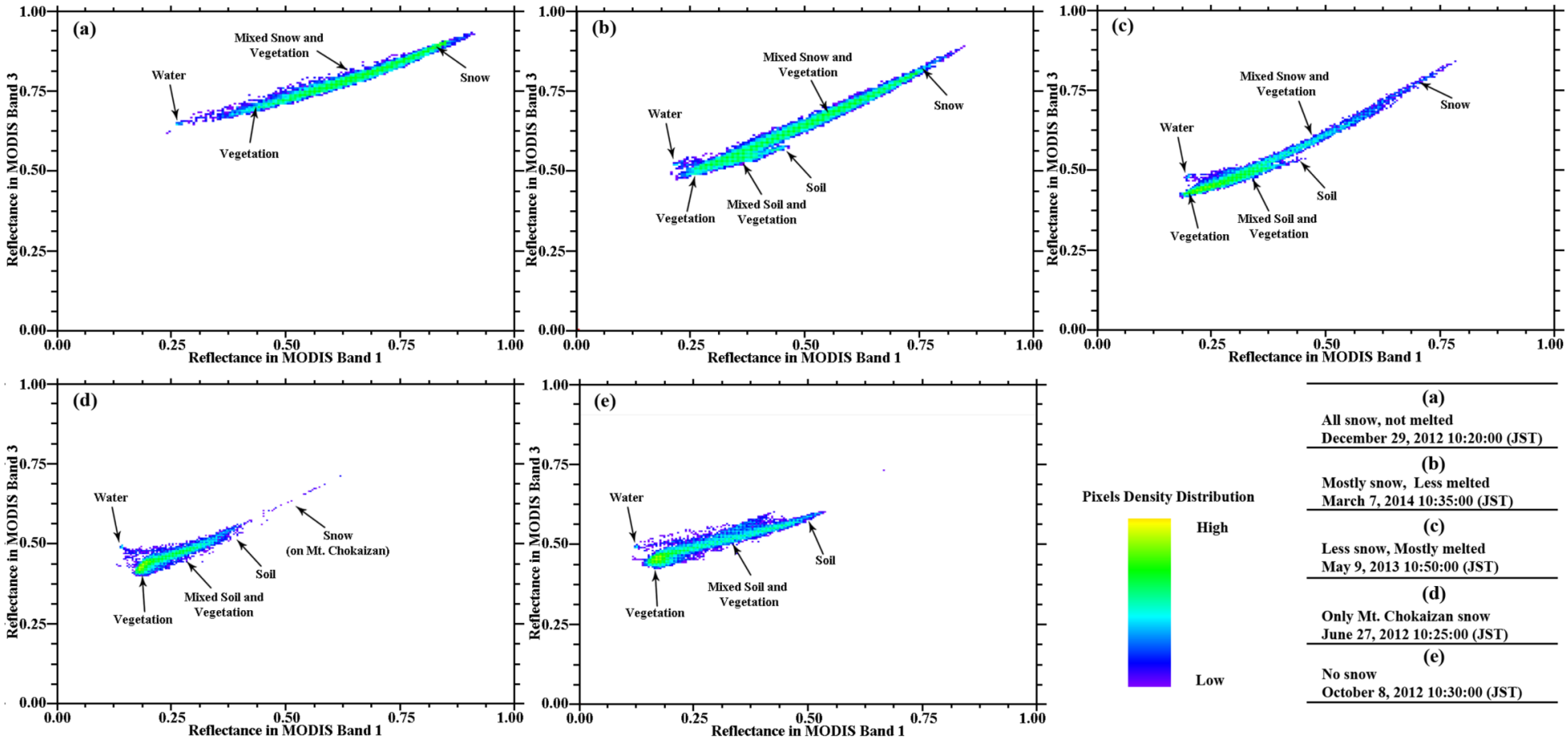

Figure 4.10: The 2-dimensional scatter plot density distributions of 5 types of images in bands 1 and 3.

almost covered by snow in winter, the pixels are mainly snow and the distributions of the pixels mainly locate at the top right part of the whole 2-dimensional scatter plot density distribution figure. With the weather warming, the snow began to melt and some of bared lands in the coastal region gradually appeared. The whole 2-dimensional scatter plot density distribution figure shows some soil pixels which located in the lower part of the snow and vegetation mixed pixels in the visible blue band 3 from Figure 4.10 (b) and Figure 4.10 (c). In Figure 4.10 (d), due to there is only still a little snow cover on the peak of Mt. Chokaizan, the snow pixels still exist at the top right part of the whole 2-dimensional scatter plot density distribution figure. And due to the bared land has become the agricultural land, the soil pixels in the 2-dimensional scatter plot also disappeared and became into the vegetation pixels again. In Figure 4.10 (e), there is not any snow cover across the whole study area, all of substances pixels become relative clearness. There are only three kinds of substances pixels which are soil, vegetation and water pixels. In addition, the reflectance of soil pixels became the biggest in the absence of snow pixels.

4.3.5. Result and Discussion

Figure 4.11 shows a composited RGB (143) true color image (a) and the snow cover detection results of proposed method (b) and MOD10_L2 (c) on April 2, 2014. Here, (a) as the reference of visual judgment is applied to be objectively compared with the snow cover detection results of (b) and (c).

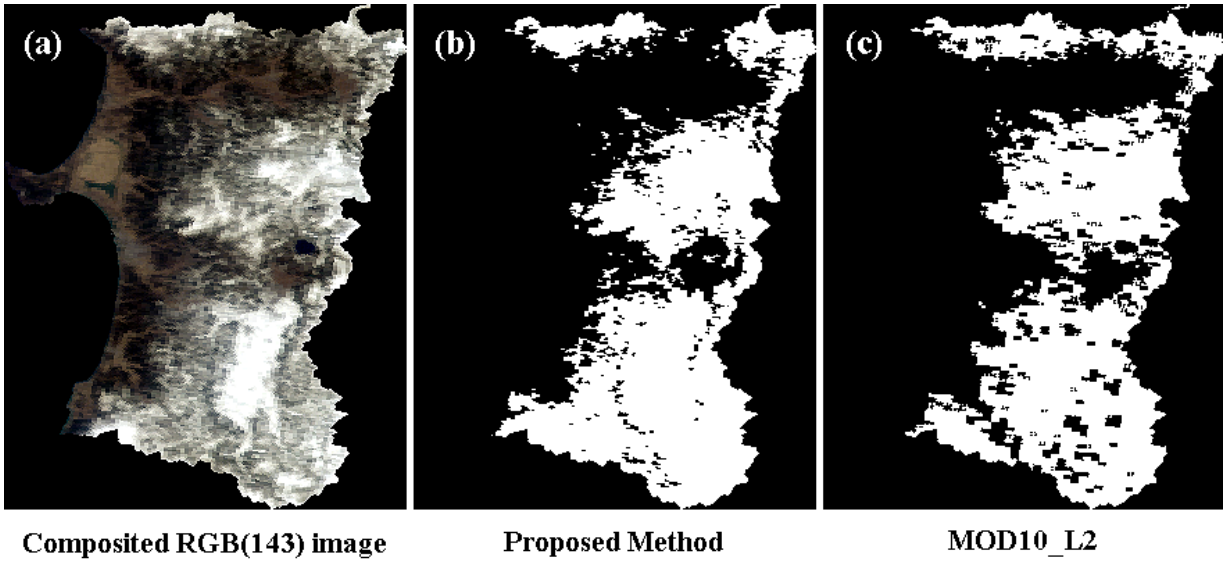

Figure 4.11: The reference image composited by RGB (1, 4, and 3) and the final results of the snow cover detection with Proposed Method (b) and MOD10_L2 (c).

From Figure 4.11 (a), it can be seen that there is snow cover in the forest and basin areas of the inland, but no snow cover in the coastal area including Oga Peninsula and the Tazawa Lake. There are some black flecks which represent that the snow pixels are not detected out near the Yokote (RSIS), Jumonji, Yuzawa (RSIS), Yokote (AMeDAS) and Yuzawa (AMeDAS) observation stations in Figure 4.11 (c), while the proposed method has detected the snow pixels of these areas out in Figure 4.11 (b), consistent with (a). Furthermore, there are also some black cracks near the Jinego observation station in Figure 4.11 (c), because of the snow pixels are not detected out.

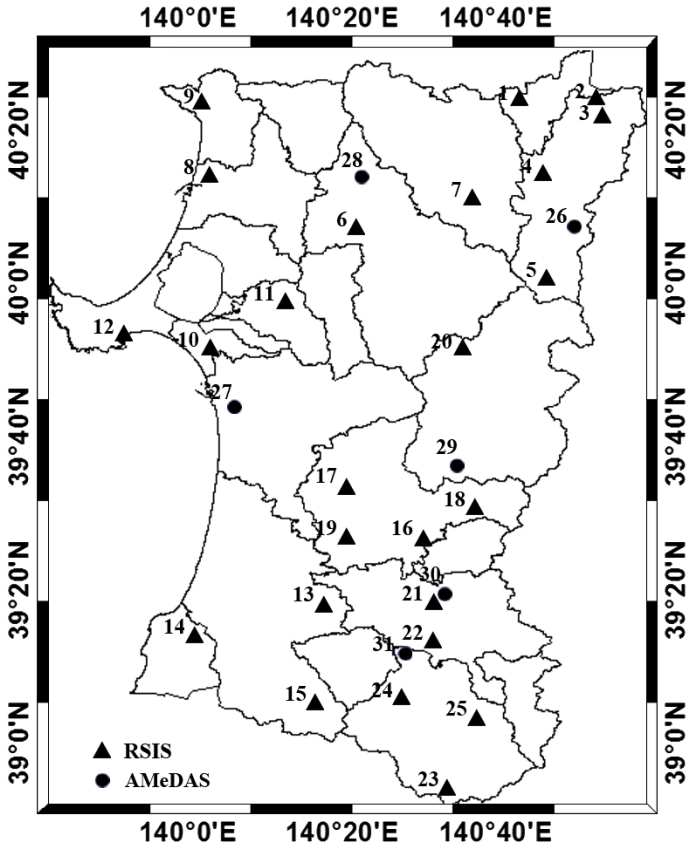

Figure 4.12: Distribution of the 31 snow depth observation sensors across the entire Akita prefecture (▲: Location of snow depth observation sensors from RSIS which have 25 observation sensors in all; ●: Location of snow depth observation sensors from AMeDAS which have 6 observation sensors in all).

On the contrary, the proposed method has detected the snow pixels of these regions in Figure 4.11 (b). It demonstrates that snow cover pixels of the study area can be detected out more accurately than MOD10_L2 according to the visual judgment.

In this work, AMeDAS snow depth data from the 6 observation stations and RSIS snow

Table 4.13: The detailed information of 31 observation stations across the entire prefecture.

Station ID Numbers	Data Type	Station Name	Station Name Abbreviation	Latitude (º North)	Longitude (º East)	Start Year
1	RSIS	Furutoobe	Fur.	40.31	140.75	1996
2	RSIS	Hakka	Hak.	40.40	140.92	1996
3	RSIS	Nakataki	Nak.	40.37	140.89	1996
4	RSIS	Towadaminami	Tow.	40.26	140.76	1996
5	RSIS	Toroko	Tor.	40.13	140.79	1996
6	RSIS	Yonaizawa	Yon.	40.04	140.55	1996
7	RSIS	Tokko	Tok.	40.19	140.60	1996
8	RSIS	Noshiro	Nos.	40.23	140.02	1997
9	RSIS	Hachimori	Hac.	40.37	140.02	1997
10	RSIS	Showa	Sho.	39.86	140.05	1997
11	RSIS	Takahi	Tak.	39.96	140.21	1997
12	RSIS	Funagawa	Fun.	39.89	139.84	1997
13	RSIS	Tateai	Tat.	39.31	140.30	1996
14	RSIS	Kamagadai	Kam.	39.24	140.03	1996
15	RSIS	Jinego	Jin.	39.10	140.28	1996
16	RSIS	Omagari	Oma.	39.45	140.48	1997
17	RSIS	Kariwano	Kar.	39.54	140.37	1997
18	RSIS	Ota	Ota	39.45	140.55	1997
19	RSIS	Nangai	Nan.	39.48	140.47	1997
20	RSIS	Tozawa	Toz.	39.86	140.57	1997
21	RSIS	Yokote	Yok.	39.30	140.53	1997
22	RSIS	Jumonji	Jum.	39.22	140.53	1997
23	RSIS	Akinomiya	Aki.	38.94	140.55	1996
24	RSIS	Yuzawa	Yuz.	39.16	140.49	1996
25	RSIS	Minase	Min.	39.06	140.63	1996
26	AMeDAS	Kazuno	Kaz.	40.22	140.79	1977
27	AMeDAS	Akita	Aki.	39.72	140.10	1998
28	AMeDAS	Takanosu	Tak.	40.23	140.37	1977
29	AMeDAS	Kakunodate	Kak.	39.60	140.56	1977
30	AMeDAS	Yokote	Yok.	39.32	140.56	1977
31	AMeDAS	Yuzawa	Yuz.	39.19	140.46	1985

Note: RSIS: Road Snow Information System

AMeDAS: Automated Meteorological Data Acquisition System

depth data from the 25 observation stations have been selected, which are Furutoobe, Hakka, Nakataki, Towadaminami, Toroko, Yonaizawa, Tokko, Noshiro (RSIS), Hachimori, Showa, Takahi, Funagawa, Tateai, Kmagadai, Jinego, Omagari, Kariwano, Ota, Nangai, Tozawa,

Yokote (RSIS), Jumonji, Akinomiya, Yuzawa (RSIS), Minase, Kazuno, Akita, Takanosu, Kakunodate, Yokote (AMeDAS) and Yuzawa (AMeDAS). Figure 4.12 shows the spatial geographic distributions of these 31 snow depth observation stations in the Akita prefecture.

Table 4.13 lists the detailed information of 31 snow depth observation stations, including the station ID numbers, data type, station name, station name abbreviation, latitude, longitude and start observation years.

Table 4.14. The snow cover detection results from in-situ Data (I), Proposed Method (II), MOD10_L2 (III) on April 2, 2014.

Station ID	Station Name	I	II	III	Station ID	Station Name	I	II	III
1	Furutoobe	65	0	0	17	Kariwano	7	1	0
2	Hakka	207	1	1	18	Ota	12	1	1
3	Nakataki	125	1	1	19	Nangai	56	1	1
4	Towadaminami	0	0	0	20	Tozawa	166	1	1
5	Toroko	195	1	0	21	Yokote	62	1	0
6	Yonaizawa	0	1	1	22	Jumonji	61	1	0
7	Tokko	0	0	0	23	Akinomiya	105	1	0
8	Noshiro	0	0	0	24	Yuzawa	45	1	0
9	Hachimori	0	0	0	25	Minase	156	1	1
10	Showa	0	0	0	26	Kazuno	0	0	0
11	Takahi	0	0	0	27	Akita	0	0	0
12	Funagawa	0	0	0	28	Takanosu	0	0	0
13	Tateai	56	1	0	29	Kakunodate	10	1	0
14	Kamagadai	42	1	0	30	Yokote	47	1	1
15	Jinego	116	1	0	31	Yuzawa	31	1	1
16	Omagari	38	1	1					

Note: I: Records of Snow Depth (cm) from In-situ Data "1": Snow covered

II: Results from Proposed Method "0": Snow Free

III: Results from MOD10_L2

Table 4.14 shows the comparison results of the in-situ data, the proposed method and MOD10_L2 product for the snow cover detection in the study area on April 2, 2014. In this table, I is the records of the RSIS and AMeDAS snow depth, II is the results from proposed method, III is the results from MOD10_L2 products. Meanwhile, “1” represents snow covered and “0” represents snow free.

From Table 4.14, it can be seen that there are snow cover pixels in the observation stations

of Toroko, Tateai, Kamagadai, Jinego, Kariwano, Yokote (RSIS), Jumonji, Akinomiya, Yuzawa (RSIS) and Kakunodate with the proposed method. But there are no snow cover pixels on these observation stations from the MOD10_L2 product.

In Furutoobe, the snow cover depth is 65 cm from the RSIS data of in-situ data, but there are not any snow cover pixels to be detected out by both the proposed method and MOD10_L2 products. In Yonaizawa, there is no snow over from the RSIS data of in-situ data, oppositely both the proposed method and MOD10_L2 product have detected snow cover pixels out wrongly.

In order to further compare and evaluate the accuracies of the snow cover detection results with the proposed method and MOD10_L2, the following validation method as Table 4.15 shown is adopted.

Table 4.15. The validation method for the snow cover detection results.

Date	In-situ Observation Station	
Proposed Method/MOD10_L2	Snow	Snow-Free
Snow	a	b
Snow-Free	c	d

In which,

a = where both the proposed method or MOD10_L2 and the in-situ observation stations detect snow;

b = where the in-situ observation stations detect snow-free and the proposed method or MOD10_L2 detects snow;

c = where the in-situ observation stations detect snow and the proposed method or MOD10_L2 detects snow-free;

d = where both the proposed method or MOD10_L2 and the in-situ observation stations detect snow-free;

Overall accuracy, over-estimation error and under-estimation error are calculated according to the following equations applying the above parameters in Table 4.15.

$$Overall\ Accuracy = \frac{a+d}{a+b+c+d} \tag{17}$$

$$Over-estimation\ Error = \frac{b}{a+b+c+d} \tag{18}$$

$$Under-estimation\ Error = \frac{c}{a+b+c+d} \tag{19}$$

Based on the above validation method and the snow cover detection results of Table 4.14, the overall accuracy, over-estimation error and under-estimation error of the proposed method are calculated, which are 93.55%, 3.23% and 3.23% respectively, and overall accuracy, over-estimation error and under-estimation error of the MOD10_L2 product are 61.29%, 3.23% and 35.48% respectively. It suggests that the snow cover detection accuracy of the proposed method is higher than MOD10_L2 products, and the under-estimation error of MOD10_L2 is greatly higher than the proposed method.

Table 4.16: The accuracy comparisons of the proposed method and the MOD10_L2 products

No.	Japan Standard Time		Proposed Method			MOD10_L2		
	Date	Time	Overall Accuracy (%)	Over-estimation Error (%)	Under-estimation Error (%)	Overall Accuracy (%)	Over-estimation Error (%)	Under-estimation Error (%)
1	January 23, 2013	10:10	100.00	0.00	0.00	54.84	0.00	45.16
2	February 1, 2013	10:05	100.00	0.00	0.00	93.55	0.00	6.45
3	April 9, 2013	10:35	74.19	3.23	22.58	48.39	3.23	48.39
4	April 16, 2013	10:40	67.74	0.00	32.26	58.06	3.23	38.71
5	March 4, 2014	10:30	100.00	0.00	0.00	61.29	0.00	38.71
6	April 1, 2014	10:55	87.10	0.00	12.90	61.29	6.45	32.26
7	April 2, 2014	10:00	93.55	3.23	3.23	61.29	3.23	35.48

In order to further compare the snow cover detection accuracies of these two methods, results of the overall accuracy, overestimation error and under-estimation error during the snowy season from May 2012 to April 2014 are calculated and listed as shown in Table 4.16.

It is clear to see that the overall accuracy of the proposed method is all higher than the MOD10_L2 products. Over-estimation errors of the proposed method are lower than or equal to the MOD10_L2 products. Under-estimation errors of the proposed method are all much lower than the MOD10_L2 products. The average values of the overall accuracy, over-estimation error and under-estimation error are 88.94%, 0.92% and 10.14% respectively from the proposed method, and are 62.67%, 2.30% and 35.02% respectively from the MOD10_L2 product. Based on above results, we can know that the average overall accuracy of the proposed method is higher than MOD10_L2 product, improved by 26.27%. These results fully prove that the effectivity of the proposed method for the snow cover detection in this work.

In order to further verify and analyze the snow cover detection results, in this work, all of the 31 observation stations across the whole study area are divided into three types according to the longitude and latitude locations of themselves, which are the forest regions (Furutoobe, Hakka, Nakataki, Yonaizawa, Takahi, Funagawa, Tateai, Kamagadai, Jinego, Tozawa, Akinomya, Minase and Kazuno), the plain regions (Towadaminami, Tokko, Toroko, Noshiro, Hachimori, Showa, Kariwano and Akita), and the basin regions (Omagari, Ota, Nangari, Yokote (RSIS), Jumonji, Yuzawa (RSIS), Takanosu, Kakunodate, Yokote (AMeDAS) and Yuzawa (AMeDAS)). Figure 4.17 shows the overall accuracy, over-estimation error and under-estimation error comparison results of these 31 observation stations based on the above three types of regions from the proposed method and the MOD10_L2 products during the snowy season from May 2012 to April 2014.

From Figure 4.17, it can be seen that there is almost no over-estimation errors for both the proposed method and the MOD10_L2 products in the plain, basin and forest regions except the Yonaizawa and Takahi in the forest areas. According to the principle of the proposed method, the reflectance of the substances is similar in visible bands 1 and 3. The reflectance of snow is much higher than other any substances, and the following is the soil.

The maximum reflectance value of the soil is defined as the threshold value, which is higher than the reflectance of other any substances excluding snow. Therefore, the pixels of other substances are difficult to be detected out as snow pixels. For MOD10_L2 products, the reflectance of snow in visible green band 4 is higher than that in short infrared band 6, while other substances in these two bands are just opposite. Only the snow pixels can be detected out with normalized difference ratio of NDSI. So the pixels of other substances are also difficult to be detected out as snow pixels.

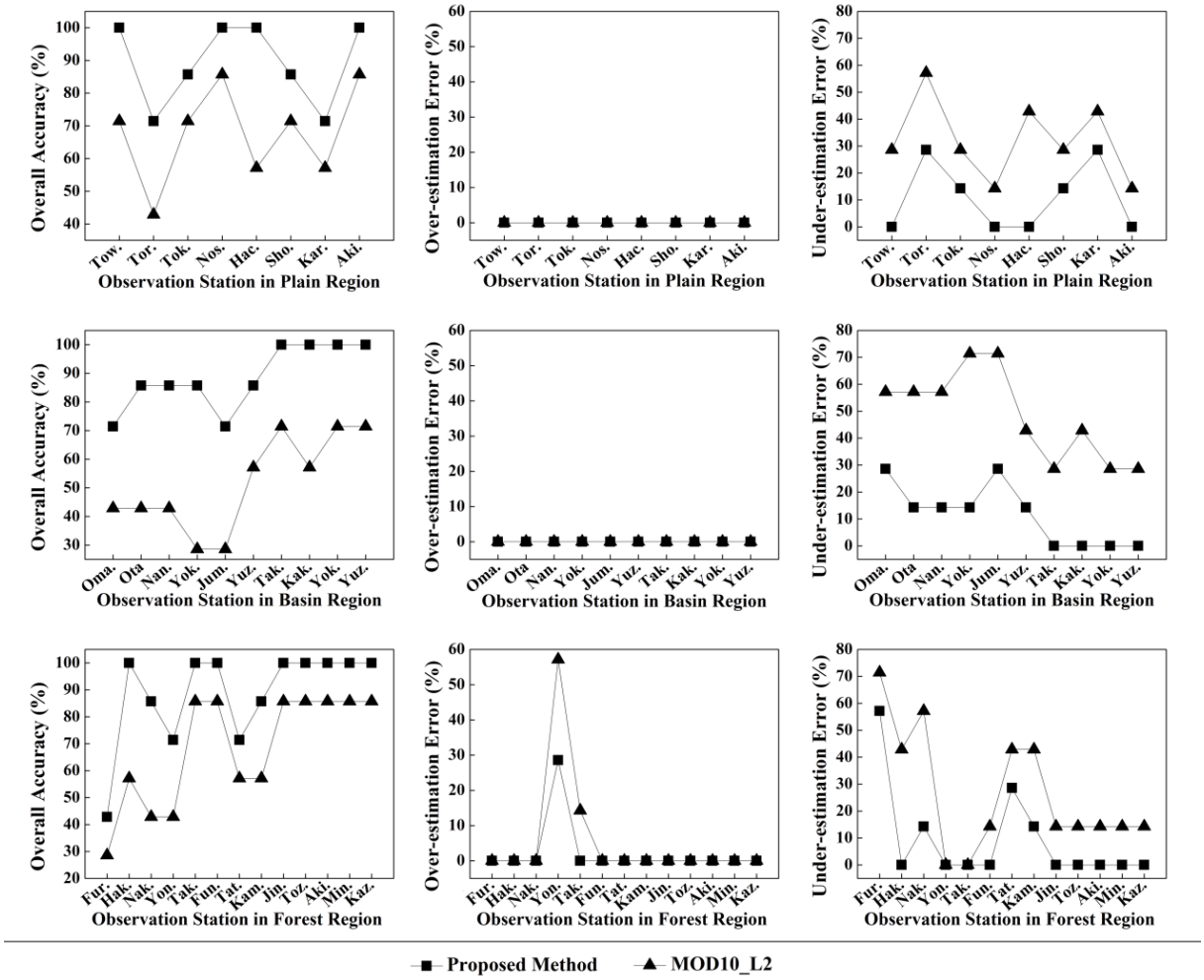

Figure 4.17: The comparison results of the overall accuracy, over-estimation error and under-estimation error from the proposed method and the MOD10_L2 products in the study area based on the types of regions.

However, there are over-estimation errors in Yonaizawa for these two methods and in Takahi for only MOD10_L2 products. It may be due to the following three reasons: first, in the present study, the MODIS 500 m image data are the coarse accuracy images. One pixel represents the actual area is from several kilometers to over ten kilometers. Therefore, there are mixed pixels in forest areas; second, the ground observation data used in this work are snow depth sensor observation data. It mainly based on the location of sensors. In mixed pixels, it is only one specific position. If there is no snow cover pixel in this position, it may be also detected out as snow pixel in other position; third, the Yonaizawa observation station locates in the southeast corner of the Takanosu Basin and is adjacent to the northeast corner of the Taihei Mountains. For MOD10_L2 products, snow pixels are detected with the

combination of NDSI and NDVI, the vegetation area is first recognized with NDVI, then the NDSI value is decreased to detect the snow cover pixels of forest areas. Therefore, the mixed pixels may be detected out as snow pixels wrongly. Moreover, the Takahi observation station locates in the northeast corner of the Akita Plain and is adjacent to the northwest corner of the Taihei Mountains. It belongs to coastal area. There are a lot of agricultural lands near the observation station. Therefore, the pixel may be the mixed pixel of agricultural, forest and snow.

From Figure 4.17, we can also know that there are many under-estimation errors of the snow cover detection results from both the proposed method and the MOD10_L2 products in the plain, basin and forest regions. The average under-estimation error of basin areas is the largest, and the following are the plain areas and forest areas respectively. But, the errors of the proposed method are less than MOD10_L2 products, because the terrain variations in basin and plain areas are less than that in forest areas. Both the proposed method and the MOD10_L2 products have only considered the terrain variations of forest areas during the process of the snow cover detection, so the errors of under-estimation in forest areas are relatively lower than the errors of under-estimation in other two types of regions. However, comparing the terrain variations of basin and plain, we can know that the terrain variations in basin areas are more than that of plain areas, which can lead to much higher errors in basin areas during the process of the snow cover detection.

In addition, the topographic correction is conducted in the proposed method, so the under-estimation error of the proposed method is lower than MOD10_L2 products. The proposed method can detect the snow cover pixels out more accurately than MOD10_L2 products. Therefore, it is feasible and effective to use the proposed method for the snow cover detection in Akita prefecture.

4.4. Snow cover detection based on two-dimensional scatter plots from MODIS imagery data

4.4.1. Methodology

In this work, the MODIS/Terra calibrated radiances 5-Min L1B Swath 500 m (MOD02HKM) product and the MODIS/Terra snow cover daily L3 Global 500 m Grid (MOD10A1) product data are applied. MOD02HKM belongs to the MODIS Level 1B dataset, and MOD10A1 belongs to the MODIS Level 3 dataset. MODIS Level 1B data are obtained

from the Level 1 and atmosphere archive and distribution system (LAADS) website [57]. MODIS Level 3 data are obtained from the next generation metadata and service discovery tool "Reverb" website of Earth observing system data and information system (EOSDIS), NASA [109].

The entire process of snow cover detection is divided into two steps: preprocessing and postprocessing, as shown in Figure 4.18. In preprocessing, the MOD02HKM data are used for geographic correction, study area clipping, atmospheric correction, and topographic correction. Snow and cloud detection are conducted during the postprocessing stage. Spectral band 1 (red: 0.620 to 0.670 μm) and band 3 (blue: 0.459 to 0.479 μm) are used to extract the snow and cloud from other ground surface features in the snow detection model, while spectral band 6 (SWIR: 1.628 to 1.652 μm) and band 7 (SWIR: 2.105 to 2.155 μm) are used to detect cloud and remove it from snow in the cloud detection model. Finally, the snow cover map of Akita Prefecture is obtained.

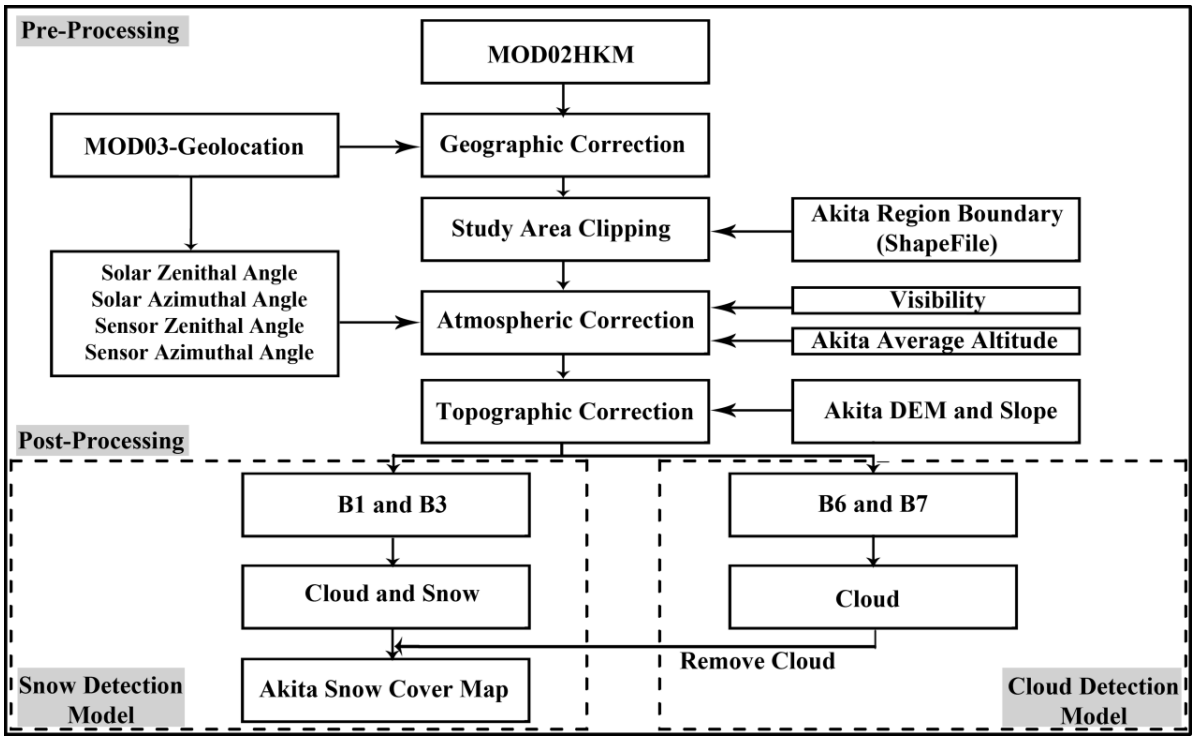

Figure 4.18: Flowchart of snow cover detection in Akita Prefecture using MODIS data.

4.4.2. Extraction of Snow and Cloud

The real ground surface reflectance in the target area can be obtained after completion of the above preprocessing methods. Figure 4.19 shows spectral reflectance curves for different

types of ground surface features in Akita Prefecture. The spectral curve of water is derived from the digital spectral library splib06a of the USGS Spectroscopy Lab [110], [111]. The spectral curves of snow, conifer, deciduous, grasses, soil, and cloud are derived from the advanced spaceborne thermal emission reflectance radiometer (ASTER) Spectral Library released on December 3, 2008. The ASTER Spectral Library is available from the SpecLib website [112], and includes data from the Johns Hopkins University Spectral Library, the jet propulsion laboratory Spectral Library, and the United States Geological Survey (USGS-Reston) Spectral Library [113].

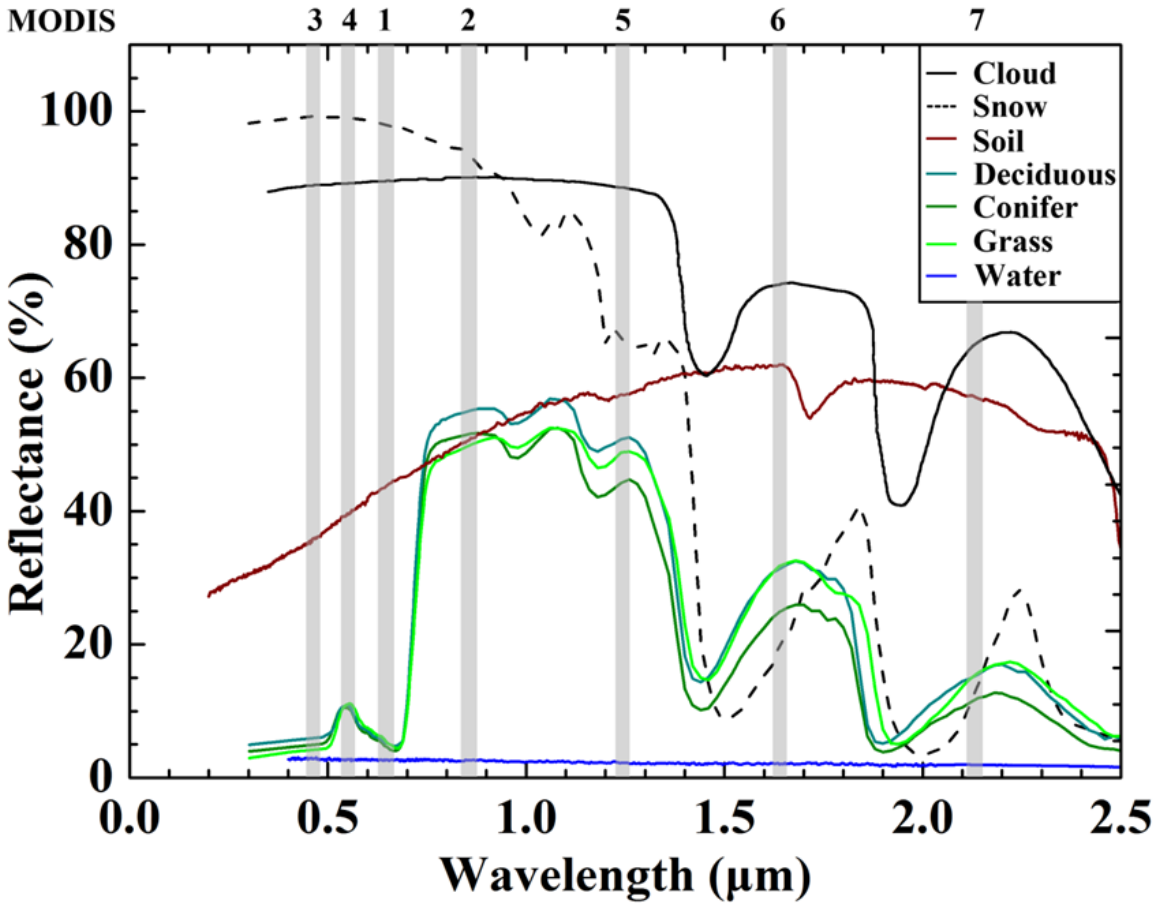

Figure 4.19: The spectral curves for cloud, snow, soil, deciduous, conifer, grass, and water.

From Figure 4.19, the reflectance spectra of different substances can be clearly distinguished in visible red band 1, blue band 3, and green band 4 (0.545 to 0.565 μm). In this region, the reflectance of snow is highest, followed in order by cloud, soil, and vegetation (grass, conifer, and deciduous). Vegetation has a much lower reflectance in this region

because of the strong chlorophyll absorption among these three wavelengths. The reflectance of water is the smallest of all the tested substances at only 5%. As green vegetation shows a small reflectance peak in band 4, there may be some difficulties in the identification of mixed snow and green vegetation pixels at this wavelength. Therefore, bands 1 and 3 are used to detect and distinguish snow and cloud pixels from other ground surface features. It should be noted that the reflectance of cloud in Figure 4.19 is representative of the reflectance over dark surfaces. When cloud occurs over a bright snow surface, the reflectance of the cloud must be higher. However, as described above, we can assume that there is no cloud shadow over the snow because only data from predominantly sunny days (in which cloud cover accounts for less than 5% of study area) are selected for snow cover detection in this work.

In this study, the pixel purity index (PPI) is used to extract pure pixels for the different features during the selection of training data pixels. The training data are selected from June 2009 to May 2010, with 10 “pure” pixels being selected for each feature in every sunny day image.

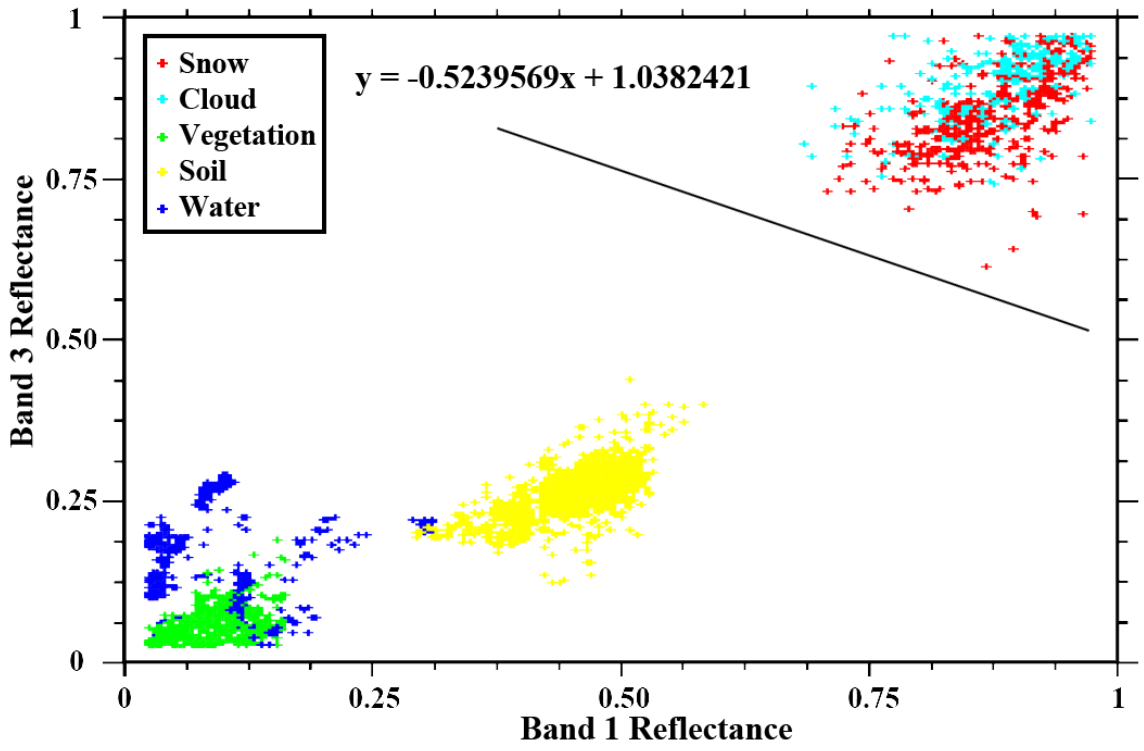

Figure 4.20: Two-dimensional (2-D) scatter plot of bands 1 and 3 reflectances.

Figure 4.20 shows a two-dimensional (2 D) scatter plot of the above-described pure pixels,

representing the reflectance of cloud, snow, soil, vegetation, and water in bands 1 and 3. Most substances are slightly distributed below a diagonal trend stretching from the top right to the bottom left of the plot. Cloud and snow have the highest values, and are located at the top right of the plot. Soils occupy the second highest values and are located near the center of the plot. Vegetation and water collectively have the lowest values and are located near the origin. There is a clear blank region between the cloud and snow pixels and the soil pixels, therefore, a threshold line can be drawn in order to extract cloud and snow pixels from pixels of other ground surface features.

The threshold line can be calculated according to the following equation:

$$y = a_{13}x + b_{13} \quad , \tag{20}$$

Where

$$a_{13} = \left(\left[(Band_3)_{\min} - (Band_3)_{\max} \right] / \left[(Band_1)_{\max} - (Band_1)_{\min} \right] \right) \quad , \tag{21}$$

$$b_{13} = (Band_3)_S + \left((Band_1)_S \times \left[(Band_3)_{\max} - (Band_3)_{\min} \right] \right) / \left[(Band_1)_{\max} - (Band_1)_{\min} \right] \tag{22}$$

$$(Band_1)_S = (Band_1)_{\min} + \left[(Band_1)_{\max} - (Band_1)_{\min} \right] \times \text{soil reflectance of } Band_1 , \tag{23}$$

$$(Band_3)_S = (Band_3)_{\min} + \left[(Band_3)_{\max} - (Band_3)_{\min} \right] \times \text{soil reflectance of } Band_3 , \tag{24}$$

Where $(Band_1)_{\min}$, $(Band_1)_{\max}$, $(Band_3)_{\min}$, and $(Band_3)_{\max}$ are the minimum and maximum values of band 1 and band 3 reflectances (excepting 0), respectively, and $(Band_1)_S$ and $(Band_3)_S$ are the digital number (DN) values of soil in band 1 and band 3, respectively.

Soil reflectances in band 1 and band 3 are 44% and 36%, respectively, calculated from Figure 4.19 in this study.

4.4.3. Detection and Removal of Cloud

As seen in Figure 4.20, it is difficult to detect and remove the cloud pixels from the cloud and snow pixel mixture based solely on the 2 D scatter plot of bands 1 and 3, as their reflectances are similar. However, the reflectance of snow is similar to that of other ground surface features in bands 6 and 7 and is distinct from the reflectance of cloud at these wavelengths.

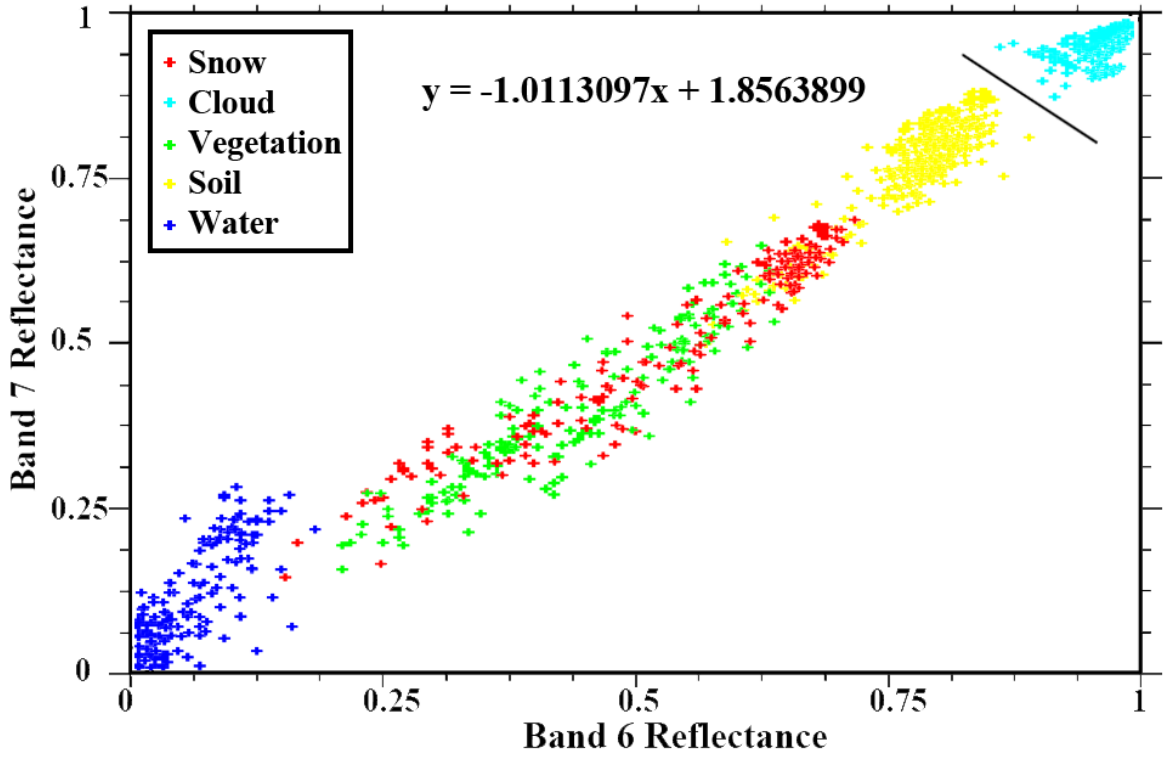

Figure 4.21: Two-dimensional scatter plot of bands 6 and 7 reflectances.

Figure 4.21 shows a 2-D scatter plot of the reflectance of cloud, snow, soil, vegetation, and water in bands 6 and 7. Training data are selected from June 2009 to May 2010, and 10 pixels are chosen from the images for each sunny day. All substances are roughly distributed along a diagonal from the origin to the top right of the chart. Cloud has the highest reflectance in both bands, located at the top right of the chart, followed by soil. Snow, vegetation, and water have the lowest values and are located within the lower quadrant of Figure 4.21. From this figure, a clear separation between cloud and soil pixels can be seen, and a threshold line can be drawn that allows cloud to be extracted from the pixels of other ground surface features.

The threshold line can be calculated with to the following equation:

$$y = a_{67}x + b_{67}, \tag{25}$$

where

$$a_{67} = \left[(Band_7)_{min} - (Band_7)_{max}\right] / \left[(Band_6)_{max} - (Band_6)_{min}\right], \tag{26}$$

$$b_{67} = (Band_7)_S + \left((Band_6)_S \times \left[(Band_7)_{max} - (Band_7)_{min}\right]\right) / \left[(Band_6)_{max} - (Band_6)_{min}\right], \tag{27}$$

$$(Band_6)_S = (Band_6)_{min} + \left[(Band_6)_{max} - (Band_6)_{min}\right] \times \text{soil reflectance of } Band_6, \text{ and} \tag{28}$$

$$(Band_7)_S = (Band_7)_{min} + \left[(Band_7)_{max} - (Band_7)_{min}\right] \times \text{soil reflectance of } Band_7, \tag{29}$$

where $(Band_6)_{min}$, $(Band_6)_{max}$, $(Band_7)_{min}$, and $(Band_7)_{max}$ are the minimum and maximum values of band 6 and band 7 reflectances (excepting 0), respectively, and $(Band_6)_S$ and $(Band_7)_S$ are the DN values of soil in band 6 and band 7, respectively.

Soil reflectances of band 6 and band 7 are 62% and 56%, respectively, calculated from Figure 4.19 in this study.

4.4.4. Extraction of Snow and Cloud

The Terra/MODIS image of Akita Prefecture, acquired on April 6, 2011, is adopted to verify the effectivity of the proposed method. Figure 4.22 (a) is a grayscale image of snow and cloud extracted from other ground surface features by the proposed method. The white and gray parts of the image represent snow or cloud. There is snow or cloud cover in the Kakunodate-Yashima-Yunodai-Yuzawa-Yokote area region to the southeast, to the southwest of the Yashima-Yunodai area, within the Kazuno-Aniai-Kakunodate area, in the southwest of the Oga Peninsula, in the vicinity of Towadako Lake, and in the most northwestern mountains of Akita Prefecture. This spatial distribution suggests that strong wind blows snow or cloud from coastal regions to inland mountainous areas in Akita Prefecture. Therefore, it can be concluded that there is relatively little or even an absence of snow cover in coastal areas, whereas a large amount of snow accumulates in the inland mountain and forest areas.

4.4.5. Detection and Removal of Cloud

Figure 4.22 (c) shows the binary black and white image of the cloud cover detection extracted from other ground surface features using the proposed method. In this figure, the white parts represent cloud cover. It is clear from this figure that cloud cover only occurs to the southwest of the Oga Peninsula. This result supports the suggestion that there is relatively less snow cover in coastal areas, and more in the inland mountains and forested areas.

The pseudocolor image composed of MODIS bands 1, 4, and 6 in Figure 4.22 (b) and the image obtained from the MODIS cloud mask product in Figure 4.22 (d) are shown to prove the effectiveness of the proposed cloud cover detection method. Snow has a high reflectance in visible red band 1 and green band 4, a low reflectance in SWIR band 6, and the reflectance of cloud is high in all these bands. Therefore, snow in Figure 4.22 (b) is displayed as yellow and cloud as almost white. From Figure 4.22 (d), we can explicitly see that the MODIS cloud mask product maps many pixels in the inland mountains and forested areas as cloud cover that do not appear as cloud cover in Figure 4.22 (b). Conversely, the result from the proposed method [Figure 4.22 (c)] is consistent with Figure 4.22 (b). That is to say, the MODIS cloud mask product overestimates the cloud cover area in study area. From these considerations, we can estimate that mixed snow and cloud pixels detected in coastal areas are most likely to represent cloud.

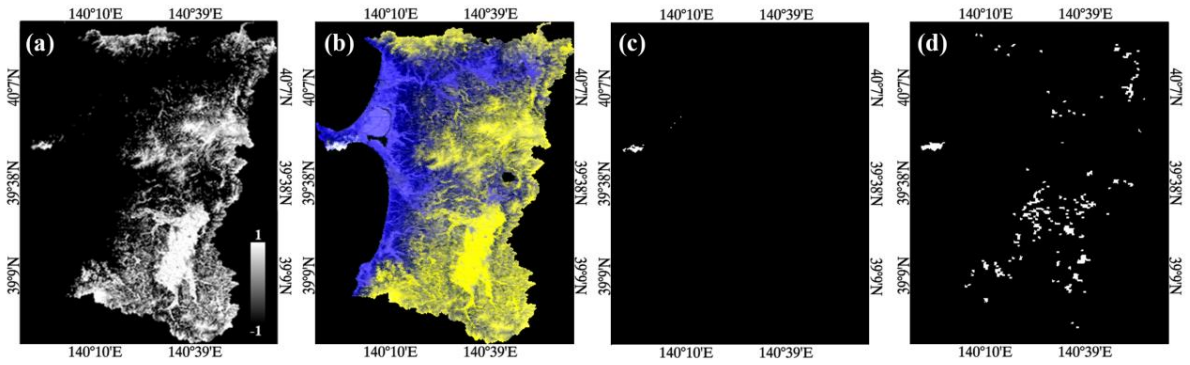

Figure 4.22: Extracted results of snow and cloud detection (a), pseudocolor image (b), image from cloud detection alone using the proposed method (c), and the result of the MODIS cloud mask product (d) (derived from the Terra/MODIS image from April 6, 2011).

4.4.6. Comparison of Cloud and No Cloud Conditions Using Aqua Satellite Image

An Aqua satellite image acquired on April 5, 2011, is adopted for comparison of reference objects in order to verify the cloud cover detection results obtained with the proposed method, as shown in Figure 4.23. Figure 4.23 (a) is the Aqua/MODIS wide area reference image from

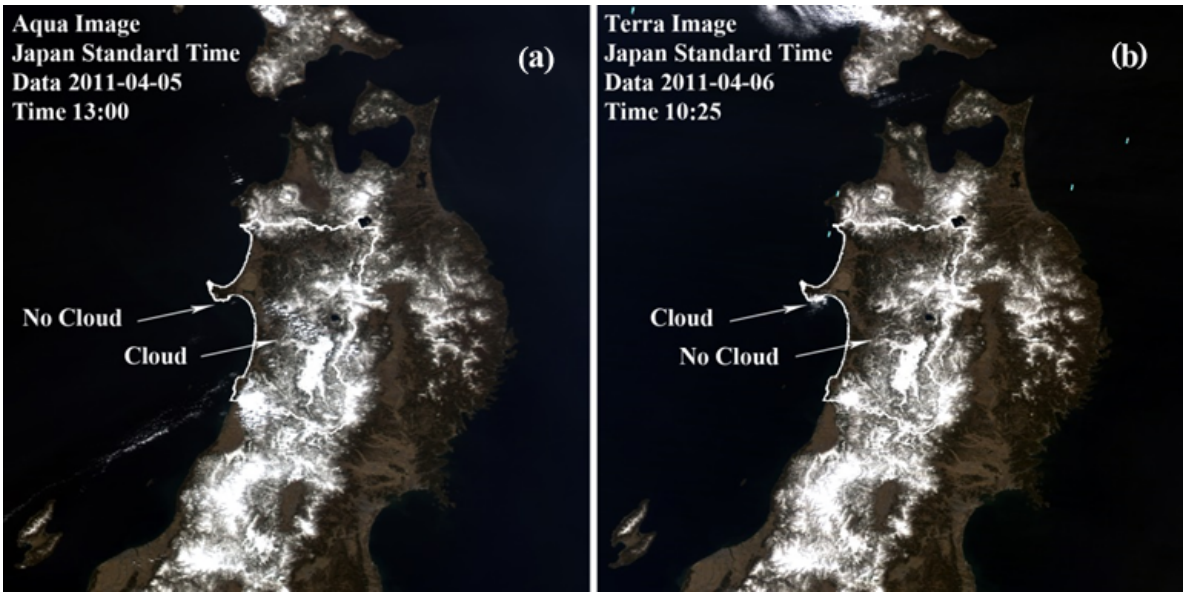

Figure 4.23: The Aqua/MODIS wide area reference image (a), and the Terra/MODIS wide area research image (b).

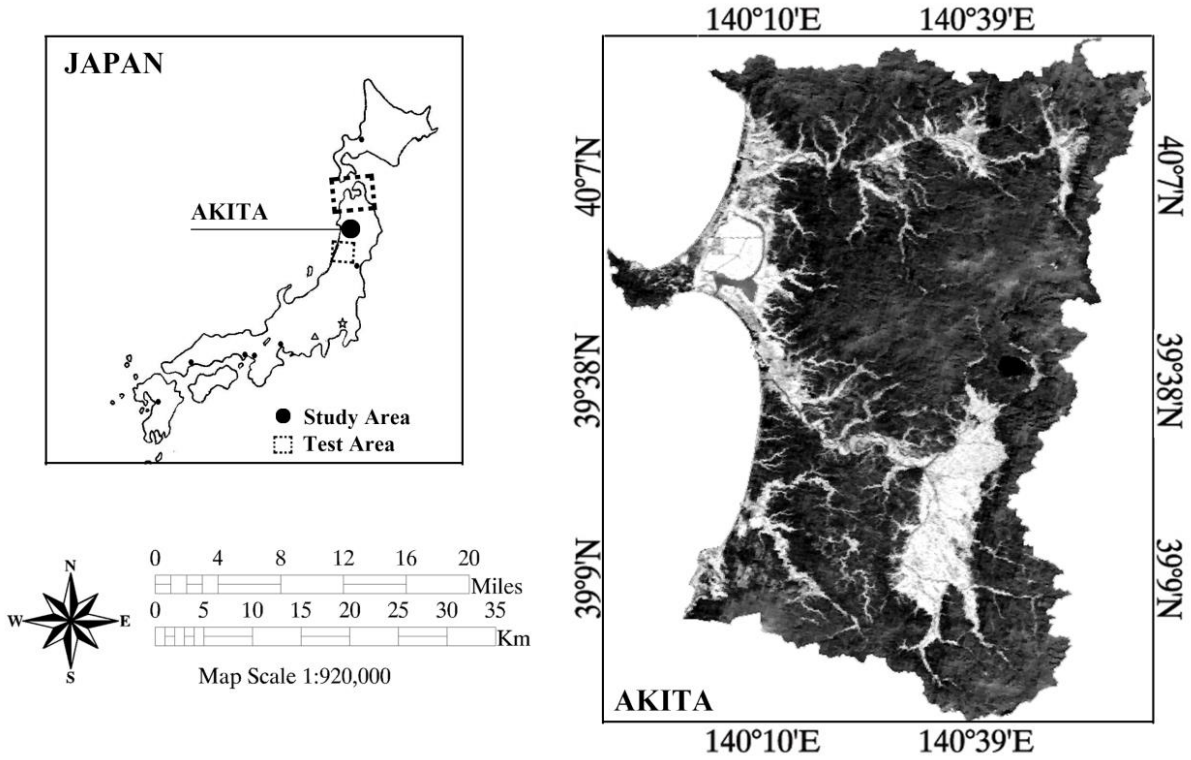

Figure 4.24: The study area of Akita Prefecture and test areas of Aomori Prefecture and Mt. Chokaizan [Left: the location of Akita Prefecture and test areas; Right: moderate resolution imaging spectroradiometer (MODIS) image of Akita Prefecture; the dark and light areas represent the presence or absence of vegetation, respectively].

13:00 (JST) on April 5, 2011, which includes Akita Prefecture, while Figure 4.23 (b) is the Terra/MODIS wide area research image from 10:25 (JST) on April 6, 2011, including Akita Prefecture. From these figures, it can be seen that there is no cloud cover over the southwest of Oga Peninsula in Figure 4.23 (a), but some clouds are present in Figure 4.23 (b). In addition, there are some convoluted clouds over Akita Prefecture in Figure 4.23 (a), but there are no such clouds in Figure 4.23 (b). In satellite images over a single area, the liquidity of clouds is greater than that of snow, and hence changes in the appearance and location of cloud on the satellite images may also be considered greater than those for snow. Therefore, it can be determined that the white areas over the southwest part of Oga Peninsula in Akita Prefecture in Figure 4.23 (b) represent cloud cover. This also supports the conclusions drawn in Chapter 4.4.5 above on cloud cover detection by the proposed method.

4.4.7. Selection of Test Areas and In-situ Data for Assessment

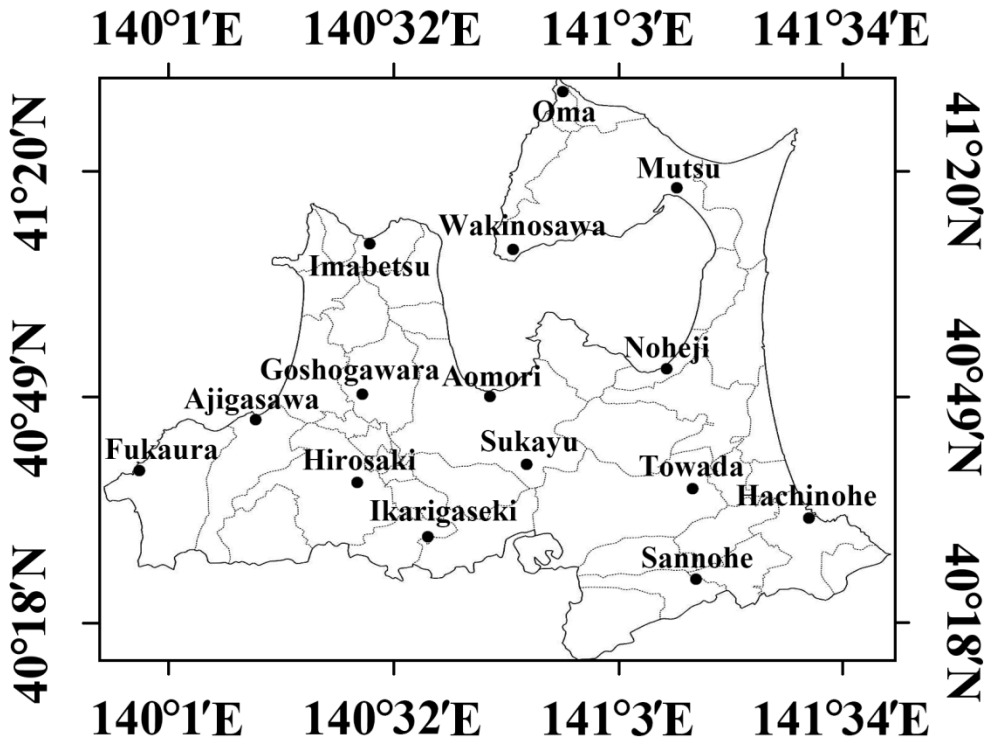

Figure 4.25: The spatial distribution of the 13 AMeDAS observation stations in Akita Prefecture (a) and the 15 AMeDAS observation stations in Aomori Prefecture (b).

Aomori Prefecture and Mt. Chokaizan, near Akita Prefecture, are selected as test areas to

verify the validity of the proposed snow cover detection method and MOD10A1 product. Their locations are marked as dotted boxes on the left-hand map in Figure 4.24. Aomori Prefecture is located in the northeast of Japan, between 40°13′04″N and 41°33′22″N, and 139°29′49″E and 141°41′00″ E [114], and the Mt. Chokaizan area is also located in the northeast of Japan, between 38°59′47.55″N and 39°12′12.75″N, and 139°54′56.65″E and 140°11′8.65″E.

In this study, AMeDAS snow depth data from the 13 observation stations in Akita Prefecture [Figure 2.5] and the 15 observation stations in Aomori Prefecture [Figure 4.25] are selected to allow for the practical objective judgment of snow depth, and to compare the snow cover results with those from the proposed method.

4.4.8. Comparison of Results with Previous Methods

The snow cover detection results from the MOD10A1 product, and the combination of NDSI and NDVI, are compared with those from the proposed method to confirm its relative effectiveness. The snow cover detection results from the combination of NDSI and NDVI are calculated using Equations (15) and (16) according to two groups of criteria. In one group, the value of $NDSI$ is greater than 0.45, $Band_2$ is greater than 0.11, and $Band_4$ is greater than 0.10. In the other group, for forested areas, the value of $NDVI$ is greater than 0.3, the value of $NDSI$ is greater than 0.38, $Band_2$ is greater than 0.11, and $Band_1$ is greater than 0.1.

Figure 4.26 shows the RGB composite image and the comparison images from snow cover detection results, all from 10:25 (JST) on April 6, 2011 [Figure 4.26 (a) shows the proposed method, Figure 4.26 (b) the MOD10A1 product, and Figure 4.26 (c) the combination of NDSI and NDVI]. Table 4.27 shows the 13 AMeDAS snow depth records from April 6, 2011, along with their latitudes, longitudes, and altitudes. From Figure 4.26 (b) and Table 4.27, it can be seen that snow cover is underestimated in Kakunodate using the MOD10A1 product. This is because Kakunodate (39°36.2′N, 140°33.4′E) is located within the northwest corner of the Yokote Basin, which connects to the easternmost part of the Taiheizan and Dewa Mountains. This region contains large areas of forest, therefore the reflectance of snow can be masked by the more dominant reflectance of forests. In addition, the MOD10A1 product is developed from a fractional snow algorithm and is mainly based on a snow-mapping algorithm that employs NDSI and other criteria that are designed to maximize snow detection

sensitivity over vegetation recognition. As a result, snow pixels are not detected, leading to an error in snow cover estimation.

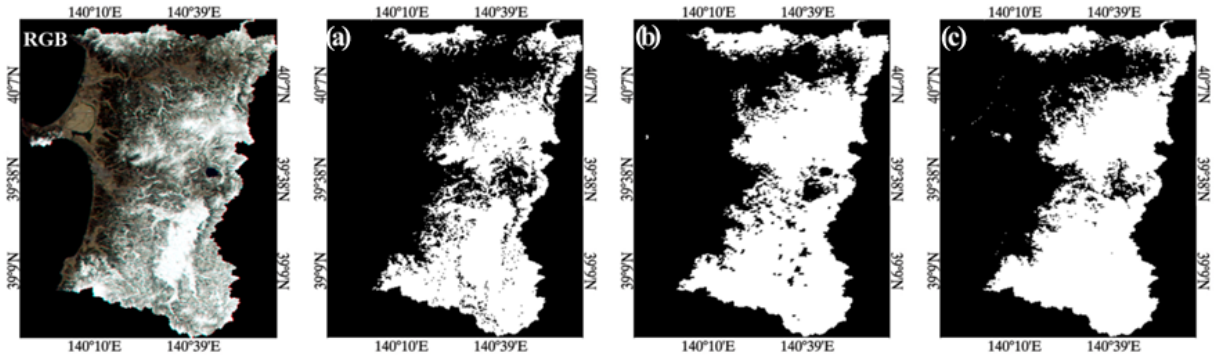

Figure 4.26: Comparison images for snow cover detection results from 10:25 (JST) on April 6, 2011, using (a) the proposed method, (b) the MOD10A1 product, and (c) normalized difference snow index (NDSI) and normalized difference vegetation index (NDVI).

Table 4.27: Snow detection results' comparison for the three methods, from April 6, 2011.

Stations	Latitude (N)	Longitude (E)	Altitude (m)	AMeDAS	April 6, 2011		
					a	b	c
Kazuno	40°12.9′	140°47.2′	123	0	0	0	0
Yunodai	38°57.6′	140°31.7′	335	84	1	1	1
Aniai	39°59.6′	140°24.2′	120	42	1	1	1
Noshiro	40°11.9′	140°1.9′	6	0	0	0	1
Akita	39°43′	140°5.9′	6	0	0	0	0
Honjo	39°21.6′	140°3.3′	11	0	0	0	0
Takanosu	40°13.6′	140°22.3′	29	0	0	0	0
Kakunodate	39°36.2′	140°33.4′	56	5	1	0	1
Yokote	39°19.2′	140°33.3′	59	18	1	1	1
Yuzawa	39°11.2′	140°27.8′	74	64	1	1	1
Gojome	39°56.3′	140°6.9′	6	0	0	0	1
Yashima	39°14.1′	140°8.2′	46	40	1	1	1
Taishouji	39°31.6′	140°14′	20	0	0	0	0

Note: AMeDAS: Records of Snow Depth (cm) from AMeDAS 0: Snow Free
a: Results from proposed method 1: Snow Covered
b: Results from MOD10A1 product
c: Results from the combination of NDSI and NDVI

It can also be seen from Figure 4.26 (c) and Table 4.27 that the snow cover is overestimated in the region of the Gojome-Noshiro-Oga Peninsula when using the

combination of NDSI and NDVI.

This is due to the Gojome observation station being located at the junction of the Akita Plain and the westernmost Taiheizan Mountains. In this region, there are mountains and rich forests to the east, and large areas of urban development known as Hachirougata Choseichi to the west. Hachirougata Choseichi was once the second largest lake in Japan, after Pipa Lake, but is now a large expanse of agricultural land planted with crops for increased food production. The Noshiro observation station is located in the middle of Noshiro Plain to the south of Yoneshiro River and is mostly flat terrain that faces the Sea of Japan to the west. Both Gojome and Noshiro are located in coastal areas and, owing to the strong sea wind, any potential snow is soon blown inland. Therefore, no snow has been recorded at these two observation stations. However, the method of combined NDSI and NDVI is not only sensitive to snow reflectance, but also to vegetation reflectance. While there are no snow depth records from Gojome and Noshiro observation stations, some snow or vegetation may exist in the areas around them. This may lead to the satisfaction of the conditions for the combined NDSI and NDVI method, leading to the incorrect detection of snow pixels and resulting in the overestimation of snow cover. In contrast to the shortcomings of the MOD10A1 product and the combined NDSI and NDVI results, barely any underestimation or overestimation is seen in the snow cover detection results from the proposed method. This suggests that the snow cover detection results from the proposed method are consistent with the real snow cover situation.

Terra/MODIS image data from 15 days between November 19, 2011, and April 21, 2012, each with cloud cover below 5%, are used to further verify the accuracy of the proposed method.

Figure 4.28 shows comparison graphs of the snow cover detection results from the three methods and the AMeDAS snow depth data from the 13 observation stations on these 15 different days. As Figure 4.28 illustrates, the average accuracies of the proposed method, the MOD10A1 product, and the combination of NDSI and NDVI are 91.28%, 70.26%, and 79.49%, respectively, for the 15 different chosen dates. Similarly, the average accuracies of the proposed method, the MOD10A1 product, and the combination of NDSI and NDVI are 91.28%, 79.49%, and 69.23%, respectively, across the 13 observation stations.

In order to further compare the possible snow cover detection methods, the 13 observation stations are divided into three groups according to their location and terrain type: mountain

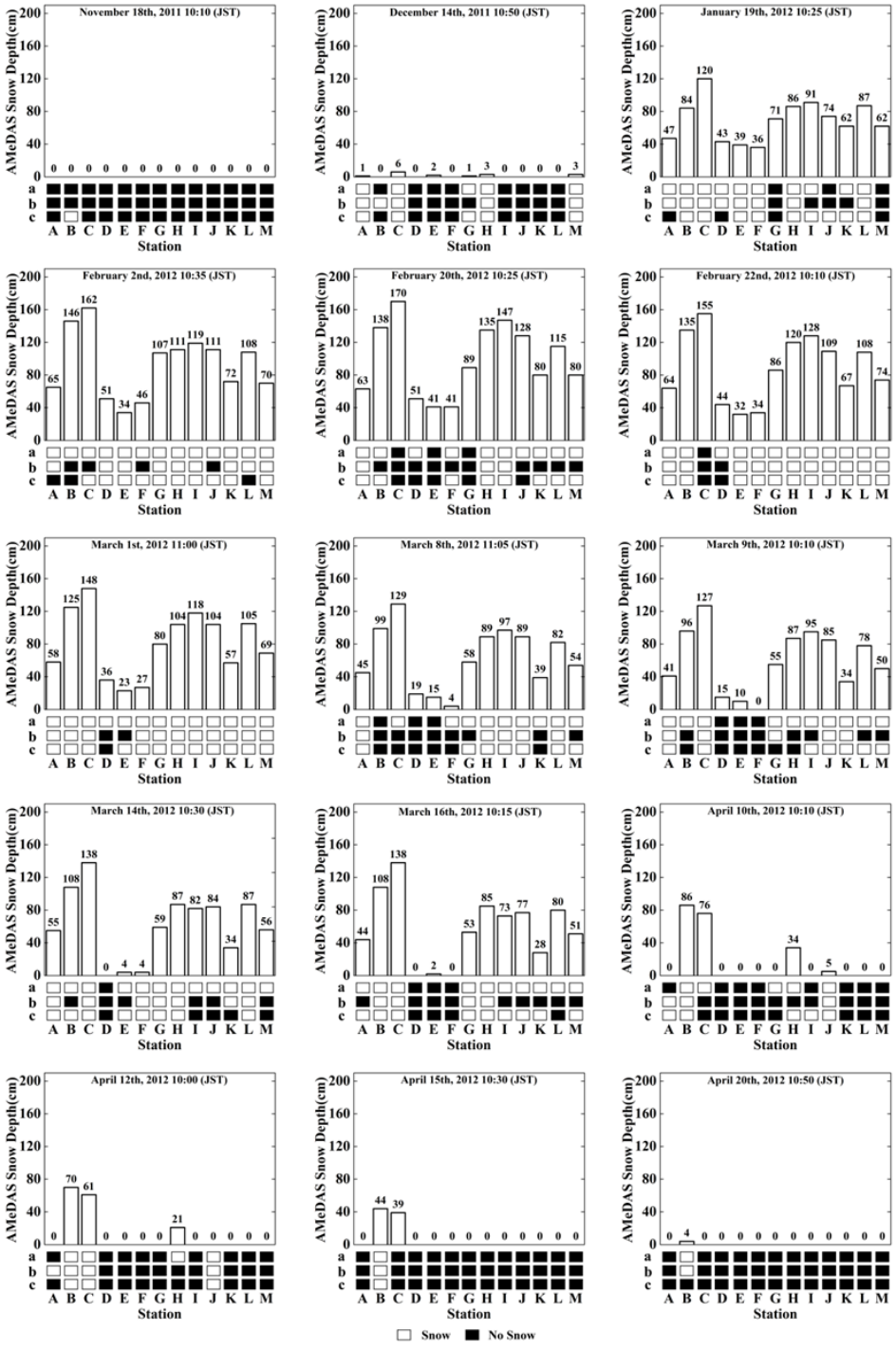

Figure 4.28: Graphs comparing the snow cover detection results for the three methods and the AMeDAS snow depth data between the 13 observation stations over 15 different dates. Histograms represent the AMeDAS snow depth data. Positive numbers represent snow, while "0" represents no snow. "a," "b," and "c" represent the snow cover detection results from the proposed method, the MOD10A1 product, and the combined NDSI and NDVI method, respectively. Letters A–M represent the observation stations of Kazuno, Yunodai, Aniai, Noshiro, Akita, Honjo, Takanosu, Kakunodate, Yokote, Yuzawa, Gojome, Yashima, and Taishouji, respectively. The white and black boxes represent conditions of snow and no snow, respectively, for each of the three methods.

areas (Kazuno, Yunodai, Aniai, Yashima, and Taishoji), plain areas (Noshiro, Akita, Honjo, and Gojome), and basin areas (Takanosu, Kakunodate, Yokote, and Yuzawa), as shown in Figure 4.29. Figure 4.29 presents a comparison of the average accuracies of the three methods within the different area types. The average accuracies in the basin areas of the proposed method, the MOD10A1 product, and the combination of NDSI and NDVI are 91.67%, 71.67%, and 83.33%, respectively, as illustrated in Figure 4.29 (a). The average accuracies in the mountain areas of the proposed method, the MOD10A1 product, and the combination of NDSI and NDVI are 93.33%, 68.00%, and 78.67%, respectively, as seen in Figure 4.29 (b). The average accuracies in the plain areas of the proposed method, the MOD10A1 product, and the combination of NDSI and NDVI are 88.33%, 76.83%, and 76.67%, respectively, as illustrated in Figure 4.29 (c). From these results, it can be seen that all three methods can be used to carry out snow cover detection in the study area. Using the MOD10A1 product, the snow cover detection results for plain and basin areas are superior to those in mountain areas. This is because the fractional snow algorithm of the MOD10A1 product is based on NDSI and other conditions that are only sensitive to snow reflectance but not to vegetation. Snow pixels in forests and mountains are easily covered, reducing the reflectance of the original pixels and increasing the reflectance of vegetation. Therefore, it is highly possible that some snow pixels are identified as vegetation pixels. Using the combination of NDSI and NDVI, the average accuracy of snow cover detection is clearly increased compared to that from the MOD10A1 product, especially in the mountain and basin areas covered by dense vegetation. This method additionally makes use of NDVI, which is able to account for the impact of vegetation under snow cover. However, considering the principles of the above two snow cover detection methods, NDSI in the MOD10A1 product makes use of the difference in reflectance between visible band 4 and infrared band 6 in MODIS images to extract snow pixels from the other ground surface pixels. In the combined NDSI and NDVI method, the NDSI is used to detect snow pixels in nonvegetated areas. In the distinction of snow pixels in vegetated areas, NDVI is first used to identify whether the target area is vegetated or not. Then, NDSI with a lowered threshold value is used to detect snow pixels in these areas. Finally, the results from the two cases are integrated. However, in the present work, the proposed method mainly focuses on the contrast between the low reflectance of vegetation and the high reflectance of snow in bands 1 and 3 in order to extract snow pixels from other ground surface features. This method not only allows the distinction of snow pixels from other features, but is also applicable to cases of mixed pixels in forested

and mountainous areas. Using the proposed method, the average accuracy for snow cover detection in the mountain, plain, and basin areas shows an obvious increase compared to the previous two methods. It can, therefore, be concluded that the proposed method can feasibly and effectively be used for snow cover detection in Akita Prefecture.

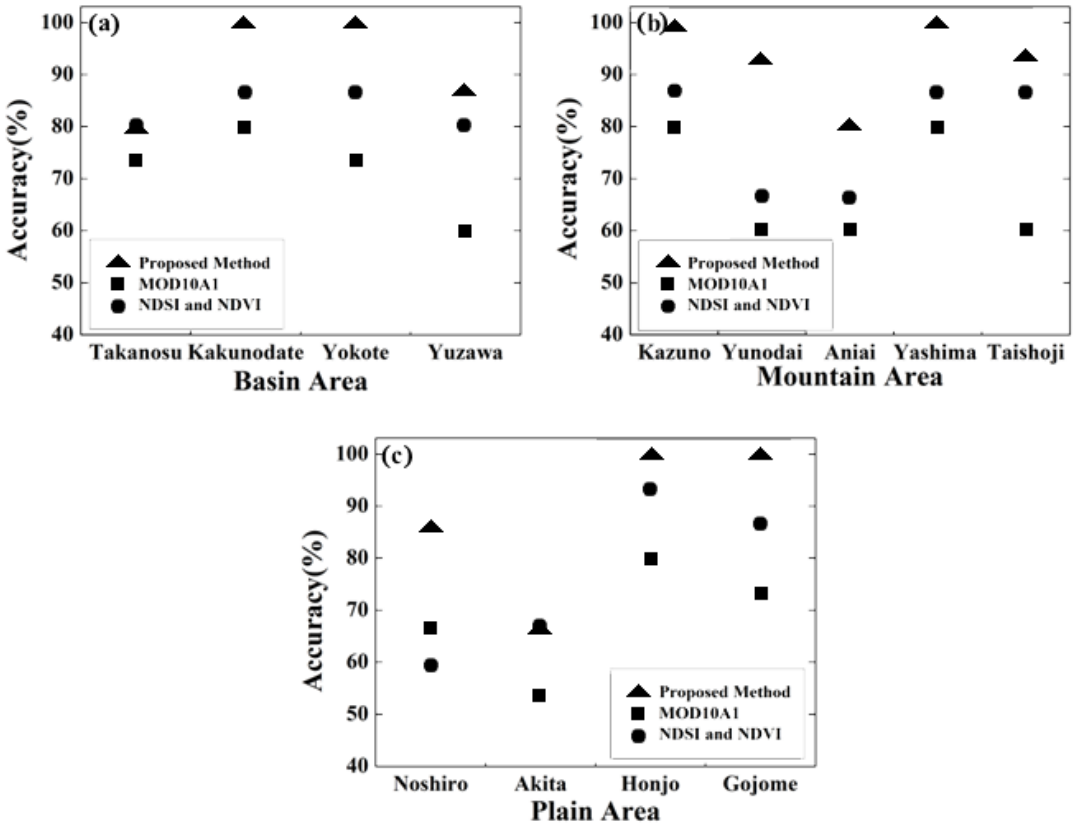

Figure 4.29: Comparison of average accuracies in the three different area types: (a) basin area, (b) mountain area, and (c) plain area.

4.4.9. Comparison of Results with the Area Image for Aomori Prefecture

In order to verify the effectiveness of the proposed method in other locations, Aomori Prefecture is selected in this work. Figure 4.30 shows the pseudocolor image composed of MODIS bands 1, 4, and 6 [Figure 4.30 (a)], and images of snow cover detection results, for comparison, from the proposed method [Figure 4.30 (b)], the MOD10A1 product [Figure 4.30 (c)], and the combined NDSI and NDVI method [Figure 4.30 (d)], all from 10:25 on April 6, 2011 (JST). As discussed in Chapter 4.4.5. and for Figure 4.22 (b), snow pixels are yellow and cloud pixels are almost white in the pseudocolor image in Figure 4.30 (a).

From Figures 4.30 (b) to 4.30 (d), it is obvious that the result of the proposed snow cover detection method [Figure 4.30 (b)] is most consistent with the pseudocolor image [Figure 4.30 (a)]. However, the snow cover is obviously underestimated in the Oma-Mutsu-Wakinosawa region by the MOD10A1 product [Figure 4.30 (c)].

For the combined NDSI and NDVI method [Figure 4.30 (d)], the snow cover is overestimated over almost the whole test area. These results demonstrate that the proposed method is more effective for snow cover detection than the MOD10A1 product and the combined NDSI and NDVI method.

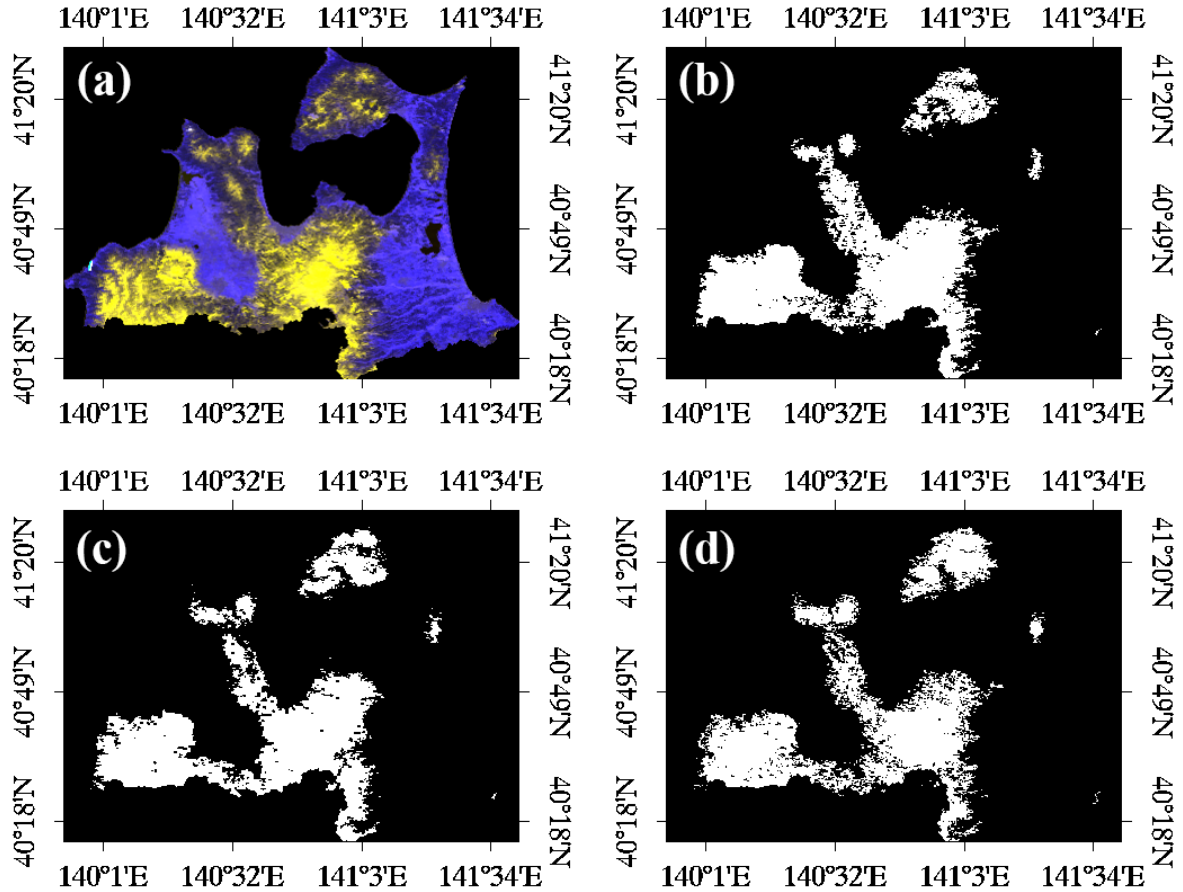

Figure 4.30: Comparison of images of snow cover detection results from 10:25 (JST) on April 6, 2011: (a) pseudocolor image, (b) proposed method, (c) MOD10A1 product, and (d) combined NDSI and NDVI.

In addition, along with the AMeDAS snow depth record data from the 15 observation stations on April 6, 2011, snow cover detection results from the three methods in the Aomori Prefecture are shown in Table 4.31. It can be seen that both the MOD10A1 product and the

Table 4.31: Snow detection results for the three compared methods in the Aomori Prefecture.

Stations	Latitude (N)		Longitude (E)		2011/4/6				2011/11/18				2011/12/14				2012/1/19				2012/2/2				2012/3/1				2012/4/15			
	Degree	Minute	Degree	Minute	AMeDAS	b	c	d	AMeDAS	b	c	d	AMeDAS	b	c	d	AMeDAS	b	c	d	AMeDAS	b	c	d	AMeDAS	b	c	d	AMeDAS	b	c	d
Mutsu	41	17	141	12.6	0	0	0	0	0	0	0	0	6	1	1	1	47	1	1	1	99	1	1	1	95	1	1	1	9	1	1	1
Aomori	40	49.3	140	46.1	0	0	0	0	0	0	0	0	13	1	1	0	107	1	1	1	136	1	1	1	128	1	1	1	8	1	1	1
Noheji	40	53.1	141	9.6	0	0	0	0	0	0	0	0	0	0	0	0	34	1	1	1	64	1	1	1	85	1	1	1	0	0	0	1
Ajigasawa	40	46.6	140	12.3	0	0	0	0	0	0	0	0	1	1	0	1	54	1	1	1	89	1	1	1	66	1	1	1	0	0	1	0
Goshogawara	40	48.5	140	27.5	0	0	0	0	0	0	1	0	3	1	1	1	82	1	1	1	107	1	1	0	106	1	1	1	0	0	0	0
Fukaura	40	38.7	139	55.9	0	0	0	0	0	0	0	1	1	1	1	1	26	1	1	1	48	1	1	1	29	1	0	1	1	0	0	0
Hirosaki	40	36.7	140	27.3	0	0	0	0	0	1	0	0	0	0	0	0	68	1	1	1	123	1	1	1	106	1	1	1	0	0	0	0
Towada	40	35.7	141	14.8	0	0	0	0	0	0	1	0	0	0	0	0	32	1	1	1	61	1	1	1	51	1	1	1	0	0	0	0
Hachinohe	40	31.6	141	31.3	0	0	0	0	0	0	0	1	1	0	1	0	3	1	0	0	15	1	0	1	13	1	0	0	2	0	0	1
Ikarigaseki	40	28.9	140	37.2	0	0	1	1	0	0	1	0	8	1	0	1	56	1	1	1	105	1	1	1	94	1	1	1	0	0	0	1
Sannohe	40	23	141	15.4	0	0	0	0	0	0	0	0	0	0	0	0	18	1	1	1	53	1	1	1	44	1	1	1	0	0	0	0
Imabetsu	41	10.8	140	28.9	0	0	0	0	0	0	0	0	1	1	1	1	93	1	1	1	140	1	1	1	116	1	1	1	2	1	0	1
Oma	41	31.6	140	54.7	0	0	0	0	0	1	0	0	0	0	0	0	10	1	1	1	69	1	1	1	43	1	1	1	0	0	0	0
Sukayu	40	38.9	140	50.9	349	1	1	1	40	1	0	0	88	1	1	1	343	1	1	1	435	1	1	1	456	1	1	1	386	1	1	1
Wakinosawa	41	8.7	140	49.3	0	0	0	0	0	0	0	0	2	1	0	1	89	1	1	1	112	1	1	1	116	1	1	1	0	0	0	0

Note: AMeDAS: Records of Snow Depth (cm) from AMeDAS; b: Results from Proposed Method; c: Results from MOD10A1 Product; d: Results from the Combination of NDSI and NDVI;

0: Snow Free; 1: Snow Covered

combined NDSI and NDVI method show incorrect evaluations at the Ikarigaseki observation station, while the proposed method is consistent with AMeDAS data.

Then, we calculate the snow cover for the entire region of Aomori Prefecture for six relatively clear days from November 2011 to April 2012 during the snowy season, as shown in Table 4.31. Only 6 days are considered because of the large size of the region and the computational expense of processing satellite data over a long period.

From this table, the overall accuracy of the proposed method, the MOD10A1 product, and the combined NDSI and NDVI method are calculated as 95.2%, 84.8%, and 88.6%, respectively, which confirms the effectiveness of the proposed method.

4.4.10. Comparison of Results with Landsat Operational Land Imager Data

In the present work, the Mt. Chokaizan region is selected as a second test region to validate the proposed method. The snow cover detection results are predominantly based on Equations (30) and (31) according to two groups of criteria. In one group, the value of $NDSI$ is greater than 0.45, $Band_5$ is greater than 0.11, and $Band_3$ is greater than 0.10. In the other group, for forested areas, the value of $NDVI$ is greater than 0.3, the value of $NDSI$ is greater than 0.38, $Band_5$ is greater than 0.11, and $Band_4$ is greater than 0.1.

$$NDSI = (Band_3 - Band_6) / (Band_3 + Band_6) \tag{30}$$

$$NDVI = (Band_5 - Band_4) / (Band_5 + Band_4) \tag{31}$$

where $Band_x$ represents the reflectance value of the corresponding Landsat OLI images after completion of the above preprocessing.

Figure 4.32 shows a comparison of the snow cover detection results from the Mt. Chokaizan region between Landsat OLI and MODIS images obtained on April 13, 2014.

Figure 4.32 (a) shows the geographic situation and coordinates of this region with a pseudocolor image composed of MODIS bands 1, 4, and 6; Figure 4.32 (b) is the snow cover detection result obtained from Landsat OLI data with a 30 m resolution and interpolated to a 500-m resolution; Figure 4.32 (c) is the snow cover detection result estimated using the proposed method with a 500 m resolution; and Figure 4.32 (d) is the snow cover detection result obtained from the MOD10A1 product with a 500-m resolution. From Figure 4.32 (b) and Figure 4.32 (c), we can clearly see that some snow pixels exist on the right-hand side of

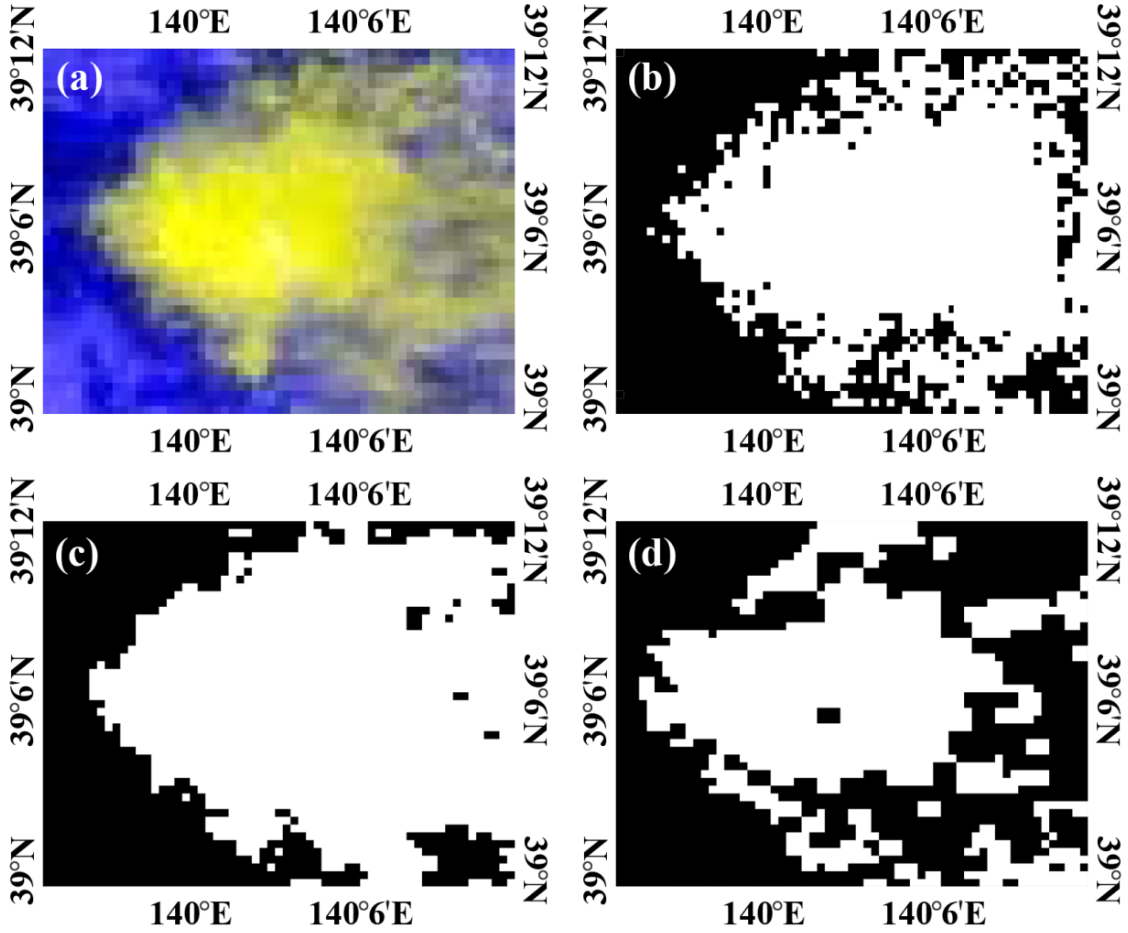

Figure 4.32: The pseudocolor composite image (a) and images of snow cover detection results for comparison from April 13, 2014: Landsat OLI data (b), proposed method (c), and MOD10A1 product (d).

the images that are consistent with Figure 4.32 (a), but are not seen in Figure 4.32 (d). This indicates that the MODIS snow cover product MOD10A1 underestimates the snow cover in the Mt. Chokaizan region. Several Landsat OLI images with a 30 m resolution, taken from January 2014 to April 2014 during the snowy season, are used to estimate snow cover, and are compared with the snow cover detection results estimated by the proposed method and the MODIS snow cover product (MOD10A1) for the same latitudes and longitudes, as shown in Figure 4.33. From this figure, it can be seen that the snow cover detection results estimated by the proposed method are consistent with the results obtained from the Landsat OLI data, which further confirms the superior accuracy of the proposed method over the MOD10A1 product.

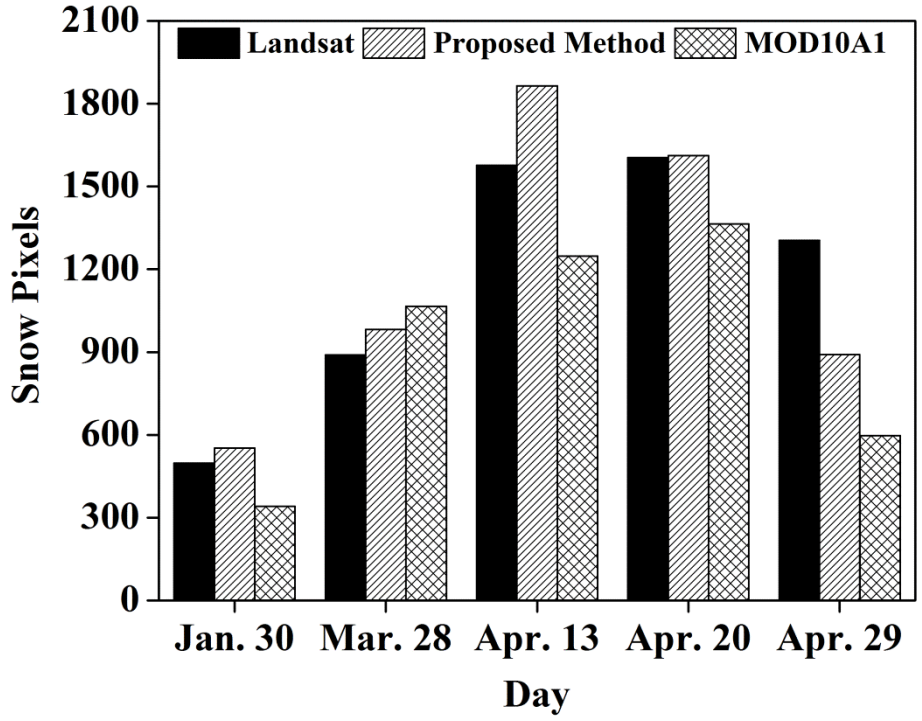

Figure 4.33: Histogram of snow pixels obtained from Landsat OLI data, the proposed method, and the MOD10A1 product on five days for the Mt. Chokaizan region.

4.5. Summary

In order to restore the real surface reflectance, in section 4.2, FLAASH model and 6S code model were used to atmospheric correction with Terra/MODIS image of Akita prefecture of Japan on April 6th, 2011. The results showed that the images with atmospheric correction model are much clearer than the images without atmospheric correction, and the brightness and contrast were also improved. FLAASH model and 6S code model have both contributed to improve the accuracy of snow cover detection for study area. The snow cover detection accuracy was improved by 40% and 46% with FLAASH model and 6S code model for atmospheric correction. Moreover, the accuracy of snow cover detection with 6S code atmospheric correction is higher than 6% compared to the FLAASH model, and it can be confirmed as optimal atmospheric correction method.

The MODIS snow cover product (MOD10_L2) is not pre-processed by the atmospheric and topographic correction, which caused many errors for the snow cover detection. In section 4.3, a new snow cover detection method based on visible red and blue channel from

MODIS imagery is proposed with fully considering the influence of atmosphere, topographic features, snow covered underlying surface and the principle of the snow cover detection from MOD10_L2. Akita prefecture in Japan with a typical climate of the Sea of Japan as the study area is selected. MOD02HKM product sunny cloud-free data from May 2012 to April 2014 are used. In order to improve the accuracy of the snow cover detection, the pre-processing is conducted before the snow cover detection. It includes the geographic correction with the MRT Swath, study area clipping with the Akita administrative regional boundary ShapeFile data, atmospheric correction with the 6S code and topographic correction with a shadowing function algorithm. In order to investigate and analyze the snow cover distributions and changes around one year at different periods in the study area, the composited true color images which represents 5 types of typical snow cover distribution situations on clear days and their corresponding 2-dimensional scatter plot density distribution figures in visible red band 1 and blue band 3 are selected as the training images. The threshold values of the reflectance are determined as greater than 0.458 in band 1 and greater than 0.60 in band 3 through all of situations analysis. Finally, the final snow cover detection map is extracted according to these threshold values. In order to evaluate the effectiveness of the proposed method, the snow depth records of 31 observation stations across the whole study area are chosen and divided into three types according to their longitude and latitude locations, which are the forest region, the plain region and basin region. Meanwhile, the overall accuracy, over-estimation error and under-estimation error as the validation method are adopted and calculated. The results suggested that the overall accuracy of the proposed method is higher than the MOD10_L2 products.

The combination of NDSI and NDVI is effective for snow cover detection in vegetated areas, but the detection conditions for snow pixels are complex and the threshold values are difficult to determine. In section 4.4, a new method for snow cover detection is proposed incorporated 2-D scatter plots from MODIS images based on terrain features and the underlying snow-covered surface in Akita Prefecture, Japan. Terra MODIS Level 1B product data and the AMeDAS snow depth records from 13 observation stations across the prefecture from the period of November 19, 2011, to April 21, 2012, were employed. In the preprocessing part, the conducted preprocessing steps are the same as those in section 4.3. To conduct the snow cover detection, mixed pixels of snow and cloud were first extracted from other ground surface features according to a 2-D scatter plot of spectral reflectances in bands 1 and 3. Then, cloud pixels were detected with a 2-D scatter plot of bands 6 and 7. Finally,

the snow cover detection results are obtained after removal of the confirmed cloud from the mixed snow and cloud pixels. Through comparisons of the final snow cover detection results from this proposed method with the previously used MOD10A1 product and the combination of NDSI and NDVI, it is found that the average accuracy obtained from the proposed method provides an improvement of 11.79% compared to the MOD10A1 product, and 22.05% compared to the NDSI and NDVI combination. Furthermore, through the selection of Aomori Prefecture and the Mt. Chokaizan region as test areas, the effectiveness of the proposed method is verified, and the results show accuracies for the proposed method that are consistent with the improvement seen for Akita Prefecture. Therefore, it is considered feasible and effective to use the proposed method for snow cover detection in Akita Prefecture, Japan with MODIS images in order to improving the environment management and agricultural development.

Chapter 5

5.1 General conclusion

In this study, several main factors of affecting the snow cover detection, such as the atmosphere, the terrain, the underlying surface of snow and cloud, are concerned and considered. The Akita Prefecture and Tohoku Region of Japan as the study area is selected. The main objective of this research is that the snow cover detection accuracy is improved and developing a snow cover detection method which is applicable to the Akita Prefecture, Japan. In this work, the MODIS images from Terra satellite and Aqua satellite are the main study use images data.

In chapter 1, snow cover detection background, the significance of snow observations, and developing snow cover detection methods was described. And the simple construction of this work was also presented.

In chapter 2, the study region and the used data are presented point-to-point. Furthermore, the preprocessing steps before the snow cover detection conducted with proposed methods in the whole of this work were also described.

In chapter 3, a new method for snow detection via the combination of NDSI and NDVI based on the terrain features and the underlying surface covered by snow was proposed used for the study area of this work, Akita Prefecture in Japan. The preprocessing, including atmospheric correction with CREFL_SPA, geographic correction with MRT, study area cutting and topographic correction with a shadowing function method was conducted before the snow detection to improve the accuracy of snow detection. NDVI was used to distinguish the mixed pixels of the snow and forests. Then the threshold value of NDSI was correspondingly lowered to improve the detecting accuracy for snow in forests. Terra MODIS Level-1 B product data and AMeDAS snow depth records in 13 observation stations during the period of December 2010 to April 2011 were selected as the comparison objects. The results showed that the accuracy of proposed method for snow detection was improved about 11% compared to the results of the MOD10_L2 product and NDSI alone. In addition, GIS forest region data and the NDVI were used for forest area discrimination with Terra/MODIS data of Tohoku region in Japan before snow cover detection during snowy season from December 2013 to April 2014. The results show that the accuracy of without the forest area

discrimination, with GIS forest region data and with the NDVI for the forest area discrimination are 78.18%, 89.35% and 86.23%, respectively. The accuracy with GIS forest region data and with NDVI for the forest area discrimination was increased by 11.17% and 8.05%, respectively. And the accuracy with GIS forest region data is higher about 3.12% than the NDVI.

In chapter 4, FLAASH model and 6S code model were used to atmospheric correcting with Terra/MODIS image of study area on April 6th, 2011. The results showed that the snow cover detection accuracy was improved by 40% and 46% with FLAASH model and 6S code model for atmospheric correction comparing to without atmospheric correction. Moreover, the accuracy of snow cover detection with 6S code atmospheric correction is higher than 6% compared to the FLAASH model, and it can be confirmed as optimal atmospheric correction method.

Then a new snow cover detection method based on visible red and blue channel from MODIS imagery was proposed with MOD02HKM product sunny cloud-free data from May 2012 to April 2014. The pre-processing similar to chapter 3 was also conducted before the snow cover detection except atmospheric corrected with the 6S code. The composited true color images which represent 5 types of typical snow cover distribution situations on clear days and their corresponding 2-dimensional scatter plot density distribution figures in visible red band 1 and blue band 3 are selected as the training images. The final snow cover detection map was extracted by determing the threshold values of the reflectance as greater than 0.458 in band 1 and greater than 0.60 in band 3 through all of situations analysis. The snow depth records of 31 observation stations across the whole study area were chosen and divided into forest region, the plain region and basin region. The overall accuracy, over-estimation error and under-estimation error as the validation method were calculated to prove the high accuracy of proposed method. The average accuracy of the proposed method is 26.27% higher than the MOD10_L2 products.

In addition, another new method for snow cover detection is proposed incorporated 2-D scatter plots from MODIS images based on terrain features and the underlying snow-covered surface in Akita Prefecture, Japan. The preprocessing steps are the same as the section 4.3. During the snow cover detection process, mixed pixels of snow and cloud were first extracted from other ground surface features according to a 2-D scatter plot of spectral reflectances in bands 1 and 3. Then, cloud pixels were detected with a 2-D scatter plot of bands 6 and 7 and removed from snow pixels. The final snow cover detection results from this method were

compared with the previously used MOD10A1 product and the combination of NDSI and NDVI. The average accuracy obtained from the proposed method provides an improvement of 11.79% compared to the MOD10A1 product, and 22.05% compared to the NDSI and NDVI combination. Furthermore, the proposed method was verified to be effective in Aomori Prefecture and the Mt. Chokaizan region. Therefore, it is considered feasible and effective to use the proposed method for snow cover detection in Akita Prefecture, Japan with MODIS images in order to improving the environment management and agricultural development..

There are, however, some shortcomings in the proposed method. First, as over 70% of the study area is covered by rich forests, the BRDF phenomenon can easily be generated. In this study, the images are corrected by BRDF during the 6S code atmospheric correction, but an evaluation of the accuracy of the radiation calculation and the impact of using routine data to correct observation angle are needed in future research.

Second, in this work, mixed snow and vegetation pixels are broadly distributed because of the presence of dense forests and the moderate resolution of MODIS images. In the 2-D scatter plot of bands 6 and 7, the distribution of snow and vegetation pixels is continuous. In order to reduce the complexity of snow cover detection, PPI is used to select pure pixels for every feature. Thus, mixed pixels are treated as pure pixels and are processed as such in this work. However, addressing the problems of decomposing such mixed pixels should be the focus of further study.

Finally, in this study, MODIS images are purposefully selected to include only those with cloud cover below 5% and with no cloud over the snow. Therefore, the cloud extraction technique of the proposed method is only proven useful for these specific cases and further development is needed to extend the applicability of the method.

Acknowledgments

This study is completed in the Graduate School of Systems Science and Technology of the Akita Prefectural University, Japan during the doctoral course under the guidance and promotion of Professor Guoyue Chen. Furthermore, in carrying out the present study, Professor Guoyue Chen gave me this opportunity to do this research, and a never stop general guidance. Moreover, in daily life, Professor Guoyue Chen often takes care of my life from public to private. In particular, Professor Guoyue Chen has taught me a lot of study methods, ways of life, and the manners and customs of Japan. Therefore, I will be here for expressing my deeply sincerely appreciations to Professor Guoyue Chen.

In process of doing this study, I obtained a large number of valuable advices from Associate Professor Kazuki Saruta and Assistant Professor Yuki Terata who work in the Faculty of Systems Science and Technology of the Akita Prefectural University in the laboratory seminar. I wish to be here for expressing my sincerely appreciations.

In addition, I will also wish to my sincerely appreciations to Professor Yohji Isoda, who is the department chairman of the Department of Electronics and Information Systems in the Faculty of Systems Science and Technology of the Akita Prefectural University and Professor Jun-ichi Kudoh who works in the Center for Northeast Asian Studies of the Tohoku University, Japan, for their valuable advices and assessments in the preparation of this manuscript.

Here, I will also express my special thanks to Professor Guoyue Chen’s wife Mrs. Zhu, who gave a great of helps to my study and life in Akita Prefectural University.

And, I will also express my special deeply thanks to my wife, Xueli Wu, for her unknown and the most powerful supports.

I will also deeply thank to the members of my research laboratory for their valuable assistances.

I will also express my heartfelt thanks to the Akita Construction Department Road Division which provided the Road Snow Information System data of Akita Prefecture.

Finally, I will express my deeply thanks to other people who helped me in study and life for their guidance and assistances.

References

[1] R. K. Pachauri and L. Meyer, “Climate Change 2014 Synthesis Report,” 2014.

[2] C. B. Field, V. Barros, T. F. Stocker, D. Qin, D. J. Dokken, K. L. Ebi, M. D. Mastrandrea, K. J. Mach, G.-K. Plattner, S. K. Allen, M. Tignor, and P. M. Midgley, *Managing the Risks of Extreme Events and Disasters to Advance Climate Change Adaptation. A Special Report of Working Groups I and II of the Intergovernmental Panel on Climate Change*. Cambridge and New York: Cambridge University Press, 2012.

[3] L. Bernstein, P. Bosch, O. Canziani, and Z. Chen, “Climate Change 2007: Synthesis Report. An Assessment of the Intergovernmental Panel on Climate Change,” Geneva, Switzerland, 2007.

[4] “Climate Change Monitoring Report 2013,” 2014.

[5] D. R. Gurung, A. Giriraj, K. S. Aung, B. Shrestha, and A. V Kulkarni, *Snow-Cover Mapping and Monitoring in the Hindu Kush-Himalayas*. Kathmandu, Nepal, 2011.

[6] J. C. Adam, A. F. Hamlet, and D. P. Lettenmaier, “Implications of global climate change for snowmelt hydrology in the twenty-first century,” *Hydrol. Process.*, vol. 23, no. 7, pp. 962–972, Mar. 2009.

[7] R. G. Barry, “The Role of Snow and Ice in the Global Climate System: A Review,” *Polar Geogr.*, vol. 26, no. 3, pp. 235–246, Jul. 2002.

[8] R. G. Barry, J.-M. Fallot, and R. L. Armstrong, “Twentieth-century variability in snow- cover conditions and approaches to detecting and monitoring changes: status and prospects,” *Prog. Phys. Geogr.*, vol. 19, no. 4, pp. 520–532, Dec. 1995.

[9] B. Metz, O. R. Davidson, P. R. Bosch, and R. Dave, *Contribution of Working Group III to the Fourth Assessment Report of the Intergovernmental Panel on Climate Change*. United Kingdom and New York: Cambridge University Press, 2007.

[10] W. G. Rees, *Remote Sensing of Snow and Ice*. CRC Press, Taylor & Francis Group, 2005.

[11] A. Merkushkin, "Observational hydrometeorological network in Uzbekistan: Status, data acquisition and control," Tokyo, 2010.

[12] J. Muñoz, J. Infante, T. Lakhankar, R. Khanbilvardi, P. Romanov, N. Krakauer, and A. Powell, "Synergistic Use of Remote Sensing for Snow Cover and Snow Water Equivalent Estimation," *Br. J. Environ. Clim. Chang.*, vol. 3, no. 4, pp. 612–627, 2013.

[13] N. J. Madan, "Snow Ecology: An Interdisciplinary Examination of Snow-covered Ecosystems.," *J. Ecol.*, vol. 89, no. 6, pp. 1097–1098, Dec. 2001.

[14] S. G. Warren, "Optical properties of snow," *Rev. Geophys.*, vol. 20, no. 1, pp. 67–89, 1982.

[15] B. Rummel, *Investigation of Landsat satellite image change detection of snow and ice cover*, Master's T. Norway: Norwegian University of Science and Technology, 2013.

[16] D. K. Hall, G. a. Riggs, V. V. Salomonson, N. E. DiGirolamo, and K. J. Bayr, "MODIS snow-cover products," *Remote Sens. Environ.*, vol. 83, no. 1–2, pp. 181–194, Nov. 2002.

[17] N. Foppa, S. Wunderle, and A. Hauser, "Operational snow cover estimation at subpixel scale using NOAA-AVHRR data," in *Proc. SPIE 4886, Remote Sensing for Environmental Monitoring, GIS Applications, and Geology II*, 2003, pp. 659–666.

[18] A. R. HARRISON and R. M. LUCAS, "Multi-spectral classification of snow using NOAA AVHRR imagery," *Int. J. Remote Sens.*, vol. 10, no. 45, pp. 907–916, Apr. 1989.

[19] R. Pimentel, J. Herrero, and M. J. Polo, “Estimating snow albedo patterns in a Mediterranean site from Landsat TM and ETM+ images,” in *Proc. SPIE 8887, Remote Sensing for Agriculture, Ecosystems, and Hydrology XV*, 2013, p. 88870L.

[20] A. J. Dietz, C. Kuenzer, U. Gessner, and S. Dech, “Remote sensing of snow – a review of available methods,” *Int. J. Remote Sens.*, vol. 33, no. 13, pp. 4094–4134, Jul. 2012.

[21] D. K. Hall, G. a. Riggs, and V. V. Salomonson, “Development of methods for mapping global snow cover using moderate resolution imaging spectroradiometer data,” *Remote Sens. Environ.*, vol. 54, no. 2, pp. 127–140, Nov. 1995.

[22] J. Dozier, “Remote sensing of snow in visible and near-infrared wavelengths,” in *Theory and Applications Of Optical Remote Sensing*, New York: John Wiley, 1989, pp. 527–547.

[23] V. . Salomonson and I. Appel, “Estimating fractional snow cover from MODIS using the normalized difference snow index,” *Remote Sens. Environ.*, vol. 89, no. 3, pp. 351–360, Feb. 2004.

[24] A. G. Klein, D. K. Hall, and G. A. Riggs, “Improving snow cover mapping in forests through the use of a canopy reflectance model,” *Hydrol. Process.*, vol. 12, no. 10–11, pp. 1723–1744, Aug. 1998.

[25] D. Vikhamar and R. Solberg, “Snow-cover mapping in forests by constrained linear spectral unmixing of MODIS data,” *Remote Sens. Environ.*, vol. 88, no. 3, pp. 309–323, Dec. 2003.

[26] S. Odagawa, T. Sanga, and M. Kato, “A Proposal for the Reduction Method of Vegetation Influence from Mixed SpectrumUsing Unit Vectorized Reflectance and NDVI Function in Vegetated Area,” *J. Remote Sens. Soc. Japan*, vol. 32, no. 5, pp. 320–329, Aug. 2012.

[27] D. M. Rogge, B. Rivard, J. Zhang, A. Sanchez, J. Harris, and J. Feng, “Integration of spatial-spectral information for the improved extraction of endmembers,” *Remote Sens. Environ.*, vol. 110, no. 3, pp. 287–303, 2007.

[28] J. J. Settle and N. A. Drake, "Linear mixing and the estimation of ground cover proportions," *Int. J. Remote Sens.*, vol. 14, no. 6, pp. 1159–1177, Apr. 1993.

[29] J. B. Adams, M. O. Smith, and P. E. Johnson, "Spectral mixture modeling: A new analysis of rock and soil types at the Viking Lander 1 Site," *J. Geophys. Res.*, vol. 91, no. B8, pp. 8098–8112, 1986.

[30] J. B. Adams, M. O. Smith, and A. R. Gillespie, *Imaging spectroscopy: Interpretation based on spectral mixture analysis*, vol. 7. New York: Cambridge University Press, 1993.

[31] D. Lu, M. Batistella, and E. Moranl, "Linear spectral mixture analysis of TM data for land-use and land-cover classification in Rondonia, Brazilian Amazon," in *Symposium on Geospatial Theory, Processing and Applications*, 2002, pp. 557–562.

[32] N. Keshava and J. F. Mustard, "Spectral unmixing," *IEEE Signal Process. Mag.*, vol. 19, no. 1, pp. 44–57, 2002.

[33] Y. J. Kaufman, R. G. Kleidman, D. K. Hall, J. V. Martins, and J. S. Barton, "Remote sensing of subpixel snow cover using 0.66 and 2.1 μm channels," *Geophys. Res. Lett.*, vol. 29, no. 16, pp. 28–31, 2002.

[34] S. Metsämäki, J. Vepsäläinen, J. Pulliainen, and Y. Sucksdorff, "Improved linear interpolation method for the estimation of snow-covered area from optical data," *Remote Sens. Environ.*, vol. 82, no. 1, pp. 64–78, Sep. 2002.

[35] D. Vikhamar and R. Solberg, "Subpixel mapping of snow cover in forests by optical remote sensing," *Remote Sens. Environ.*, vol. 84, no. 1, pp. 69–82, Jan. 2003.

[36] J. J. Simpson, J. R. Stitt, and M. Sienko, "Improved estimates of the areal extent of snow cover from AVHRR data," *J. Hydrol.*, vol. 204, no. 1–4, pp. 1–23, Jan. 1998.

[37] A. W. Nolin, J. Dozier, and L. a. K. Mertes, "Mapping alpine snow using a spectral mixture modelling technique," *Ann. Glaciol.*, vol. 17, no. 1, pp. 121–124, 1993.

[38] W. Rosenthal and J. Dozier, "Automated Mapping of Montane Snow Cover at Subpixel Resolution from the Landsat Thematic Mapper," *Water Resour. Res.*, vol. 32, no. 1, pp. 115–130, Jan. 1996.

[39] N. Foppa, S. Wunderle, A. Hauser, D. Oesch, and F. Kuchen, "Operational sub-pixel snow mapping over the Alps with NOAA AVHRR data," *Ann. Glaciol.*, vol. 38, no. 1, pp. 245–252, Jan. 2004.

[40] G. Martelloni, S. Segoni, D. Lagomarsino, R. Fanti, and F. Catani, "Snow accumulation/melting model (SAMM) for integrated use in regional scale landslide early warning systems," *Hydrol. Earth Syst. Sci.*, vol. 17, no. 3, pp. 1229–1240, 2013.

[41] K. J. Bormann, M. F. McCabe, and J. P. Evans, "Satellite based observations for seasonal snow cover detection and characterisation in Australia," *Remote Sens. Environ.*, vol. 123, pp. 57–71, Aug. 2012.

[42] M. J. Kim, J. a. Weinman, W. S. Olson, D. E. Chang, G. Skofronick-Jackson, and J. R. Wang, "A physical model to estimate snowfall over land using AMSU-B observations," *J. Geophys. Res.*, vol. 113, no. D9, pp. 1–16, 2008.

[43] E. F. Vermote, N. Z. El Saleous, and C. O. Justice, "Atmospheric correction of MODIS data in the visible to middle infrared: first results," *Remote Sens. Environ.*, vol. 83, no. 1, pp. 97–111, 2002.

[44] V. Balthazar, V. Vanacker, and E. F. Lambin, "Evaluation and parameterization of ATCOR3 topographic correction method for forest cover mapping in mountain areas," *Int. J. Appl. Earth Obs. Geoinf.*, vol. 18, no. 1, pp. 436–450, Aug. 2012.

[45] "The Geospatial Information of Akita," *The Geospatial Information Authority of Japan*. [Online]. Available: http://www.gsi.go.jp/KOKUJYOHO/CENTER/kendata/akita_heso.htm. [Accessed: 08-Jul-2015].

[46] "Data of Akita Prefecture," *The Geospatial Information Authority of Japan (GSI)*. [Online]. Available: http://uub.jp/47/akita/. [Accessed: 08-Jul-2015].

[47] "Climate Change in Tohoku," *Sendai Dist. Meteorol. Obs. Hakodate Mar. Obs.*, vol. 12, pp. 54–64, 2011.

[48] "Past rainfall weather data search of Japan Meteorological Agency (JMA)," *Japan Meteorological Agency*. [Online]. Available: http://www.data.jma.go.jp/gmd/risk/obsdl/index.php. [Accessed: 10-Jul-2015].

[49] "Weather characteristic of Akita Prefecture," *Akita Local Meteorological Observatory*. [Online]. Available: http://www.jma-net.go.jp/akita/4season/4season.htm. [Accessed: 10-Jul-2015].

[50] "Summary of Forest and Forestry in Akita Report 2013," Akita, 2013.

[51] "Position information of Prefectures," *The Geospatial Information Authority of Japan (GSI)*. [Online]. Available: http://www.gsi.go.jp/KOKUJYOHO/CENTER/zenken.htm. [Accessed: 08-Jul-2015].

[52] "Climate of the Tohoku Region," *Japan Meteorological Agency*. [Online]. Available: http://www.jma-net.go.jp/sendai/wadai/touhokukikou/kikou-index.htm. [Accessed: 08-Jul-2015].

[53] "Information of Terra Satellite," *National Aeronautics and Space Administration*. [Online]. Available: http://terra.nasa.gov/about. [Accessed: 09-Jul-2015].

[54] "Aqua Earth-observing satellite mission," *National Aeronautics and Space Administration*. [Online]. Available: http://aqua.nasa.gov/. [Accessed: 09-Jul-2015].

[55] W. L. Barnes, T. S. Pagano, and V. V. Salomonson, "Prelaunch characteristics of the Moderate Resolution Imaging Spectroradiometer (MODIS) on EOS-AM1," *IEEE Trans. Geosci. Remote Sens.*, vol. 36, no. 4, pp. 1088–1100, Jul. 1998.

[56] D. K. Hall, G. A. Riggs, and J. S. Barton, *Algorithm Theoretical Basis Document (ATBD) for the MODIS Snow and Sea Ice-Mapping Algorithms*. 2001.

[57] "The Level 1 and Atmosphere Archive and Distribution System (LAADS) web of MODIS," *Goddard Space Flight Center of National Aeronautics and Space*

Administration (NASA). [Online]. Available: https://ladsweb.nascom.nasa.gov/. [Accessed: 08-Jul-2015].

[58] "The Landsat 8 satellite website of U.S. Geological Survey," *United States Geological Survey*. [Online]. Available: http://landsat.usgs.gov/landsat8.php. [Accessed: 08-Jul-2015].

[59] "USGS Global Visualization Viewer of Earth Resources Observation and Science Center (EROS)," *United States Geological Survey*. [Online]. Available: http://glovis.usgs.gov/. [Accessed: 08-Jul-2015].

[60] T. Toutin, "Impact of terrain slope and aspect on radargrammetric DEM accuracy," *ISPRS J. Photogramm. Remote Sens.*, vol. 57, no. 3, pp. 228–240, Dec. 2002.

[61] "CGIAR-CSI SRTM 90m DEM Digital Elevation Database," *The CGIAR Consortium for Spatial Information (CGIAR-CSI)*. [Online]. Available: http://srtm.csi.cgiar.org/. [Accessed: 08-Jul-2015].

[62] "Automated Meteorological Data Acquisition System of Japan Meteorological Agency," *Japan Meteorological Agency*. [Online]. Available: http://www.jma.go.jp/jma/kishou/know/amedas/kaisetsu.html. [Accessed: 08-Jul-2015].

[63] "Akita Local Meteorological Observatory," *Japan Meteorological Agency*. [Online]. Available: http://www.jma-net.go.jp/akita/. [Accessed: 08-Jul-2015].

[64] "Past weather data search of Japan Meteorological Agency (JMA)," *Japan Meteorological Agency*. [Online]. Available: http://www.data.jma.go.jp/obd/stats/etrn/index.php. [Accessed: 08-Jul-2015].

[65] "Akita Construction Department Road Division," *Goverment of Akita Prefecture*. [Online]. Available: http://www.pref.akita.lg.jp/www/genre/0000000000000/1000000001048/index.html. [Accessed: 09-Jul-2015].

[66] "MODIS Reprojection Tool Swath User Manual," The Land Processes Distributed Active Archive Center (LP DAAC), Sioux Falls, 2010.

[67] "MODIS Reprojection Tool Swath of LP DAAC," *the Land Processes Distributed Active Archive Center of the U.S. Geological Survey*. [Online]. Available: https://lpdaac.usgs.gov/tools/MODIS_reprojection_tool_swath. [Accessed: 08-Jul-2015].

[68] "ShapeFile library of RjpWiki," *PukiWiki Developers Team*. [Online]. Available: http://www.okadajp.org/RWiki/?ShapeFile%E3%83%A9%E3%82%A4%E3%83%96%E3%83%A9%E3%83%AA. [Accessed: 08-Jul-2015].

[69] R. Richter, "A spatially adaptive fast atmospheric correction algorithm," *Int. J. Remote Sens.*, vol. 17, no. 6, pp. 1201–1214, Apr. 1996.

[70] Y. J. Kaufman, A. E. Wald, L. A. Remer, Bo-Cai Gao, Rong-Rong Li, and L. Flynn, "The MODIS 2.1-μm channel-correlation with visible reflectance for use in remote sensing of aerosol," *IEEE Trans. Geosci. Remote Sens.*, vol. 35, no. 5, pp. 1286–1298, 1997.

[71] P. S. J. Chavez, "Image-based atmospheric corrections - revisited and improved," *Photogramm. Eng. Remote Sensing*, vol. 62, no. 9, pp. 1025–1036, 1996.

[72] B. Tang, B. Shrestha, Z. Li, G. Liu, H. Ouyang, D. R. Gurung, A. Giriraj, and K. S. Aung, "Determination of snow cover from MODIS data for the Tibetan Plateau region," *Int. J. Appl. Earth Obs. Geoinf.*, vol. 21, pp. 356–365, 2013.

[73] "Direct Readout Laboratory of NASA," *National Aeronautics and Space Administration*. [Online]. Available: http://directreadout.sci.gsfc.nasa.gov/?id=software. [Accessed: 11-Jul-2015].

[74] S. Y. Kotchenova, E. F. Vermote, R. Matarrese, and F. J. Klemm, Jr., "Validation of a vector version of the 6S radiative transfer code for atmospheric correction of satellite data. Part I: Path radiance," *Appl. Opt.*, vol. 45, no. 26, p. 6762, Sep. 2006.

[75] S. Y. Kotchenova and E. F. Vermote, "Validation of a vector version of the 6S radiative transfer code for atmospheric correction of satellite data. Part II. Homogeneous Lambertian and anisotropic surfaces," *Appl. Opt.*, vol. 46, no. 20, p. 4455, Jul. 2007.

[76] E. F. Vermote, D. Tanre, J. L. Deuze, M. Herman, and J. J. Morcrette, "Second Simulation of the Satellite Signal in the Solar Spectrum, 6S: An Overview," *IEEE Trans. Geosci. Remote Sens.*, vol. 35, no. 3, pp. 675–686, 1997.

[77] "6S Vector Code," *MODIS Land Surface Reflectance Science Computing Facility*. [Online]. Available: http://6s.ltdri.org/. [Accessed: 11-Jul-2015].

[78] J. D. Colby, "Topographic Normalization in Rugged Terrain," *Photogramm. Eng. Remote Sensing*, vol. 57, no. 5, pp. 531–537, 1991.

[79] M. Faraklioti and M. Petrou, "Illumination invariant unmixing of sets of mixed pixels," *IEEE Trans. Geosci. Remote Sens.*, vol. 39, no. 10, pp. 2227–2234, 2001.

[80] J. Dozier and J. Frew, "Rapid calculation of terrain parameters for radiation modeling from digital elevation data," *IEEE Trans. Geosci. Remote Sens.*, vol. 28, no. 5, pp. 963–969, 1990.

[81] J. P. Wilson and J. C. Gallant, *Terrain Analysis: Principles and Applications*. New York: John Wiley & Sons, Inc., 2000.

[82] R. Dubayah, "Estimating net solar radiation using Landsat Thematic Mapper and digital elevation data," *Water Resour. Res.*, vol. 28, no. 9, pp. 2469–2484, Sep. 1992.

[83] B. Hapke, "Bidirectional reflectance spectroscopy: 3. Correction for macroscopic roughness," *Icarus*, vol. 59, no. 1, pp. 41–59, Jul. 1984.

[84] S. Liang, P. Lewis, R. Dubayah, W. Qin, and D. Shirey, "Topographic effects on surface bidirectional reflectance scaling," *J. Remote Sens.*, vol. 1, pp. 82–93, Oct. 1997.

[85] S. Liang, *Wiley: Quantitative Remote Sensing of Land Surfaces - Shunlin Liang*. New Jersey: John Wiley & Sons, Inc., 2003.

[86] H. S. He, D. J. Mladenoff, V. C. Radeloff, and T. R. Crow, "Integration of GIS Data and Classified Satellite Imagery for Regional Forest Assessment," *Ecol. Appl.*, vol. 8, no. 4, pp. 1072–1083, 1998.

[87] G. A. Riggs, D. K. Hall, and V. V. Salomonson, "MODIS snow products user guide to collection 5," 2006.

[88] G. A. Riggs, J. S. Barton, D. K. Hall, and V. V. Salomonson, "MODIS Snow Products Users' Guide," *The Institute for Computational Earth System Science(ICESS) in the University of California*, 2000. [Online]. Available: http://www.icess.ucsb.edu/modis/SnowUsrGuide/usrguide.html. [Accessed: 07-Jul-2015].

[89] A. Huete, C. Justice, and W. van Leeuwen, "MODIS Vegetation Index (MOD 13) Algorithm Theoretical Basis Document," 1999.

[90] J. Dozier, "Spectral signature of alpine snow cover from the landsat thematic mapper," *Remote Sens. Environ.*, vol. 28, pp. 9–22, Apr. 1989.

[91] P. Pan, K. Saruta, Y. Terata, and G. Chen, "Observations for Snow Cover Detection in Akita via the Combination of Normalized Difference Vegetation Index and Normalized Difference Snow Index," *Trans. Japan Soc. Aeronaut. Sp. Sci. Aerosp. Technol. Japan*, vol. 12, no. ists29, pp. 1–7, 2014.

[92] R. Richter, "Atmospheric correction of satellite data with haze removal including a haze/clear transition region," *Comput. Geosci.*, vol. 22, no. 6, pp. 675–681, Jul. 1996.

[93] S. Liang, H. Fang, and M. Chen, "Atmospheric correction of Landsat ETM+ land surface imagery. I. Methods," *IEEE Trans. Geosci. Remote Sens.*, vol. 39, no. 11, pp. 2490–2498, 2001.

[94] X. Zhao, S. L. Liang, S. H. Liu, J. Di Wang, J. Qin, Q. Li, and X. W. Li, "Improvement of dark object method in atmospheric correction of hyperspectral remotely sensed data," *Sci. China, Ser. D Earth Sci.*, vol. 51, no. 3, pp. 349–356, 2008.

[95] Y. Lin, H. He, Z. Yin, and F. Chen, "Rotation-Invariant Object Detection in Remote Sensing Images Based on Radial-Gradient Angle," *IEEE Geosci. Remote Sens. Lett.*, vol. 12, no. 4, pp. 746–750, Apr. 2015.

[96] D. Paronis and N. Sifakis, "Satellite aerosol optical thickness retrieval over land with contrast reduction analysis using a variable window size," in *IGARSS 2003. 2003 IEEE International Geoscience and Remote Sensing Symposium. Proceedings (IEEE Cat. No.03CH37477)*, 2003, vol. 2, pp. 1276–1278.

[97] L. Chen, G. Yan, T. Wang, H. Ren, J. Calbo, J. Zhao, and R. McKenzie, "Estimation of surface shortwave radiation components under all sky conditions: Modeling and sensitivity analysis," *Remote Sens. Environ.*, vol. 123, pp. 457–469, 2012.

[98] R. T. Wilson, "Py6S: A Python interface to the 6S radiative transfer model," *Comput. Geosci.*, vol. 51, pp. 166–171, Feb. 2013.

[99] B. C. Gao, M. J. Montes, C. O. Davis, and A. F. H. Goetz, "Atmospheric correction algorithms for hyperspectral remote sensing data of land and ocean," *Remote Sens. Environ.*, vol. 113, no. SUPPL. 1, pp. S17–S24, 2009.

[100] E. Vermote, M. Herman, J. J. Morcrette, and S. Y. Kotchenova, "Second Simulation of a Satellite Signal in the Solar Spectrum - Vector (6SV)," *MODIS L. Surf. Reflectance Sci. Comput. Facil.*, vol. 3, no. 2, pp. 1–55, 2006.

[101] P. P. Pan, K. Saruta, Y. Terata, and G. Y. Chen, "Comparison of FLAASH and 6S Code Atmospheric Correction on Snow Cover Detection in Akita Prefecture, Japan Using MODIS Imagery Data," *Appl. Mech. Mater.*, vol. 541–542, pp. 1394–1397, Mar. 2014.

[102] P. Pan, G. Chen, K. Saruta, and Y. Terata, "Snow Cover Detection Based on Visible Red and Blue Channel from MODIS Imagery Data," *Int. J. Geosci.*, vol. 6, no. January, pp. 51–66, 2015.

[103] A. Gafurov and A. Bárdossy, "Cloud removal methodology from MODIS snow cover product," *Hydrol. Earth Syst. Sci.*, vol. 13, no. 7, pp. 1361–1373, Jul. 2009.

[104] S. Ackerman, K. Strabala, P. Menzel, R. Frey, C. Moeller, and L. Gumley, "Discriminating clear-sky from cloud with MODIS algorithm theoretical basis document (MOD35)," Wisconsin, 2010.

[105] D. K. Hall, G. a. Riggs, J. L. Foster, and S. V. Kumar, "Development and evaluation of a cloud-gap-filled MODIS daily snow-cover product," *Remote Sens. Environ.*, vol. 114, no. 3, pp. 496–503, Mar. 2010.

[106] A. E. Tekeli, Z. Akyürek, A. Arda Şorman, A. Şensoy, and A. Ünal Şorman, "Using MODIS snow cover maps in modeling snowmelt runoff process in the eastern part of Turkey," *Remote Sens. Environ.*, vol. 97, no. 2, pp. 216–230, Jul. 2005.

[107] D. K. Hall and G. A. Riggs, "Accuracy assessment of the MODIS snow products," *Hydrol. Process.*, vol. 21, no. 12, pp. 1534–1547, Jun. 2007.

[108] P. Pan, G. Chen, K. Saruta, and Y. Terata, "Snow cover detection based on two-dimensional scatter plots from MODIS imagery data," *J. Appl. Remote Sens.*, vol. 9, no. 1, p. 096083, Feb. 2015.

[109]"The Earth Observing System Data and Information System (EOSDIS) web of NASA," *National Aeronautics and Space Administration*. [Online]. Available: https://earthdata.nasa.gov/. [Accessed: 08-Jul-2015].

[110] R. N. Clark, G. A. Swayze, R. Wise, E. Livo, T. Hoefen, R. Kokaly, and S. J. Sutley, "USGS digital spectral library splib06a," *United States Geological Survey*, 2007. [Online]. Available: http://speclab.cr.usgs.gov/spectral.lib06/. [Accessed: 07-Jul-2015].

[111] Clark, R. N., and U. S. G. Survey, *USGS digital spectral library splib06a*, Rev. Sept. Denver: U.S. Geological Survey, 2007.

[112] "ASTER Spectral Library," *Jet Propulsion Laboratory, California Insitute of Technology*. [Online]. Available: http://speclib.jpl.nasa.gov/. [Accessed: 14-Jul-2015].

[113] A. M. Baldridge, S. J. Hook, C. I. Grove, and G. Rivera, "The ASTER spectral library version 2.0," *Remote Sens. Environ.*, vol. 113, no. 4, pp. 711–715, Apr. 2009.

[114] "The Geospatial Information of Aomori," *The Geospatial Information Authority of Japan*. [Online]. Available: http://www.gsi.go.jp/KOKUJYOHO/CENTER/kendata/aomori_heso.htm. [Accessed: 14-Jul-2015].

Publications list

Peer-reviewed Professional Journal Papers

1. Paipai Pan, Guoyue Chen, Kazuki Saruta, and Yuki Terata. Snow-cover Detection Based on Two-dimensional Scatter Plots from MODIS Imagery Data. Journal of Applied Remote Sensing, 9(1), 096083 (2015). (IF= 0.892)

2. Paipai Pan, Guoyue Chen, Kazuki Saruta, and Yuki Terata. Snow Cover Detection Based on Visible Red and Blue Channel from MODIS Imagery Data. International Journal of Geosciences, 6, 51-66, (2015). (IF=0.77)

3. Paipai Pan, Kazuki Saruta, Yuki Terata, Guoyue Chen. Observations for Snow Cover Detection in Akita via the Combination of Normalized Difference Vegetation Index and Normalized Difference Snow Index, Transactions of The Japan Society for Aeronautical Space Sciences Aerospace Technology Japan, Vol.12, No.ists29p.Pn_1-Pn_7 (2014). (EI)

4. Paipai Pan, Kazuki Saruta, Yuki Terata, Guoyue Chen. Comparison of FLAASH and 6S Code Atmospheric Correction on Snow Cover Detection in Akita Prefecture, Japan Using MODIS Imagery Data, Applied Mechanics and Materials, Vols. 541-542, pp. 1394-1397 (2014). (EI)

International Academic Conference

1. Paipai Pan, Kazuki Saruta, Yuki Terata, Guoyue Chen. Comparison of FLAASH and 6S Code Atmospheric Correction on Snow Cover Detection in Akita Prefecture, Japan Using MODIS Imagery Data, The 2014 International Conference on Mechanical, Electronics and Computer Engineering (CMECE 2014), CMECE2014-2-081, Sanya, China. January 24-26, 2014.

2. Paipai Pan, “Observations for Snow Cover Detection in Akita via the Combination of

NDVI and NDSI". The 29th International Symposium on Space Technology and Science (29th ISTS), 2013-s-82-n, Nagoya, Japan. June 2-9, 2013.

Japan Domestic Academic Conference

1. Paipai Pan, Kazuki Saruta, Yuki Terata, Guoyue Chen. Observations of climate change of Akita Prefecture using MODIS images. Proceedings of Forum on Information Technology 2011, No. 10 (3), pp. 295-296, Hakodate University, Hokkaido, Japan, September 7-9, 2011.

2. Paipai Pan, Kazuki Saruta, Yuki Terata, Guoyue Chen. Analysis of snow cover in Akita Prefecture using remote sensing. Proceedings of Tohoku-Section Joint Convention of Institutes of Electrical and Information Engineers, Japan, No.1D13, pp.129, Tohoku Gakuin University, Miyagi, Japan, August 25-26, 2011.